UNIVERSITÀ DEGLI STUDI DI PADOVA

DEPARTMENT OF CIVIL, ENVIRONMENTAL AND ARCHITECTURAL ENGINEERING

MASTER THESIS IN WATER AND GEOLOGICAL RISK ENGINEERING

BASIN-SCALE HYDROLOGICAL IMPACTS FROM CLIMATIC CHANGES: A MODEL ASSESSMENT IN THE HORN OF AFRICA

SUPERVISOR
PROFESSOR MARCO MARANI

MASTER CANDIDATE:
HUNDESA SIRAJ MOHAMMED
STUDENT ID NUMBER: 2089747

ACADEMIC YEAR 2024/2025

ACKNOWLEDGEMENTS

This work would not have been possible without the unwavering support and encouragement of many individuals and institutions. First and foremost, I express my deepest gratitude to my mother, who, despite having no formal education, raised me with resilience and determination. It is because of her sacrifices and unwavering belief in me that I stand here today. To my father, who was always a pillar of strength and support but is not here to witness this achievement—this work is dedicated to him. I did it, and I hope he is proud. I extend my heartfelt appreciation to my supervisor, Professor Marco Marani, whose guidance, patience, and exceptional mentorship have been instrumental throughout this journey. His unwavering support, insightful discussions, and constant encouragement made this research a reality. He is more than just a professor—his understanding and dedication are truly inspiring. I am deeply grateful to the Italian Government, particularly the Ministry of Foreign Affairs, for granting me the scholarship that made this opportunity possible. Without this support, pursuing my academic journey in Italy would not have been feasible. A special thank you to Valentina Zanaga, whose kindness and encouragement ensured that I never gave up, even during the most challenging times. I also extend my sincere appreciation to my friends, who stood by me through the highs and lows, offering their unwavering support, motivation, and companionship. Their presence made this journey bearable and meaningful. A special thank you to Hydronova stuff for their technical assistance and contributions to this research. Above all, I thank myself for not giving up, for pushing through challenges, and for believing in my ability to achieve this milestone. This journey has been demanding, but it has also been incredibly rewarding, and I am proud of how far I have come.

ABSTRACT

Water resources modelling and management in arid catchments must face three main challenges: 1) the quantification of flood magnitudes, 2) the quantification of groundwater recharge for sustainable water extraction, 3) the evaluation of shifts in surface/subsurface hydrologic partitioning as a consequence of climate change. Tackling these challenges requires the development and use of a diverse set of tools, ranging from continuous hydrological modelling to the estimation of rainfall in ungauged areas, to the evaluation of quantitative climate change scenarios. The present thesis develops and applies these tools in the context of the Gheba River Basin, with outlet at Adi-Kumsi (Tigray, Ethiopia). This area exhibits strong seasonal and spatial rainfall fluctuations, whose quantitative characterization is made very challenging by observational data scarcity. This study integrates ground-based observations (1999–2002), global precipitation datasets (CHIRPS, TRMM, ERA5, TerraClimate), and stochastic weather generation to produce an enhanced evaluation of available precipitation input and to evaluate hydrologic partitioning in the Gheba Basin. CHIRPS and TRMM outperformed other datasets in a comparison with observations, with CHIRPS exhibiting lower bias and TRMM capturing peak flows more effectively. ERA5 and TerraClimate showed significant biases, limiting their suitability for hydrological applications. A 100-year hourly precipitation dataset was then generated using a Bartlett-Lewis stochastic weather generator, calibrated on the 1999–2002 observed precipitation period. The generated dataset closely preserved key statistical properties of the observed data, including mean, variance, and wet-dry cycle patterns, though it underestimated extreme events. Three climate scenarios were applied, with the first scenario directly informed by CMIP5 simulation results, while the remaining two represent hypothetical experiments designed to explore potential climate extremes. These include: (i) Moderate Increase Scenario (+10% annual precipitation, +17% wet-season); (ii) Intensified Rainfall Scenario (+30% daily mean, +50% variance); and (iii) Prolonged Dry Scenario (-30% mean precipitation, +10–25% dry fraction). A HEC-HMS model was calibrated on the available rainfall and discharge observations and was subsequently used to evaluate the water balance at the basin scale. Results reveal that Scenario 2 led to a 54% increase in total precipitation, amplifying total flow (187%) and direct runoff (292%), posing heightened flood and erosion risks. Conversely, Scenario 3 resulted in a 43% reduction in precipitation, leading to a 53% decline in aquifer recharge and a 48% reduction in total flow, exacerbating drought conditions. Scenario 1 yielded an increase in infiltration and groundwater recharge. These findings demonstrate that hydrological shifts in response to climate perturbations are nonlinear and strongly influenced by precipitation distribution rather than mean changes alone. While some deviations were observed between imposed and modelled changes, these are expected given that the stochastic model was calibrated using only four years of observed precipitation and a single 100-year simulation. The results underscore the inherent variability in stochastic hydrological modeling, where changes in precipitation characteristics can lead to amplified or dampened hydrological responses. A longer observational record and ensemble-based simulations would improve alignment with imposed changes and strengthen confidence in projections. Despite these uncertainties, this study provides a robust framework for assessing climate-induced hydrological shifts in data-scarce, semi-arid environments. The results highlight the Gheba Basin's dual vulnerability to both extreme flood and drought conditions, emphasizing the need for adaptive water resource management strategies to enhance resilience in the face of increasing climate variability.

Keywords: Hydrological Modeling, Climate Change, Precipitation Datasets, Stochastic Weather Generator, HEC-HMS, Gheba Basin, Ethiopia.

Table of Contents

LIST OF FIGURES

LIST OF TABLES

1. INTRODUCTION

Water is a fundamental resource for human survival, agriculture, and economic development, particularly in semi-arid and drought-prone regions such as Ethiopia's Tigray region. The country's economy is predominantly agrarian, with more than 85% of the population engaged in rain-fed agriculture. Given this dependence on rainfall, variations in precipitation patterns, extreme weather events, and prolonged droughts pose a significant risk to water security, food production, and hydrological stability.

Ethiopia's climate variability poses significant challenges to water resource management and agricultural planning, particularly as extreme events like droughts and floods have become more frequent in recent decades. This variability underscores the importance of accurate hydrological modeling and data management to ensure sustainable resource utilization. Droughts and occasional floods are recurrent issues in the Tigray region, exacerbated by climate variability and environmental degradation. These climatic extremes have a direct impact on the sustainability of water resources, making accurate hydrological modelling and efficient water management essential for the region's socioeconomic stability [1].

The Tigray region, located in northern Ethiopia, demonstrates semi-arid to sub-humid rainfall characteristics. The region primarily relies on the *Kiremt* season for its annual precipitation, which ranges from 450 mm in the lowland areas to 850 mm in the highland zones [2,3]. This variation is shaped by the region's rugged terrain, including high mountains, dissected plateaus, and valleys. Rainfall in Tigray is essential for sustaining its predominantly agrarian economy, yet it is highly erratic, often leading to droughts or, occasionally, excessive flooding. Such variability exacerbates challenges for water resource management and agricultural productivity in the region [4].

The Gheba Basin, located in the Tigray region of Ethiopia, is an example of a hydrologically sensitive and data-scarce basin where climate variability has major implications for water resource management and flood risk assessment. Changes in seasonal precipitation, runoff behaviour, and evapotranspiration directly impact groundwater recharge, soil moisture availability, and streamflow dynamics. However, limited ground-based observations in the region make it challenging to accurately model hydrological responses under current and future climate conditions.

Hydrological models such as HEC-HMS provide a scientific basis for simulating water balance components, but their reliability is largely dependent on accurate precipitation inputs. In regions like Gheba Basin, where observed data is sparse and discontinuous, researchers often turn to global precipitation datasets such as ERA5-Land, CHIRPS, TRMM, and many more. These datasets provide valuable insights but come with uncertainties that need to be quantified before they are used for hydrological applications.

To overcome these challenges, this study integrates multiple precipitation datasets and a stochastic weather generator (SWG) (Bartlett-Lewis model). After validating the generated precipitation data on observed precipitation from 1999–2002. A synthetic 100-year hourly precipitation dataset were produced. Using this long-term synthetic dataset as a baseline, three climate change scenarios are simulated:

- Moderate Increase Scenario (+10% mean annual precipitation, +17% wet-season increase)
- Intensified Rainfall Scenario (+30% 24-hour mean precipitation, +50% variance increase)
- Prolonged Dry Scenario (-30% mean precipitation, +10–25% increase in dry fraction)

By assessing the hydrological responses to these projected climate conditions, this study aims to provide a robust framework for evaluating water resource risks and resilience in the Gheba Basin. The findings will contribute to the development of adaptive water management strategies that address both flood risk mitigation and drought resilience in the face of increasing climate variability.

1.1. PROBLEM STATEMENT

Hydrological modeling in data-scarce regions like the Gheba Basin presents significant challenges due to limited ground-based observations, uncertainty in global datasets, and the impact of climate variability on precipitation patterns. A reliable precipitation dataset is essential for hydrological model calibration, streamflow prediction, and future climate impact assessment, yet existing observational records are limited (1999–2002), making long-term hydrological projections difficult.

To address this challenge, this study first calibrated and validated a continuous hydrological model (HEC-HMS) using observed precipitation and streamflow data from the Adi-Kumsi station. However, due to the limited temporal coverage of ground-based precipitation data, an evaluation of global precipitation datasets (CHIRPS, ERA5, TRMM) was conducted to determine the most reliable dataset for hydrological modeling in the Gheba Basin.

To establish a long-term baseline precipitation dataset, interpolated precipitation data from the calibrated HEC-HMS model was used as input for stochastic weather generation. A Bartlett-Lewis Stochastic Weather Generator (SWG) was calibrated based on interpolated precipitation data and used to generate a 100-year hourly precipitation dataset, forming the baseline climate scenario. The statistical properties of this dataset were then compared with observed and interpolated data to ensure consistency and reliability.

Once the baseline dataset was validated, three climate change scenarios were applied to analyze future hydrological impacts:

- Moderate Increase Scenario—Simulating a 10% increase in mean annual precipitation and a 17% increase during the rainy season (July–September).
- Intensified Rainfall Scenario—Increasing 24-hour precipitation by 30% and variability by 50%, representing the potential for more extreme storm events.
- Prolonged Dry Scenario—Simulating a 30% decrease in mean precipitation and a 10–25% increase in dry fraction, representing extended drought conditions.

This study compares and analyses the statistical differences between observed precipitation, global datasets, interpolated precipitation, and generated climate scenarios to identify the most suitable precipitation dataset for hydrological modeling. The findings will contribute to climate impact studies and water resource management strategies in the Gheba Basin, ensuring better preparedness for future hydrological extremes.

1.2. OBJECTIVES

General Objectives:

The main objective of this study is to assess the hydrological response of the GHEBA Basin to current and future climate conditions by utilizing a calibrated and validated continuous hydrological model (HEC-HMS) and a stochastic weather generator (SWG) to produce long-term precipitation simulations.

Specific Objectives:

- Calibrate and validate the HEC-HMS hydrological model using observed precipitation and streamflow data from the Adi-Kumsi station (1999–2002).
- Evaluate and compare global precipitation datasets (CHIRPS, ERA5, TRMM, etc.) to identify the most suitable dataset for hydrological simulations in the study region.
- Generate a 100-year hourly baseline precipitation dataset using a Bartlett-Lewis Stochastic Model, calibrated based on interpolated precipitation from the HEC-HMS model.
- Validate the generated baseline dataset by comparing its statistical properties with observed and interpolated precipitation statistics.
- Apply climate change scenarios to assess their impact on precipitation partitioning and hydrological balance in the basin.
- Compare the hydrological impacts of various precipitation datasets (observed, global datasets, interpolated, and generated climate scenarios) to analyze how climate change influences the basin's hydrological behaviour.

1.3. STRUCTURE OF THE THESIS

This thesis is organized into the following chapters, each focusing on different aspects of the study to provide a comprehensive understanding of the comparative analysis of hydrological modeling using different precipitation datasets and evaluating climate change impacts on hydrology in the GHEBA Basin.

Chapter 1, Introduction provides an overview of the research problem, objectives, and significance of the study. It introduces the GHEBA Basin, highlights the challenges of hydrological modeling in data-scarce regions. It also outlines the structure of the thesis and its contribution to understanding climate change impacts on basin hydrology

Chapter 2, Background establishes the theoretical foundation of the study by discussing the relationship between climate and hydrology, the importance of precipitation datasets in hydrological modeling, and the application of stochastic weather generators for long-term climate simulations. The chapter also covers hydrological modeling using HEC-HMS, the relevance of global precipitation datasets such as CHIRPS, ERA5, and TRMM.

Chapter 3, Study Area Description presents the physical and hydrological characteristics of the GHEBA Basin. It describes the basin's geography, climate, seasonal rainfall distribution, and topographical influences on hydrology. Additionally, the land use, soil characteristics, and water resource features of the basin are discussed to provide context for the hydrological modeling approach.

Chapter 4, Data and Methods outlines the data sources and methodological framework used in the study. It details the collection and processing of observed precipitation and streamflow data from the Adi-Kumsi station, the evaluation of global precipitation datasets such as CHIRPS, ERA5, and TRMM, and the interpolation of precipitation using HEC-HMS. The chapter also describes the calibration and validation of the HEC-HMS model using observed data, including the use of performance metrics such as the Nash-Sutcliffe Efficiency (NSE), Root Mean Square Error (RMSE), and Percent Bias (PBIAS) to assess model accuracy. The setup and calibration of the stochastic weather generator (SWG) based on interpolated precipitation data are also presented, along with the generation of a 100-year hourly precipitation dataset for the baseline climate scenario. Finally, the application of climate change scenarios, including RCP8.5, extreme rainfall, and prolonged dry spell scenarios, is discussed, along with the methods used to analyze changes in runoff, infiltration, and water balance under different conditions.

Chapter 5, Results and Discussion presents the findings from the hydrological simulations and the statistical validation of the precipitation datasets. It includes an analysis of the baseline precipitation statistics, comparing observed, interpolated, and SWG-generated precipitation to assess the reliability of the generated dataset. The performance of the HEC-HMS model using different precipitation inputs is evaluated, and the model's response to global datasets is discussed.

Chapter 6, Conclusion and Recommendations summarizes the key findings of the study and discusses their implications for hydrological modeling and water resource management. It highlights the effectiveness of stochastic weather generators in generating long-term precipitation data and the role of different precipitation datasets in hydrological modeling.

Chapter 7 Recommendation also outlines the limitations of the study and offers recommendations for future research, including the integration of machine learning techniques and extension of stochastic modeling to temperature and evapotranspiration projections.

Appendix and Annex contains relevant data snapshots and also some important links to the code used and file downloaded from global datasets.

2. BACKGROUND

2.1. OVERVIEW OF CLIMATE AND HYDROLOGY

The relationship between climate and hydrology is fundamental to understanding water resource dynamics. Climate directly influences the hydrological cycle through precipitation, temperature, and evaporation processes. These variables govern the distribution, movement, and storage of water across the Earth's surface and subsurface systems. Hydrology, in turn, reflects these climatic interactions through processes like runoff, infiltration, and evapotranspiration, which are critical for maintaining water availability [5].

A central concept in hydrological studies is the water balance equation, which represents the continuity of water within a system. The equation is expressed as:

$$P = ET + Q + \Delta S \qquad (1)$$

where P is precipitation, ET is evapotranspiration, Q is runoff, and ΔS represents the change in water storage (in soil or groundwater). This equation is essential for evaluating water availability, particularly in regions prone to climatic variability or stress. It provides a framework for assessing how changes in any of these components—driven by climate or human activity—affect overall hydrological behaviour [5].

Climate change poses significant challenges to hydrological processes, especially in semi-arid regions like Ethiopia. Changes in precipitation patterns, the frequency of extreme events, and rising temperatures alter evapotranspiration rates and runoff dynamics, leading to increased variability in water availability. Semi-arid regions are particularly vulnerable because of their dependence on limited rainfall and their exposure to prolonged droughts or intense seasonal rains. These changes underscore the importance of studying rainfall variability and runoff in the context of climate projections to develop effective water resource management strategies [6].

2.2. STOCHASTIC WEATHER GENERATORS (SWGS)

Stochastic weather generators (SWGs) are widely used tools in hydrological and climate research for simulating synthetic climate data while preserving statistical properties of historical observations. These models are particularly valuable in regions where observed meteorological data is limited or incomplete. The ability to generate long sequences of synthetic climate data allows researchers to analyze climate variability, extreme events, and the potential impacts of climate change on hydrological systems [7].

Precipitation, in particular, exhibits high temporal and spatial variability, making it challenging to predict. Stochastic weather generators simulate precipitation using probability distributions and statistical relationships derived from historical climate records. One of the most frequently used models for stochastic precipitation generation is the Bartlett-Lewis Rectangular Pulse Model (BLRPM), which captures the clustered nature of rainfall events through a Poisson [8].

These models play an essential role in hydrological applications such as flood forecasting, water resource management, and climate impact assessments [9]. Their effectiveness lies in their ability to

reproduce observed climate characteristics while allowing for sensitivity analyses under different climate scenarios.

2.2.1. STOCHASTIC MODELS OF PRECIPITATION

Precipitation at a specific location exhibits extreme variability and irregularity over time, making it well-suited for a probabilistic approach. This is because the numerous factors influencing its occurrence and intensity are challenging to identify and quantify. Additionally, the highly nonlinear nature of the physical processes involved makes accurate prediction infeasible, even if precise measurements were possible. Consequently, precipitation analysis must rely on stochastic methods, focusing on the probability distributions of the associated random variables. In hydrology, various stochastic models have been developed to effectively characterize the hydrometeorological properties of a given area. These models operate by identifying key random variables and assigning appropriate probability distributions, whose parameters are estimated using historical data. One notable example of such models is the Bartlett-Lewis model, which will be discussed in the following section [10].

2.2.2. BARTLETT-LEWIS STOCHASTIC MODEL

The Bartlett-Lewis model is a stochastic precipitation model that schematizes the succession of perturbations through a process of Poissonian arrivals with parameter λ. The probability P of events is characterized as follows:

$$P(s) = (\lambda \Delta t)^s \frac{e^{-\lambda \Delta t}}{s!} \qquad (2)$$

in which: s is the number of perturbations that begin in the time interval Δt

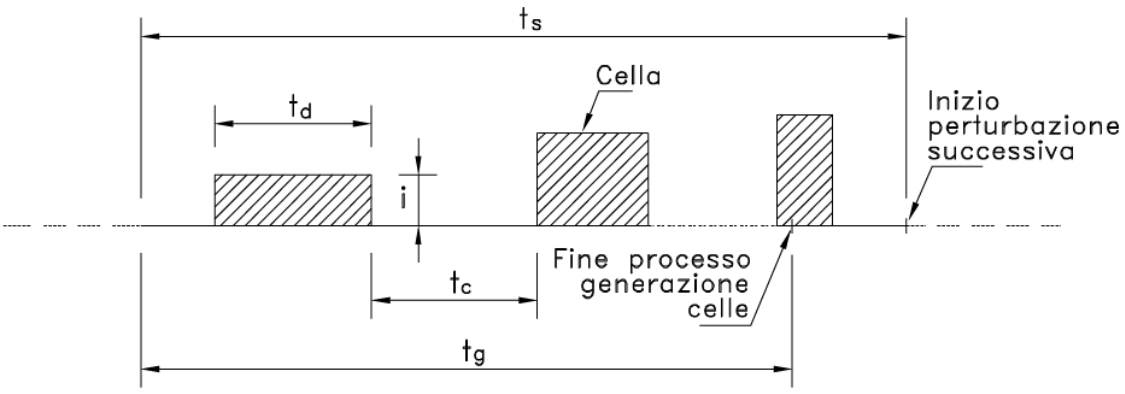

Figure 1. Random variables that define a Bartlett-Lewis process [10]

In the figure 1 above represent the original diagram from Processi e Modelli dell'Idrologia: Un'introduzione by Professor Marco Marani (2017) [10] and was originally labeled in Italian. The translated terms used in the figure are as follows:

Cella → Cell
Inizio perturbazione successiva → Start of next perturbation
Fine processo generazione celle → End of cell generation process.

The process of Poissonian arrivals implies that the moments of onset of the disturbances, t_s, are distributed exponentially as follows:

$$P(T_s \leq t_s) = 1 - e^{-\lambda t_s} \quad (3)$$

where T_s indicates the time between the arrival of two successive disturbances, i.e. interarrival time). In correspondence to each perturbation, there is a process of precipitation cell generation cells, which represent the spatial path of the perturbations, also assumed to be of the Poissonian type:

$$P(c) = (\beta \Delta t)^c \frac{e^{-\beta \Delta t}}{c!} \quad (4)$$

(where c indicates the number of cells that start in the time interval Δt). We therefore have:

$$P(T_c \leq t_c) = 1 - e^{-\beta t_c} \quad (5)$$

in which T_c indicates the arrival time of two successive cells. According to the Bartlett-Lewis model, the cell generation process ends after a time that is also exponentially distributed:

$$P(T_g \leq t_g) = 1 - e^{-\gamma t_g} \quad (6)$$

The lifetime of the cells is also distributed according to an exponential law:

$$P(T_d \leq t_d) = 1 - e^{-\eta t_d} \quad (7)$$

and so is also the intensity at I of precipitation:

$$P(I \leq i) = 1 - e^{-i/\mu_i} \quad (8)$$

2.2.3. MODIFIED BARTLETT-LEWIS MODEL

The Bartlett-Lewis model has certain limitations that make it less suitable for applications involving inflow-outflow models, which are of primary interest in this context. Like many other point-based models, it significantly overestimates the likelihood of dry periods. Since the hydrological response of a basin—a key application of hydrological modeling—relies heavily on the accurate representation of alternating dry and wet periods, a realistic reproduction of these sequences is essential.

To improve the model's ability to generate reliable flow simulations, modifications to the previously introduced framework are necessary. One approach to achieving a more accurate representation of rainfall probability is by introducing an additional degree of freedom, as suggested by Rodriguez-Iturbe, Cox, and Isham [8]. Specifically, instead of assuming a fixed cell duration, the model allows variability in cell lifetimes across different perturbations. This adjustment enables the incorporation of perturbations with distinct structures, meaning the precipitation within them can originate from different statistical distributions.

The η parameter, which represents the lifetime of individual cells, is thus modelled using a Gamma distribution, with its probability density function defined as follows

$$f(\eta) = \frac{\nu^\alpha}{\Gamma(\alpha)} e^{-\nu\eta} \eta^{\alpha-1} \quad (9)$$

For ease of calculation, the following is posed: k =β/η Φ=γ/η the parameters β and γ are then varied, as η change, so as to keep k and φ constant. The definition of this stochastic model therefore requires the specification of six parameters:

$$\lambda, \kappa, \varphi, \nu, \alpha, \mu i$$

The model calibration procedure consists in solving a system of (non-linear) equations in which some statistical quantities (e.g. means, variances or autocorrelations) are expressed as a function of the model parameters. In order to consider, the way in which the characteristics of precipitation vary with the variation of the aggregation interval, statistical quantities have been considered referring both to aggregations of data over 24 hours and to aggregations of the same data over 48 hours. The statistical quantities chosen for the purpose of calibrating the model are: Aggregated data over 24 hours [10]:

- medium (E1).
- variance (V ar1).
- autocovariance with lag equal to one (Cov1).
- fraction of dry days (P1). Aggregated data over 48 hours:
- variance (V ar2).
- fraction of dry days (P2).

On the basis of the probability distributions introduced above, it is possible to obtain expressions of these statistical quantities, in which the parameters of the model appear. In fact, we have:

$$\begin{aligned}
E_1 &= \frac{h\lambda\mu_c\mu_x\nu}{\alpha-1} \\
Var_1 &= 2A_1[h(\alpha-3)\nu^{2-\alpha} - \nu^{3-\alpha} + (\nu+h)^{3-\alpha}] - 2A_2[h\phi(\alpha-3)\nu^{2-\alpha} - \nu^{3-\alpha} + (\nu+h\phi)^{3-\alpha}] \\
Cov_1 &= A_1[(\nu+2h)^{3-\alpha} - 2(\nu+h)^{3-\alpha} + \nu^{3-\alpha}] - A_2[(\nu+2h\phi)^{3-\alpha} - 2(\nu+h\phi)^{3-\alpha}\nu^{3-\alpha}] \\
P_1 &= exp\{-h\lambda - \frac{\lambda}{\phi}\frac{\nu}{\alpha-1} + [1+\phi(k+\phi) - \frac{1}{4}\phi(k+\phi)(k+4\phi) + \\
&+ \frac{1}{72}\phi(k+\phi)(4k^2+27k\phi+72\phi^2)] + \frac{\lambda\phi}{\phi+k}\frac{1}{\phi}\frac{\nu}{\alpha-1}(1-k-\phi+\frac{3}{2}k\phi+\phi^2+\frac{1}{2}k^2)\} \\
Var_2 &= 2A_1[2h(\alpha-3)\nu^{2-\alpha} - \nu^{3-\alpha} + (\nu+2h)^{3-\alpha}] - 2A_2[2h\phi(\alpha-3)\nu^{2-\alpha} - \nu^{3-\alpha} + (\nu+2h\phi)^{3-\alpha}] \\
Cov_2 &= A_1[(\nu+4h)^{3-\alpha} - 2(\nu+2h)^{3-\alpha} + \nu^{3-\alpha}] - A_2[(\nu+4h\phi)^{3-\alpha} - 2(\nu+4h\phi)^{3-\alpha}\nu^{3-\alpha}] \\
P_2 &= \exp\{-2h\lambda - \frac{\lambda}{\phi}\frac{\nu}{\alpha-1}[1+\phi(k+\phi) - \frac{1}{4}\phi(k+\phi)(k+4\phi) + \\
&+ \frac{1}{72}\phi(k+\phi)(4k^2+27k\phi+72\phi^2)] + \frac{\lambda\phi}{\phi+k}\frac{1}{\phi}\frac{\nu}{\alpha-1}(1-k-\phi+\frac{3}{2}k\phi+\phi^2+\frac{1}{2}k^2)\}
\end{aligned}$$

where: h indicates the basic interval of aggregation of the data used (h = 24 hours in the case in question), and the constants A1 and A2 are defined by:

$$A_1 = \frac{\lambda\mu_c k\mu_x^2\nu^\alpha}{(\alpha-1)(\alpha-2)(\alpha-3)}(2\mu_x^2 + \frac{k\phi\mu_x^2}{\phi^2-1});$$

$$A_2 = \frac{\lambda\mu_c k\mu_x^2\nu^\alpha}{\phi^2(\phi^2-1)(\alpha-1)(\alpha-2)(\alpha-3)}.$$

The relations introduced constitute, once the values deriving from the time series have been substituted for the first member, a system of six nonlinear equations in six unknowns. For the solution of such a system, the nonlinear system was first transformed into the problem of minimizing the objective function:

$$F = (1 - E_1/E_1*)^2 + (1 - Var_1/Var_1*)^2 + (1 - Var_2/Var2*)^2 \\ +(1 - Cov_1/Cov_1*)^2 + (1 - P_1/P_1*)^2 + (1 - P_2/P_2*)^2$$

in which the terms marked with an asterisk, $*$, represent the values obtained from the time series, while the remaining ones represent the quantities evaluated through the expressions just introduced. The solution of the minimum problem is obtained with standard numerical techniques. It is hardly necessary to recall that it is necessary to introduce some constraints on the parameters, such as, for example, non-negativity. The method used is that of the simplex, which, although not characterized by a high order of convergence, normally guarantees the achievement of a value close to the minimum. The calibration of the model presented is carried out on the basis of daily precipitation data, dividing the year into sub-intervals of approximately one month duration, which can be assumed to be meteorologically homogeneous. The statistical parameters are then calculated and the model parameters for each of these intervals are calculated. Subsequently, on the basis of the parameters thus calculated, it is possible to generate a synthetic succession of hourly rainfall that reproduces the values of the statistical quantities used for calibration [10].

2.3. HYDROLOGICAL MODELING IN CLIMATE CHANGE STUDIES

Hydrologic models, which integrate key hydrologic processes, are essential tools for assessing water resources and evaluating hydrological phenomena. These models simplify complex real-world systems and are indispensable for water resource management, flood forecasting, and hydrological analysis. However, accurate hydrological modeling remains a challenging task, especially in regions with limited data availability. To provide reliable results, hydrological models require proper calibration and performance evaluation to ensure their suitability for a given study [11].

2.3.1. HYDROLOGIC MODELING USING HEC-HMS

The HEC-HMS (Hydrologic Engineering Centre–Hydrologic Modeling System) is a widely used hydrologic model developed by the U.S. Army Corps of Engineers. This model is specifically designed to simulate the rainfall-runoff processes in watersheds and is employed in various applications, including flood frequency analysis, flood warning system design, urban flooding studies, reservoir spillway capacity evaluation, and stream restoration [12]. Its flexibility and adaptability make HEC-HMS an appropriate choice for both large and small-scale watershed studies [13].

The Hydrologic Modeling System (HEC-HMS) is designed to simulate the complete hydrologic processes of dendritic watershed systems. The software includes many traditional hydrologic analysis procedures such as event infiltration, unit hydrographs, and hydrologic routing. HEC-HMS also includes procedures necessary for continuous simulation including Evapo-transpiration, snowmelt, and soil moisture accounting. Advanced capabilities are also provided for gridded runoff simulation using the linear quasi-distributed runoff transform (ModClark). Supplemental analysis tools are provided for model optimization, forecasting streamflow, depth-area reduction, assessing model uncertainty, erosion and sediment transport, and water quality.

Hydrologic models in HEC-HMS can be categorized into two main types: event-based models and continuous models. Event-based models are designed to simulate individual storm events, focusing on short-term rainfall-runoff processes. These models are particularly useful for flood analysis and extreme event predictions, where the primary concern is capturing peak flows and event-specific

dynamics. In contrast, continuous models simulate the hydrologic cycle over extended periods, accounting for processes such as soil moisture changes, evapotranspiration, and groundwater flow. Continuous models are ideal for assessing long-term water balance, seasonal variations, and climate change impacts [11].

To enhance its capabilities for continuous simulations, the HEC-HMS incorporates methods that model soil moisture dynamics and their interactions with hydrologic processes. Among these, the Soil Moisture Accounting (SMA) method (described in 2.3.2) is particularly significant as it captures the movement and storage of water within the soil and groundwater layers, offering a comprehensive representation of watershed hydrology.

2.3.2. SOIL MOISTURE ACCOUNTING (SMA) METHOD

The Soil Moisture Accounting (SMA) method in HEC-HMS is a robust approach for modeling the movement of water through vegetation, surface interception, soil layers, and groundwater systems. This method is particularly effective for continuous hydrologic simulations and is widely used in studies involving water resource assessment, groundwater-surface water interactions, and evapotranspiration analysis [13].

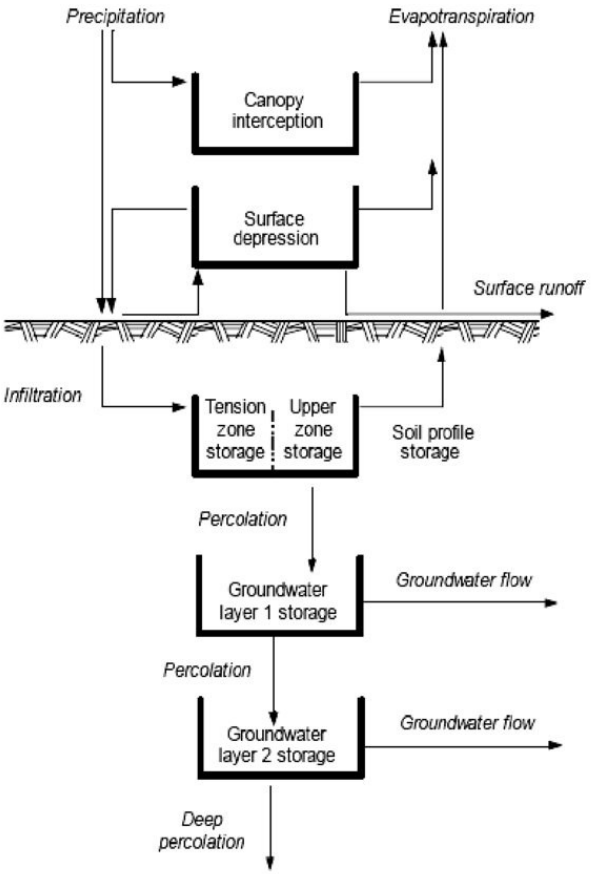

Figure 2.Conceptual schematic of the continuous soil moisture accounting algorithm [14]

2.3.2.1. STORAGE COMPONENTS IN THE SMA METHOD

CANOPY-INTERCEPTION STORAGE

This layer captures precipitation that is intercepted by vegetation such as trees, shrubs, and grasses. Precipitation is the only input to this layer. Water first fills the canopy storage, and only once this is full can precipitation contribute to other storage components. Water stored in the canopy is eventually removed via evaporation.

SURFACE-INTERCEPTION STORAGE

Representing water temporarily held in shallow surface depressions, this storage receives inflow from precipitation that surpasses the canopy storage and exceeds the soil's infiltration capacity. Outflows include infiltration into the soil profile and evaporation. When the volume of surface storage is exceeded, the excess water contributes directly to surface runoff.

SOIL PROFILE STORAGE:

This storage represents water stored in the upper soil layer and is divided into two zones: Upper Zone: Contains water available for both evaporation and percolation and Tension Zone: Contains water bound to soil particles, which can only be lost through evaporation. Evaporation first depletes the upper zone, then reduces the tension zone at a slower rate to account for the increasing difficulty in removing water bound to soil particles. Inflows to this layer come from infiltration, while outflows include evapotranspiration and percolation to groundwater layers.

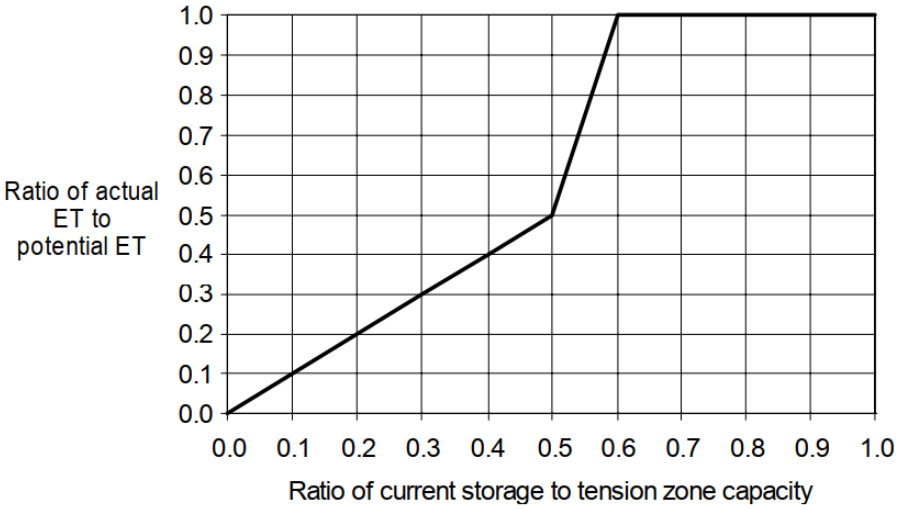

Figure 3.ET as a function of tension zone storage [14]

GROUNDWATER STORAGE:

Groundwater layers in the SMA represent horizontal interflow processes. The SMA model can include either one or two such layers. Water percolates into groundwater storage from the soil profile. The percolation rate is a function of a user-specified maximum percolation rate and the current storage in the layers between which the water flows. Losses from a groundwater storage layer are due to groundwater flow or to percolation from one layer to another. Percolation from the soil profile enters the first layer. Stored water can then percolate from layer 1 to groundwater layer 2 or from

groundwater layer 2 to deep percolation. In the latter case, this water is considered lost from the system; aquifer flow is not modelled in the SMA.

2.3.2.2. FLOW COMPONENT

The SMA model computes flow into, out of, and between the storage volumes. This flow can take the form of:

PRECIPITATION:

Precipitation is an input to the system of storages. Precipitation first contributes to the canopy interception storage. If the canopy storage fills, the excess amount is then available for infiltration.

INFILTRATION:

Infiltration refers to the process by which water enters the soil from the ground surface. The water available for infiltration during a specific time step consists of precipitation that bypasses canopy interception, and any water already stored on the surface.

The amount of water infiltrated during a given time period depends on three factors: the volume of water available for infiltration, the current saturation level (as a fraction of the soil's capacity), and the maximum infiltration rate defined by the user in the model. For each time interval in the analysis, the SMA model calculates the potential infiltration volume, denoted as PotSoilInfl.

$$PotSoilInfl = MaxSoilInfl - \left(\frac{CurSoilStore}{MaxSoilStore}\right) \times MaxSoilInfl \qquad (10)$$

Where MaxSoilInfl represents the maximum infiltration rate, CurSoilStore is the amount of water stored in the soil at the start of the time step, and MaxSoilStore is the maximum capacity of soil storage. The actual infiltration rate is determined as the lesser value between the potential infiltration volume (PotSoilInfl) and the available water for infiltration. Any water exceeding this calculated infiltration rate is directed to surface interception storage [15]

PERCOLATION

Percolation is the process where water moves downward from the soil profile into groundwater layers or a deep aquifer. In the SMA model, the rate of percolation between the soil profile and groundwater layers, as well as between two groundwater layers, depends on the volume in the source and receiving layers. Percolation is highest when the source layer is full, and the receiving layer is empty, while it decreases when the opposite is true. The potential percolation rate from the soil profile to groundwater layer 1 is calculated as following, (refer to figure 2):

$$PotSoilPerc = MaxSoilPerc\left(\frac{CurSoilStore}{MaxSoilStore}\right)\left(1 - \frac{CurGwStore}{MaxGwStore}\right) \qquad (11)$$

where PotSoilPerc = the potential soil percolation rate; MaxSoilPerc = a user-specified maximum percolation rate; CurSoilStore = the calculated soil storage at the beginning of the time step; MaxSoilStore = a user-specified maximum storage for the soil profile; CurGwStore = the calculated groundwater storage for the upper groundwater layer at the beginning of the time step; and MaxGwStore = a user-specified maximum groundwater storage for groundwater layer.

The potential percolation rate computed with Equation 3 is multiplied by the time step to compute an actual percolation volume. The available water for percolation is equal the initial soil storage plus

infiltration. The minimum of the potential volume and the available volume percolates to groundwater layer 1. [15].

A similar equation is used to compute *PotGwPerc*, the potential percolation from groundwater layer 1 to layer 2:

$$PotGwPerc = MaxPercGw\left(\frac{CurSoilStore}{MaxSoilStore}\right)\left(1 - \frac{CurGwStore}{MaxGwStore}\right) \quad (12)$$

where *MaxPercGw* = a user-specified maximum percolation rate; *CurGwStore* = the calculated groundwater storage for the groundwater layer 2; and *MaxGwStore* = a user-specified maximum groundwater storage for layer 2. The actual volume of percolation is computed as described above.

For percolation directly from the soil profile to the deep aquifer in the absence of groundwater layers, for percolation from layer 1 when layer 2 is not used, or percolation from layer 2, the rate depends only on the storage volume in the source layer. In those cases, percolation rates are computed as:

$$PotSoilPerc = MaxSoilPerc\left(\frac{CurSoilStore}{MaxSoilStore}\right) \quad (13)$$

and

$$PotGwPerc = MaxPercGw\left(\frac{CurSoilStore}{MaxSoilStore}\right) \quad (14)$$

respectively, and actual percolation volumes are computed as described in soil percolation section.

SURFACE RUNOFF AND GROUNDWATER FLOW

Surface runoff is the water that exceeds the infiltration rate and overflows the surface storage. This volume of water is direct runoff. Groundwater flow is the sum of the volumes of groundwater flow from each groundwater layer at the end of the time interval. The rate of flow is computed as:

$$GwFlow_{i+1} = \frac{ActSoilPerc + CurGw_iStore - PotGw_iPerc - \frac{1}{2}GwFlow_t \cdot TimeStep}{RoutGw_iStore + \frac{1}{2}TimeStep} \quad (15)$$

where $GwFlowt$ and $GwFlowt$+1= groundwater flow rate at beginning of the time interval t and t+1, respectively; ActSoilPerc = actual percolation from the soil profile to the groundwater layer; $PotGwiPerc$ = potential percolation from groundwater layer i; $RoutGwiStore$ = groundwater flow routing coefficient from groundwater storage i; TimeStep = the simulation time step; and other terms are as defined previously.

The volume of groundwater flow that the watershed releases, GwVolume, is the integral of the rate over the model time interval. This is computed as:

$$GwVolume = \frac{1}{2}(GwFlow_{t+1} + GwFlow_t)TimeStep \quad (16)$$

This volume may be treated as inflow to a linear reservoir model to simulate baseflow. [15]

EVAPOTRANSPIRATION (ET)

ET is the loss of water from the canopy interception, surface depression, and soil profile storages. In the HEC-HMS SMA model, potential ET demand currently is computed from monthly pan evaporation depths, multiplied by monthly-varying pan correction coefficients, and scaled to the time interval.

The potential ET volume is satisfied first from canopy interception, then from surface interception, and finally from the soil profile. Within the soil profile, potential ET is first fulfilled from the upper zone, then the tension zone. If potential ET is not completely satisfied from one storage in a time interval, the unsatisfied potential ET volume is filled from the next available storage.

When ET is from interception storage, surface storage, or the upper zone of the soil profile, actual ET is equivalent to potential ET. When potential ET is drawn from the tension zone, the actual ET is a percentage of the potential, computed as

$$ActEvapSoil = PotEvapSoil \cdot f(CurSoilStore, MaxTenStore) \quad (17)$$

where *ActEvapSoil* = the calculated ET from soil storage; *PotEvapSoil* = the calculated maximum potential ET; and *MaxTenStore* = the user specified maximum storage in the tension zone of soil storage.

2.3.3. TRANSFORM METHOD: CLARK UNIT HYDROGRAPH MODEL

The Clark unit hydrograph method utilizes the concept of an instantaneous unit hydrograph to route excess precipitation to the subbasin outlet. An instantaneous unit hydrograph is derived by instantaneously applying a unit depth (e.g. one inch) of excess precipitation over a watershed [16]. The resultant unit hydrograph is entirely theoretical (i.e. real precipitation cannot be applied instantaneously to a watershed) but it has the distinct advantage of characterizing the watershed's response to rainfall without reference to the duration of excess precipitation. This method explicitly represents two critical processes in the transformation of excess precipitation to runoff: 1) the translation (or movement) of excess precipitation from its origin throughout the watershed to the outlet and 2) the attenuation (or reduction) of the magnitude of the discharge as the excess precipitation is temporarily stored throughout the watershed [15].

Conceptually, water is translated from remote points to the watershed outlet with delay but without attenuation. Attenuation is then incorporated, conceptually speaking, at the watershed outlet. Two parameters are utilized within this method: Time of concentration (T_c), which is equivalent to the time it takes for excess precipitation to travel from the hydraulically-most remote point of the watershed to the outlet. Watershed storage coefficient (R), which is equivalent to attenuation due to storage effects throughout the watershed [17].

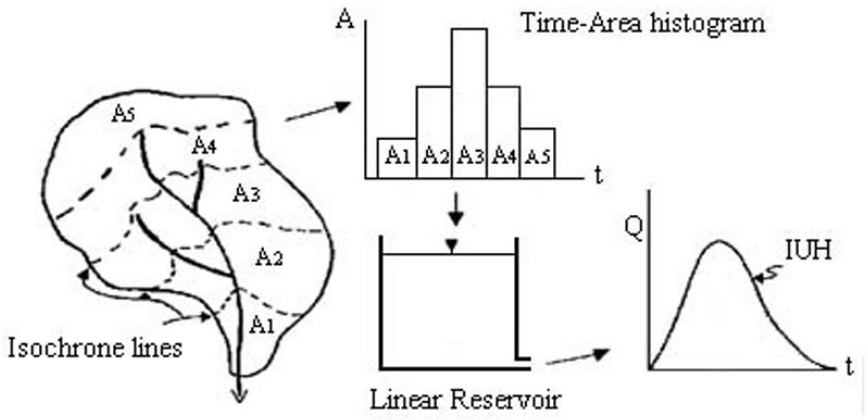

Figure 4. The conceptual model of Clark method

The time of concentration is defined as the time duration for a drop of water falling in the most remote point of a drainage basin to travel to the outflow point. The time of concentration is important to the hydrological analysis of watersheds.

3. STUDY AREA DESCRIPTION

3.1. ETHIOPIA: NATIONAL CONTEXT

Ethiopia's climate is largely influenced by its diverse topography and proximity to the equator. The country experiences a range of climatic zones, from arid and semi-arid regions in the lowlands to cool, temperate conditions in the highlands [1]. Rainfall in Ethiopia is highly variable both spatially and temporally. The primary rainy season, known as *kiremt*, occurs from June to September, delivering the majority of the annual rainfall in the highlands. A shorter rainy period, *belg*, spans from February to May and is particularly significant in the southern and southeastern regions. The dry season, *bega*, extends from October to January and is characterized by minimal precipitation and higher evaporation rates [18].

These seasons contribute to the country's rainfall variability, with the *kiremt* providing the bulk of precipitation, especially in the highlands, while the *belg* season is more prominent in southern and southeastern regions. Rainfall across Ethiopia ranges from over 2,000 mm annually in the western highlands to less than 200 mm in the arid eastern lowlands [19].

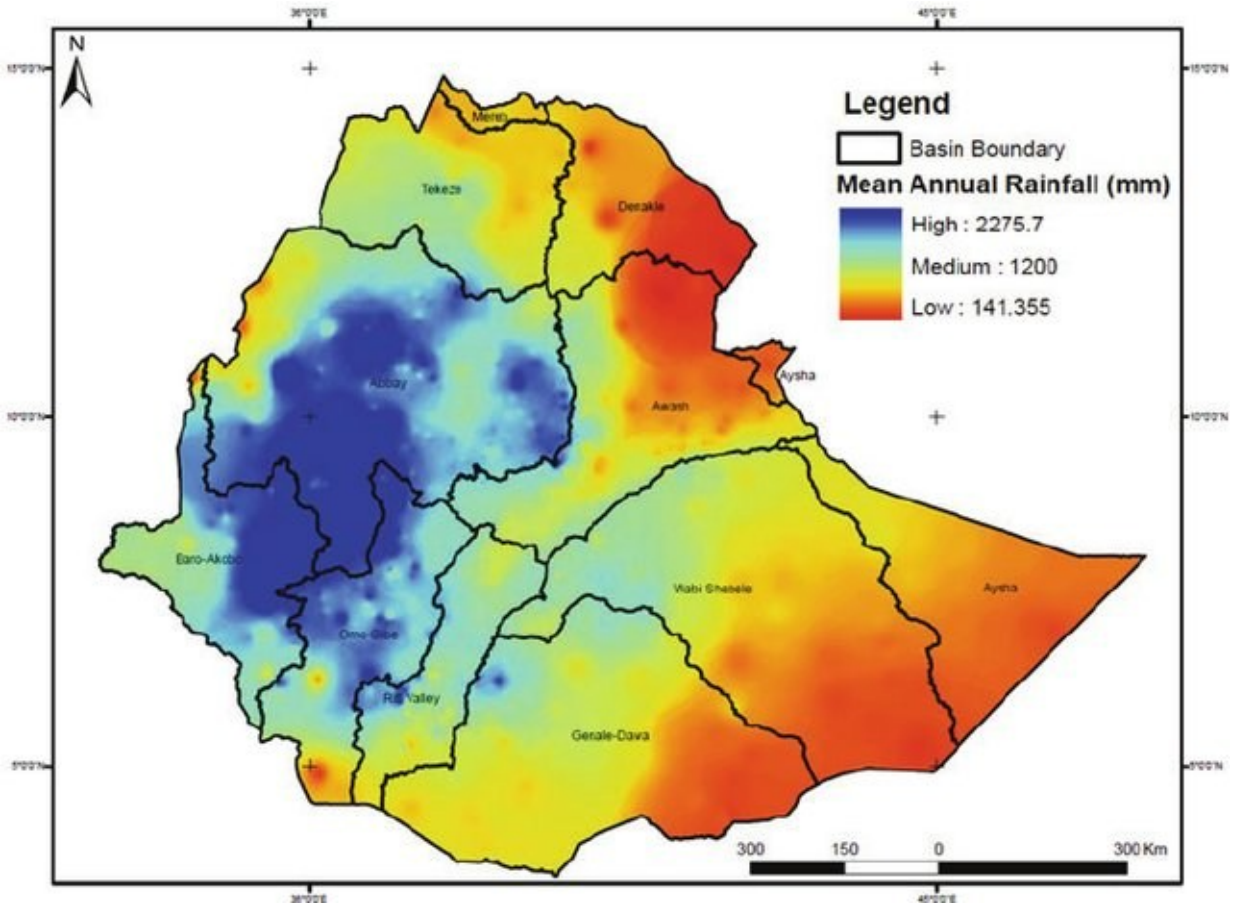

Figure 5.Spatial variability of rainfall in Ethiopia [18]

Temperature in Ethiopia varies with elevation. The lowland areas, lying below 1,500 meters above sea level, experience average annual temperatures ranging from 25°C to 30°C. In contrast, the highlands, above 2,500 meters, enjoy cooler conditions, with annual average temperatures between 10°C and 15°C. The combined effects of temperature, altitude, and rainfall distribution significantly

influence agricultural productivity and water resource availability across the country (Leul, 1994; NMA, 2007).

CLIMATE ZONES OF ETHIOPIA

Ethiopia's diverse topography and geographical location create distinct climate zones, each with unique characteristics that influence the country's ecosystem, agriculture, and water resources. These zones can be classified broadly into five main categories based on altitude, temperature, and rainfall [18]

Bereha (Hot Arid Zone): This zone lies at altitudes below 500 meters, primarily covering areas like the Danakil Depression. Bereha experiences extremely high temperatures, often exceeding 40°C, and minimal rainfall of less than 200 mm annually. Vegetation is sparse and adapted to arid conditions. Human activities in this zone mainly involve salt mining and pastoralism [16].

Kolla (Warm Semi-Arid Zone): Found at elevations between 500 and 1,500 meters, Kolla experiences average annual temperatures of 22°C to 29°C. Rainfall ranges from 400 to 1,200 mm, supporting crops such as sorghum, maize, and millet. This zone is significant for its contribution to Ethiopia's grain production, particularly in the western lowlands [18]

Weyna Dega (Cool Sub-Humid Zone): Situated at altitudes between 1,500 and 2,500 meters, Weyna Dega enjoys moderate temperatures, ranging from 16°C to 20°C, and receives rainfall between 800 and 1,200 mm annually. The region supports mixed farming systems, producing staple crops like wheat and barley, along with coffee in suitable areas. Its favorable climate makes it the most densely populated zone in the country [19].

Dega (Cool and Humid Zone): This zone spans elevations of 2,500 to 3,200 meters, with temperatures averaging 10°C to 16°C. Rainfall ranges from 1,000 to 2,000 mm annually, enabling the cultivation of highland crops such as barley, pulses, and potatoes. The Dega zone also supports extensive livestock farming and serves as an important watershed for the country [20].

Wurch (Cold and Moist Zone): Found above 3,200 meters, this zone experiences average temperatures below 10°C and receives rainfall of around 900 mm annually. Vegetation is sparse, dominated by Afro-alpine flora, and agriculture is limited to subsistence-level barley cultivation and livestock grazing. This zone is critical for preserving biodiversity and maintaining ecological balance [19].

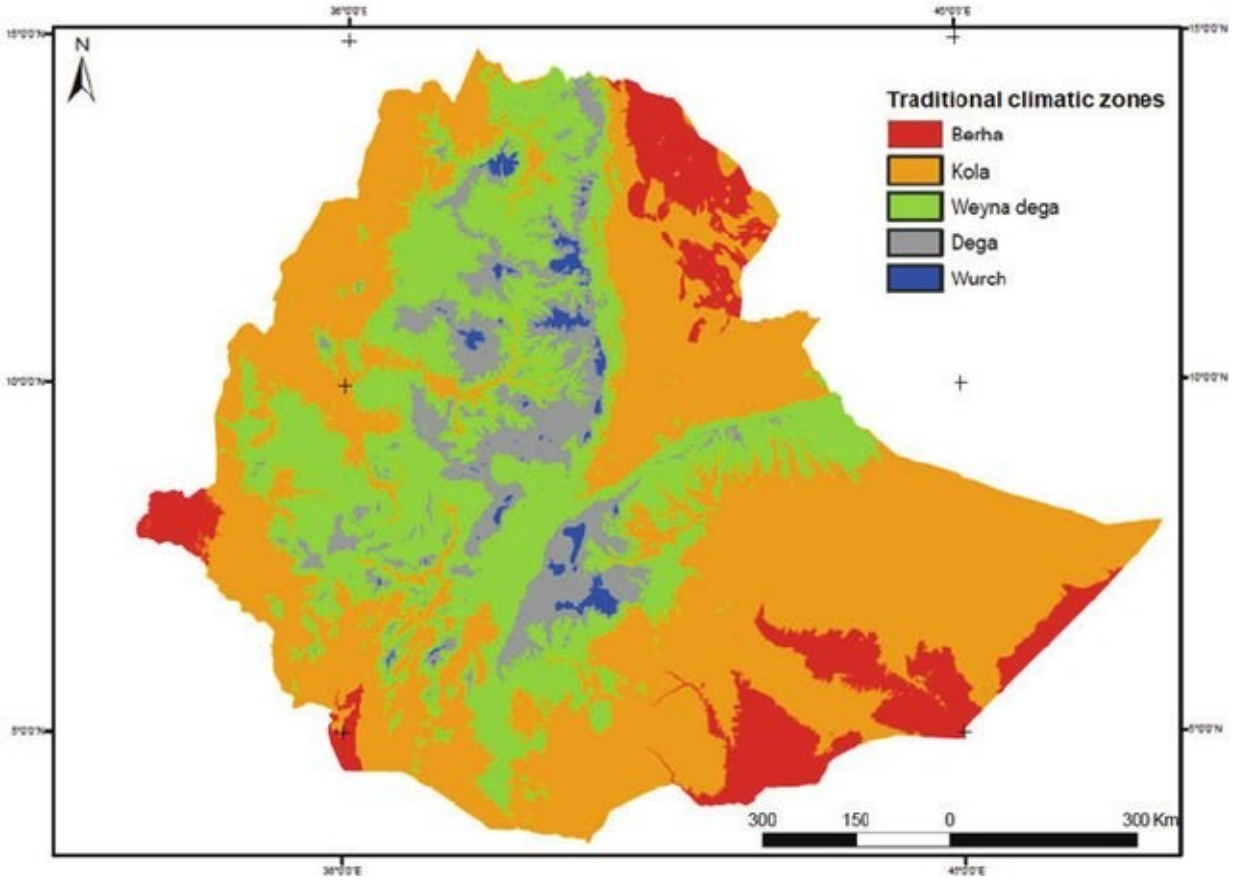

Figure 6.Traditional climatic zones of Ethiopia [18]

The Tigray region in northern Ethiopia, where the Gheba subbasin is located, exhibits a semi-arid to sub-humid climate, heavily influenced by its varied topography and latitude. The region experiences marked seasonal rainfall patterns, with most precipitation occurring during the *kiremt* season (June to September). Rainfall in Tigray is highly variable, ranging from 450 mm annually in lowland areas to over 850 mm in some highland zones. This variability significantly affects agricultural productivity and water availability [2,3].

Temperature also varies with elevation. Lowland areas often experience temperatures exceeding 30°C, while highland regions typically have cooler conditions, with average annual temperatures ranging from 15°C to 20°C. Seasonal fluctuations further compound the challenges of resource management in the region [21].

3.2. GHEBA: BASIN CONTEXT

3.2.1. LOCATION AND EXTENT

The Gheba basin is situated in northern Ethiopia, extending between 38°38′ to 39°48′ E longitude and 13°14′ to 14°16′ N latitude. Covering an area of approximately 5116 km², the subbasin includes Mekelle, the capital city of the Tigray regional state. It forms the headwaters of the Upper Tekeze River Basin, a major tributary of the Nile River. This subbasin is a significant hydrological study area because of its complex terrain, variable rainfall patterns, and its role in contributing to the Nile's flow [4].

3.2.2. CLIMATE AND RAINFALL VARIABILITY

The Gheba subbasin experiences a semi-arid climate, with the majority of rainfall occurring between June and September. Approximately 70% of the annual rainfall is concentrated in July and August, driven by the seasonal migration of the intertropical convergence zone (ITCZ) [3]. Rainfall is characterized by high spatial and temporal variability, ranging from 450 mm/year in the lower valleys to over 650 mm/year in the highland areas near Mugulat. This variability has a profound influence on hydrological processes, particularly surface runoff and recharge [22].

3.2.3. TOPOGRAPHY AND DRAINAGE

The subbasin's topography is dominated by rugged highlands in the northern and northeastern regions, with elevations ranging from 930 m.a.s.l. at the outlet to 3300 m.a.s.l. at the Mugulat Mountains near Adigrat. The central part of the basin features plateaus dissected by numerous rivers that drain southwest into the Tekeze River at Chemey. The mean elevation is 2144 m, with significant topographic variability [22]. These elevation differences greatly influence drainage patterns, surface water flow, and sediment [22]

3.2.4. LAND USE AND LAND COVER (LULC)

Land use in the Gheba subbasin is predominantly agricultural, covering 39% of the area, followed by bush and shrubland (30%), bare land (11%), and smaller percentages of grassland, forested areas, and settlements. Over the past two decades, small-scale irrigated agriculture has increased significantly, while natural vegetation cover has shown signs of recovery due to watershed management programs [22]. These LULC changes have directly influenced evapotranspiration rates and surface runoff, critical factors in hydrological modeling.

3.2.5. GEOLOGY AND SOILS

The geology of the Gheba subbasin comprises formations such as Enticho Sandstone, Adigrat Sandstone, Antalo Supersequence, and various metamorphic rocks [23]). Soils vary from clay loam (40%) and sandy clay loam (30%) to clay (19%), with finer soils in undulating pediments and deep alluvial deposits in lower terraces. However, much of the basin features shallow, rocky soils due to the prevalence of hard rock outcrops. These soil characteristics are vital in understanding infiltration, groundwater recharge, and the overall water balance [23].

3.2.6. HYDROLOGY

The Gheba subbasin contains four main sub-catchments: Siluh, Genfel, Agula, and Illala. These sub-catchments drain into the Tekeze River through a network of tributaries, with flow patterns significantly influenced by rainfall intensity and topography. Annual runoff is erratic due to variable rainfall, with the majority occurring during short, intense storms in the rainy season [22]. Reservoirs and small dams constructed as part of watershed management programs have enhanced water storage and availability, mitigating water scarcity in drier periods [3].

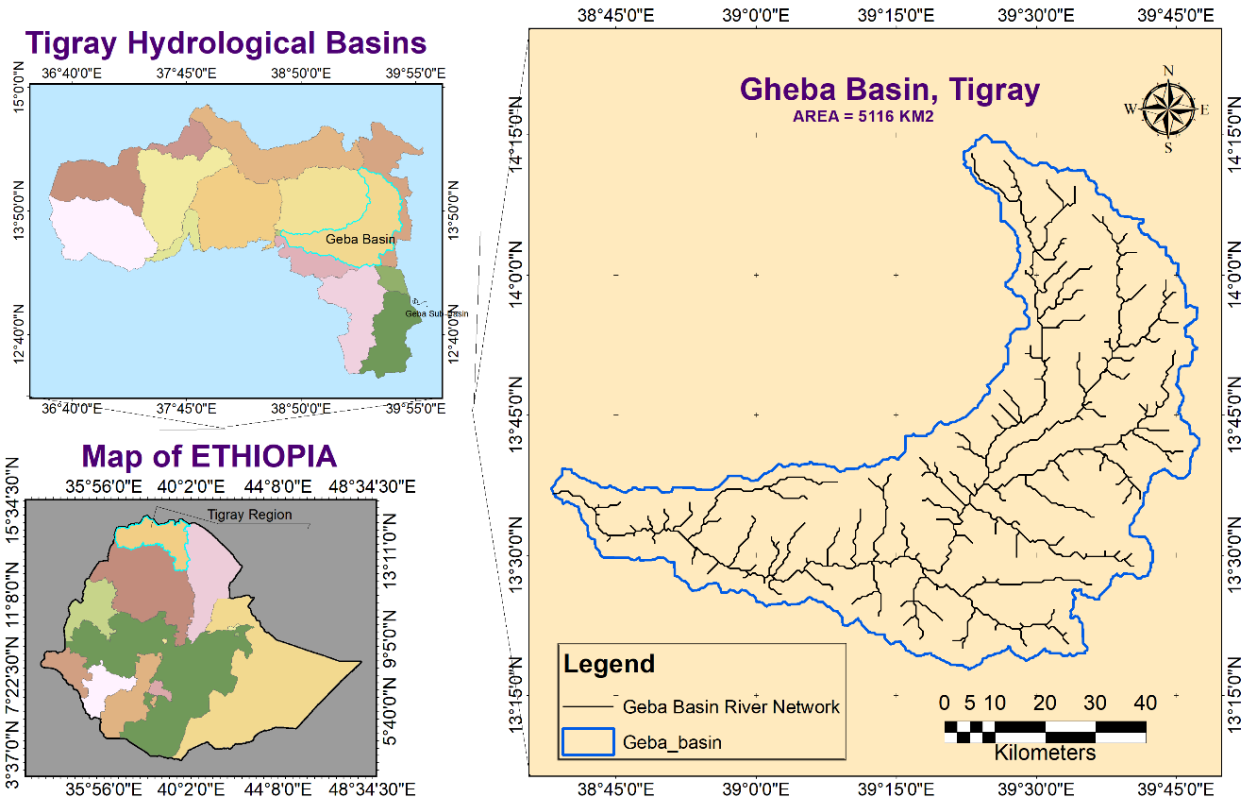

Figure 7.Study Area Map

4. DATA AND METHODS

4.1. DATA

4.1.1. DATA ACQUISITION AND PRELIMINARY QUALITY ASSESSMENT

To conduct this research, an official request letter was sent to the National Meteorological Institute (NMI) in Addis Ababa, Ethiopia. The request sought daily meteorological data—precipitation, minimum temperature, maximum temperature, and average temperature—for five stations in the Tigray region: Mekele (Airport), Adigrat, Alamata, Adi-Gudom, and Edaga Hamus. The goal was to obtain data from 1 January 1960 to 30 December 2023, thus capturing a long-term record for both retrospective hydrological modeling and future climate projections.

The NMI provided the requested datasets in digital format. However, initial quality checks revealed significant gaps and inconsistencies, especially in the rainfall series at certain stations (e.g., missing entire months or years). Such inconsistencies rendered portions of the dataset unsuitable for continuous hydrological modeling without extensive gap-filling.

By analysing both spatial proximity of each station to the Gheba Basin and record consistency, it was determined that only three of the original five stations—Mekele Airport, Adigudom, and Edaga Hamus—had relatively complete daily precipitation series suitable for hydrological modeling. These three stations lie within or near the Gheba Basin boundaries, ensuring more representative climate inputs. Consequently, they were selected for further analysis and model calibration.

4.1.2. METEOROLOGICAL DATA: PRECIPITATION AND TEMPERATURE

After evaluating data completeness, 1999–2002 was identified as the optimal window for continuous hydrological modeling. During this period, the three selected stations exhibited fewer missing values and greater internal consistency, which facilitated Soil Moisture Accounting (SMA) model calibration.

Although the stations recorded data from 1970 onward, 1999–2002 was identified as the optimal window for hydrological modeling. This timeframe demonstrated fewer missing values and greater internal consistency across the three stations, ensuring reliable inputs for the subsequent Soil Moisture Accounting (SMA) model calibration. The daily precipitation data during these years were used in tandem with observed streamflow measurements at the Gheba Basin outlet to calibrate and validate the hydrological model.

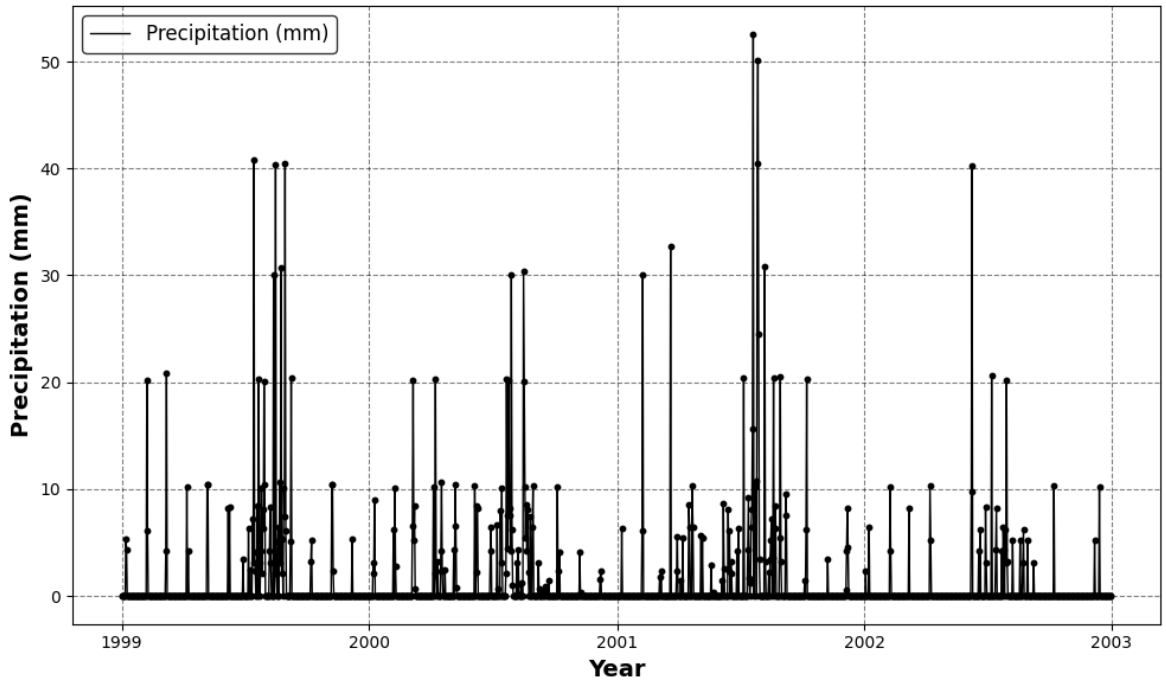

Figure 8.Adigudom Station Daily Precipitation 1999-2002

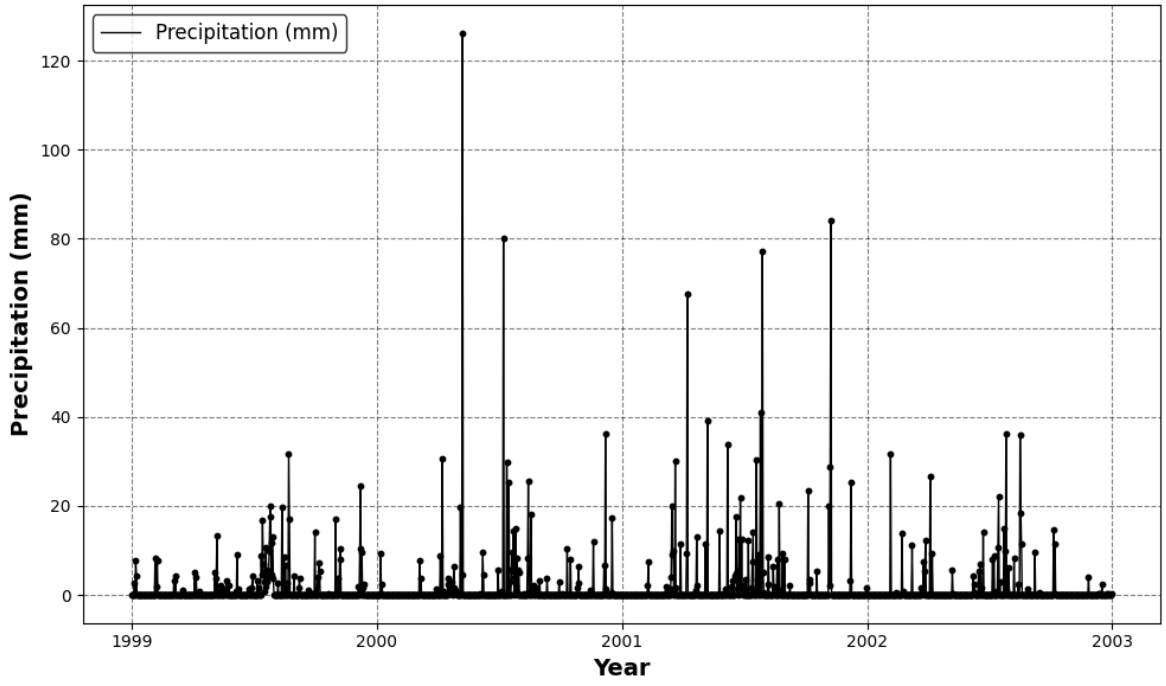

Figure 9.Edaga-Hamus Station Daily Precipitation 1999-2002

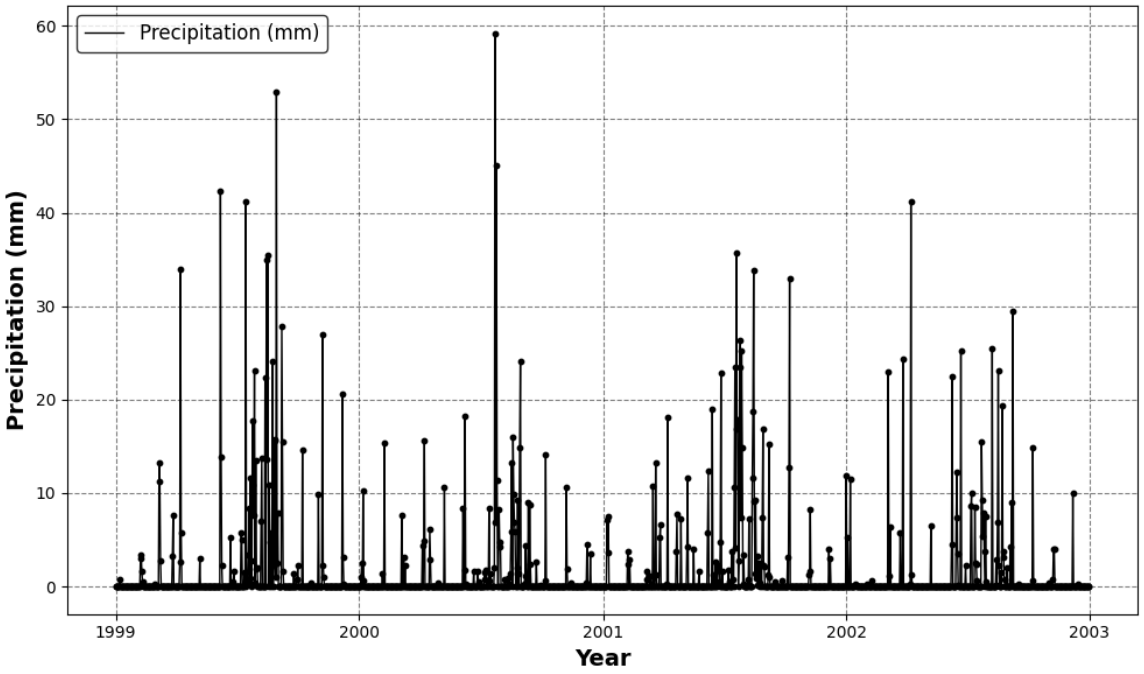

Figure 10.Mekele Airport Station Daily Precipitation 1999-2002

Extended Dataset (Mekele Airport station, 1999–2019): To evaluate the reliability of multiple global precipitation datasets, an extended precipitation series from Mekele Airport (1999–2019) was used as a reference for comparison. This dataset, due to its more continuous and long-term record, served as a benchmark for assessing the accuracy of global datasets such as CHIRPS, ERA5, TERRACLIMATE, and TRMM. By comparing these datasets against the extended Mekele Airport data, the study was able to identify and rule out those datasets that significantly deviated from local observations, ensuring that only the most reliable precipitation inputs were considered for hydrological modeling in the Gheba Basin.

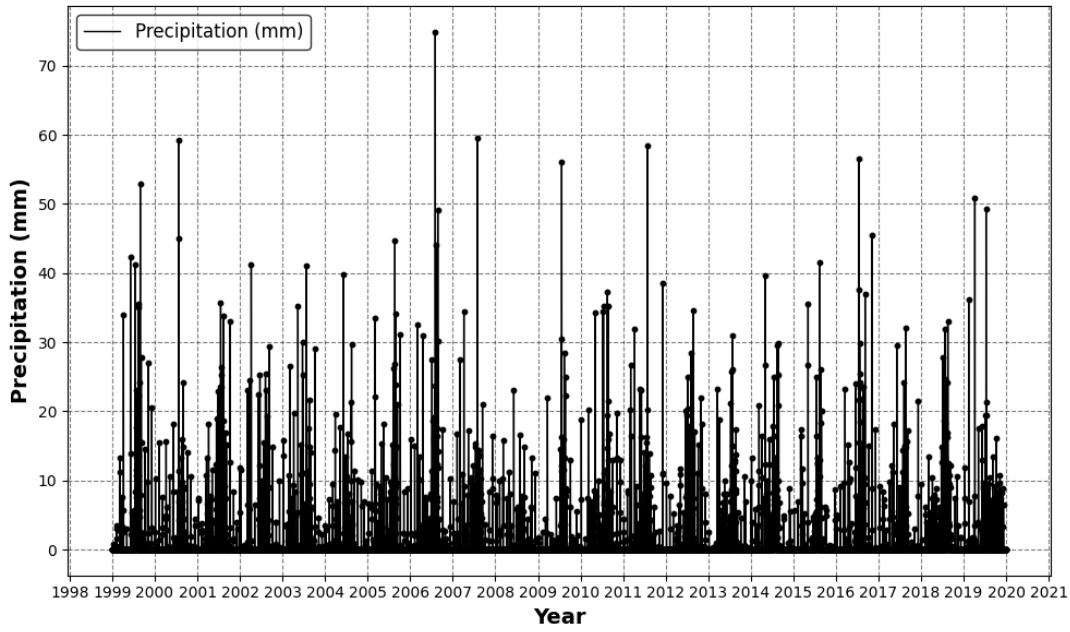

Figure 11. Mekele Airport Station Daily Precipitation 1999-2019

4.1.2.1. COMPARISON OF THE ANNUAL PRECIPITATION FOR THE THREE STATIONS

The annual precipitation data for the three stations (Mekelle Airport *(lat:13.4705, long: 39.5312)*, Adi-Gudom (*lat:13.2466, long: 39.5123*), and Edaga Hamus (*lat:14.1845, long: 39.5620*)) reveal significant temporal variability from 1999 to 2002. Edaga Hamus consistently recorded the highest annual precipitation, with a peak of 862 mm in 2001, indicating its significant contribution to the basin's hydrological processes. Mekelle Airport showed substantial rainfall but was generally lower than Edaga Hamus, except in 1999, when it recorded the highest precipitation at 717.10 mm. Adi-Gudom, on the other hand, consistently received the lowest rainfall, with its minimum observed in 2002 at 253.10 mm.

Temporally, the year 2001 stands out as the wettest year, with all stations experiencing increased precipitation, reflecting a basin-wide anomaly. Conversely, 2002 was relatively dry, particularly for Adi-Gudom, which exhibited a sharp decline in annual rainfall. These results highlight the importance of both spatial and temporal variability in precipitation and their implications for the basin's hydrological response, particularly in streamflow generation and discharge patterns during wet and dry years.

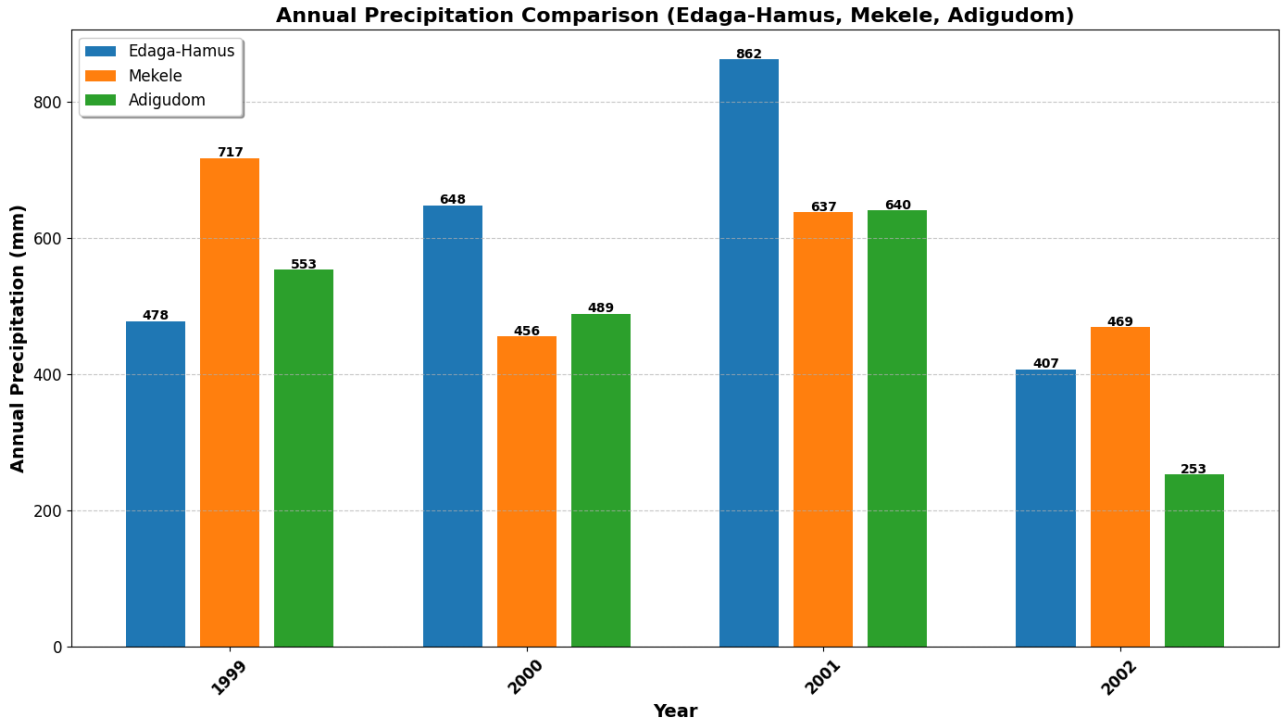

Figure 12.Annual Precipitation Comparison for the three Ground-Stations (mm)

4.1.3. STREAMFLOW DATA (1999–2002)

Initially, streamflow data from the Gheba nr. Mekelle station, representing a smaller subbasin of approximately 2,300 km², were considered. However, this dataset contained significant missing values, particularly during critical months essential for understanding hydrological processes. Due to these limitations, streamflow data from the Gheba nr. Adi-Kumsi station, which represents the larger Gheba subbasin (over 5,125 km²), were selected. This dataset, covering the period 1999 to 2002,

offered greater consistency and completeness, making it more suitable for the study's objectives, including the calibration of the continuous hydrological model.

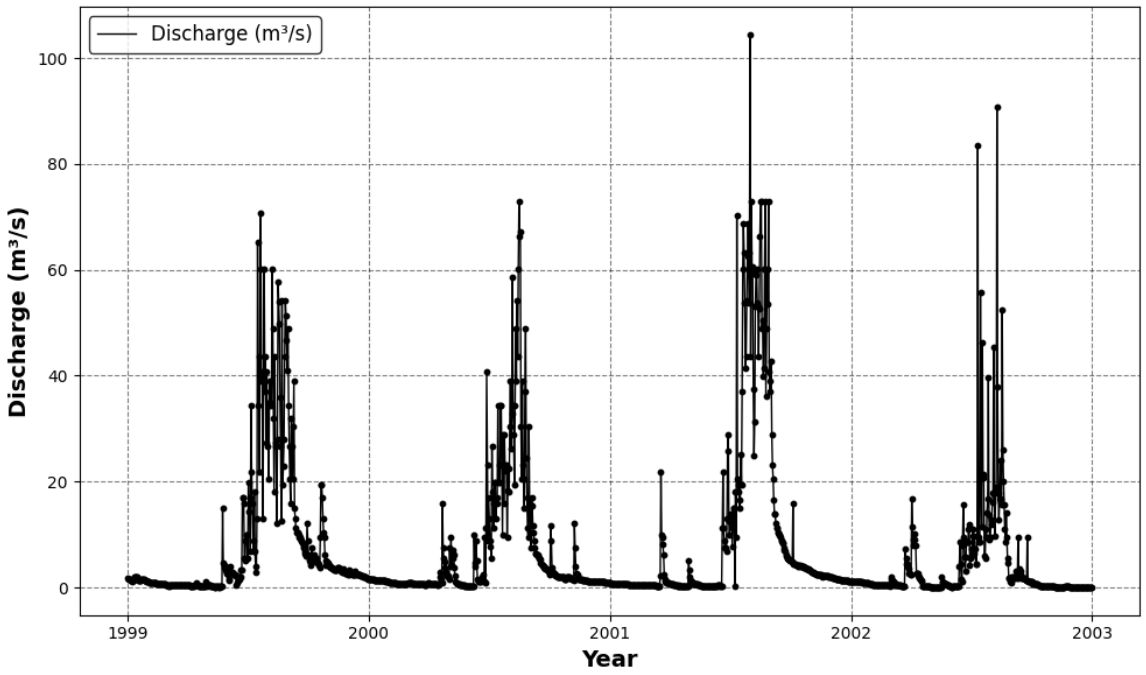

Figure 13.Daily Discharge at Adi-Kumsi Station 1999-2002

4.1.4. DIGITAL ELEVATION MODEL (DEM) DATA FOR GHEBA BASIN

The DEM data for the Gheba Basin was obtained from NASA's SRTM 30m, widely used for hydrological and geomorphological studies. It was reprojected to UTM Zone 37N, clipped to the basin boundary, and processed by filling sinks and smoothing noise to enhance accuracy. The elevation ranges from 965m to 3,228m, with steep slopes in the northern and eastern regions leading to rapid runoff, while lower elevations in the south and west facilitate infiltration. This DEM serves as a basis for hydrological modeling, stream extraction, and flood risk assessment, aiding water resource management.

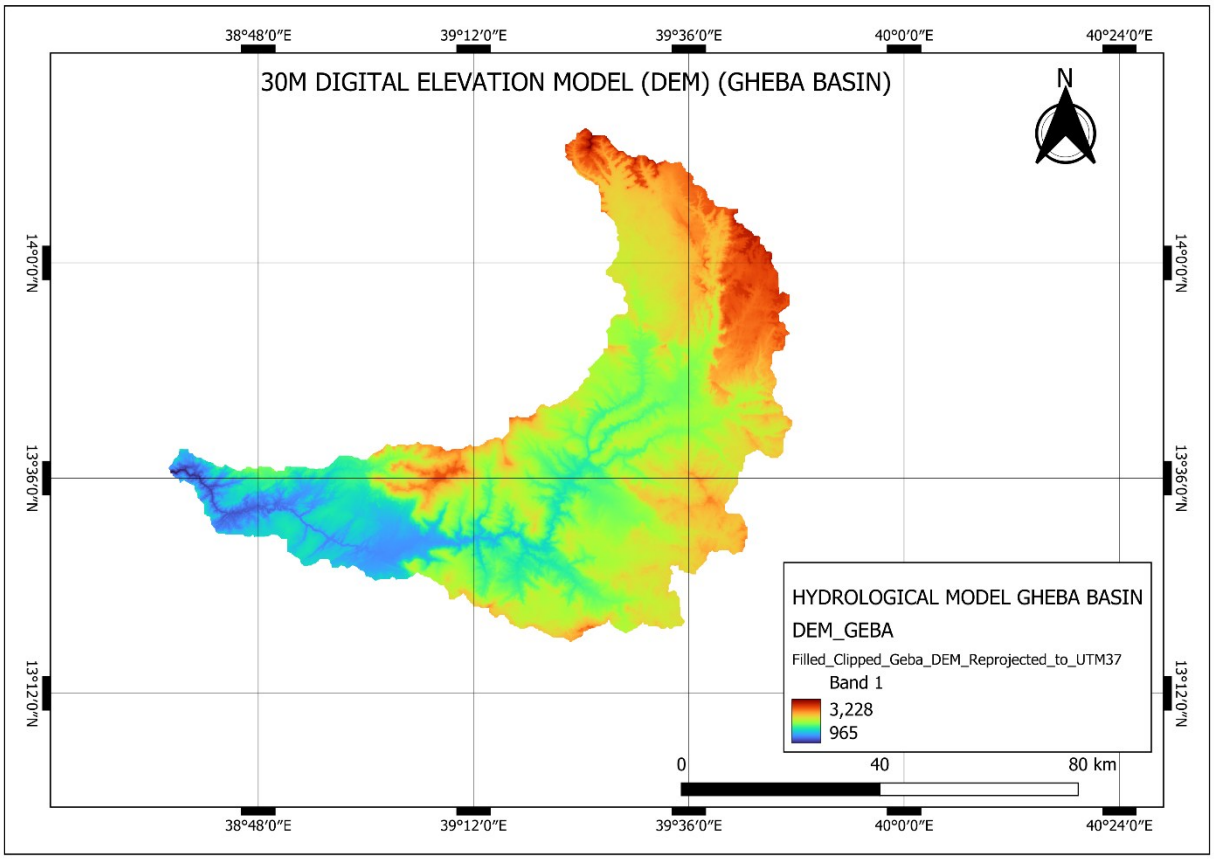

Figure 14. Digital Elevation Model for Gheba basin

4.1.5. POTENTIAL EVAPOTRANSPIRATION (PET) DATA

In this study, Potential Evapotranspiration (PET) data for the Gheba Basin in the Tigray region, Northern Ethiopia was used. PET is a critical hydrological variable for understanding water balance and is often used in hydrological modeling. For this analysis, we obtained monthly PET data spanning from 1999to 2002. The data was processed and visualized to analyse the temporal variations of PET over the period of interest. The dataset was processed using both Google Earth Engine (GEE) and python via Google Colab for visualization.

The Potential Evapotranspiration (PET) data was obtained from the NASA Earth Observing System Data and Information System (EOSDIS), specifically from the TerraClimate dataset. This dataset provides global climate data at a high spatial resolution of approximately 4.6 km and a monthly temporal resolution, spanning from 1958 to the present. The PET values in TerraClimate are derived using a combination of monthly temperature, precipitation, and other atmospheric variables from both satellite observations and climate models, making it a reliable source for climatic analysis.

The TerraClimate dataset, hosted on Google Earth Engine (GEE), was used to extract PET data for the Gheba Basin. The basin shapefile was uploaded to GEE and applied as a spatial filter to isolate data for the specific geographic area of interest. PET data for the study period (1999–2002) was extracted by filtering the dataset for the variable of interest and selecting monthly values corresponding to each year within the specified timeframe.

To process the data, the monthly PET values were averaged for each month of the year (January to December) across all five years of the study period. A scaling factor of 0.1 was applied to the PET

values to adjust for the dataset's specific formatting. Finally, the processed data was exported in two CSV formats: one containing the monthly mean PET values for each year from 1999 to 2002 and another containing the average PET for each month across the entire study period. These CSV files were exported to Google Drive for further analysis and visualization.

The visualization highlighted seasonal variations in PET, with the x-axis representing months (January to December) and the y-axis showing the average PET values in millimetres. This approach provided a clear and concise representation of the seasonal dynamics of PET for the study period.

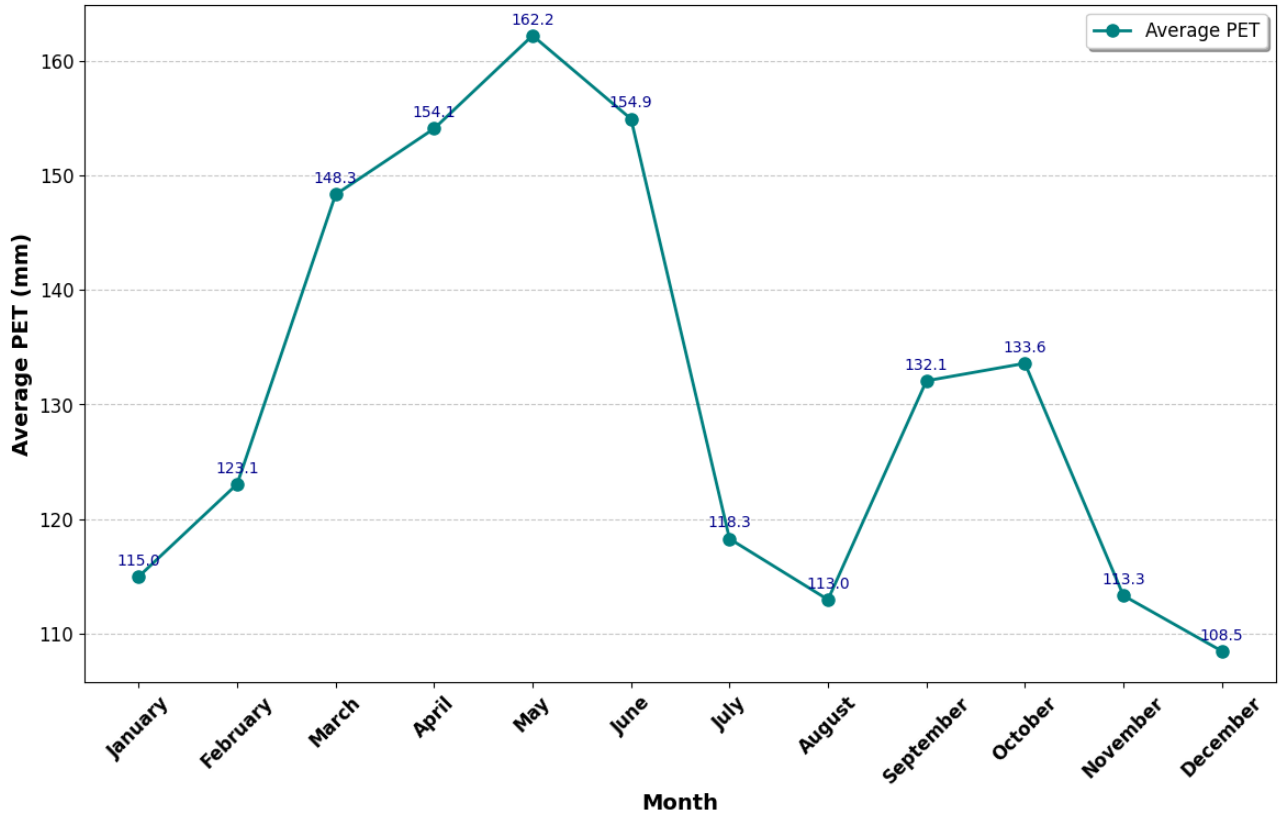

Figure 15.Average Monthly Potential Evapotranspiration over Gheba Basin 1999-2002

4.1.6. GLOBAL PRECIPITATION DATASETS

The Gheba Basin, located in the Tigray region of Ethiopia, exhibits complex hydrological dynamics, making accurate precipitation data crucial for effective water resource management and climate impact assessments. Understanding precipitation variability is essential for assessing water availability, modeling runoff, and developing sustainable hydrological strategies. However, obtaining reliable precipitation measurements in this region remains challenging due to limited ground-based observations and the spatial variability of rainfall patterns.

To address these challenges, this study analyses multiple global precipitation datasets, including ERA5-LAND, Tropical Rainfall Measuring Mission (TRMM), Climate Hazards Group InfraRed Precipitation with Station Data (CHIRPS), and (TERRACLIMATE). These datasets, derived from satellite observations, reanalysis models, and interpolated station data, vary in their spatial resolution, temporal coverage, and underlying methodologies, offering complementary insights into precipitation trends over the Gheba Basin.

The precipitation data were accessed through Google Earth Engine (GEE), an advanced cloud-based geospatial analysis platform that enables efficient data extraction, preprocessing, and large-scale analysis. GEE's JavaScript interface facilitated streamlined spatial averaging of precipitation data across the Gheba Basin, aligning with ground-based station observations to produce both daily and annual precipitation datasets for analysis. By integrating high-resolution satellite, reanalysis, and interpolated datasets, this approach demonstrates the potential of modern remote sensing technologies to enhance hydrological studies in data-scarce and hydrologically complex regions.

The datasets used in this study are publicly available through Google Earth Engine: (**TRMM 3B42**, **ERA5-LAND**, **CHIRPS Daily**, **TerraClimate**)

This study highlights the power of satellite-driven datasets and cloud computing technologies in overcoming data limitations, providing robust insights into precipitation variability, and supporting improved hydrological modeling in regions with sparse in-situ measurements.

4.1.6.1. ERA5-LAND HOURLY PRECIPITATION DATA

The ERA5-Land dataset, developed by the European Centre for Medium-Range Weather Forecasts (ECMWF), offers high-resolution atmospheric and land-surface data at a 9 km spatial resolution, which is significantly more detailed than the ERA5 dataset, which has a resolution of 31 km. This reanalysis dataset provides an enhanced view of land variables over multiple decades, offering hourly data from 1950 up to three months before real-time. ERA5-Land is generated by running the land component of the ECMWF's ERA5 climate reanalysis model, which combines observational data and model outputs into a globally consistent dataset. This dataset enables a comprehensive understanding of the evolution of land conditions over time, making it valuable for applications in hydrology, meteorology, and climate studies.

The data in ERA5-Land is available through the Copernicus Climate Data Store (CDS), and it has been re-gridded to a regular latitude-longitude grid of 0.1x0.1 degrees. Additionally, ECMWF member states with access to the Meteorological Archival and Retrieval System (MARS) can retrieve the data in its native 9 km grid. This dataset offers a reliable and accurate historical climate description, which is vital for studying long-term trends and variations in climate and land-surface conditions [24].

The high spatial and temporal resolution of ERA5-Land, its extended period, and the consistency of the fields produced makes it a valuable dataset to support hydrological studies [25]

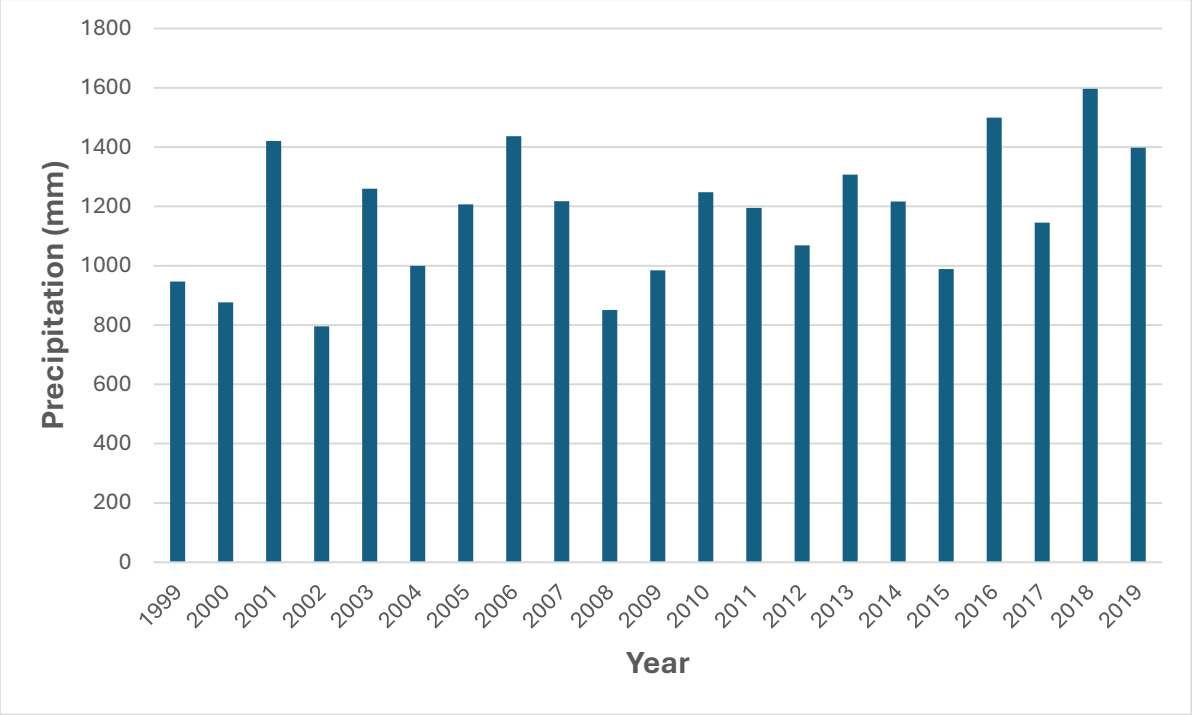

Figure 16. ERA5-LAND Annual precipitation over Gheba basin 1999-2019

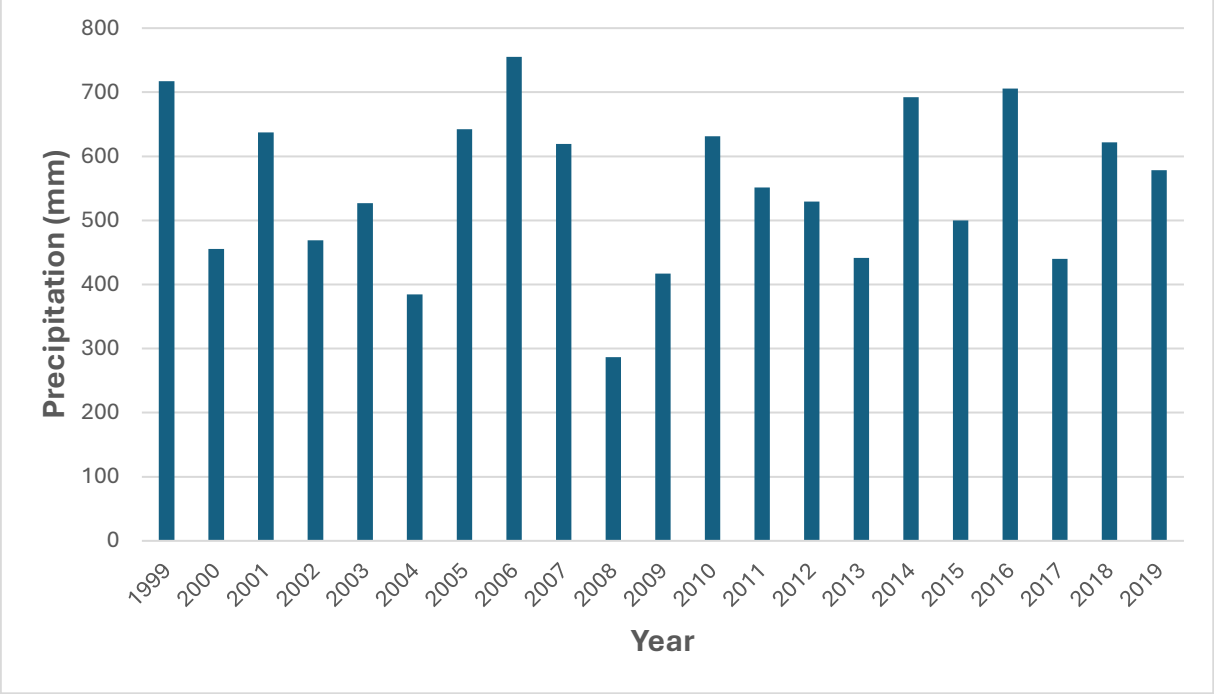

Figure 17. Mekele-Airport station Annual precipitation over Gheba basin 1999-2019

4.1.6.2. TRMM 3B42 3-HOURLY PRECIPITATION DATA

The Tropical Rainfall Measuring Mission (TRMM) is a collaborative effort between NASA and Japan's National Space Development Agency, designed to monitor and analyze tropical and subtropical precipitation along with its associated energy release. To achieve this, TRMM utilizes a combination of active and passive remote sensing instruments, including the Precipitation Radar (PR), TRMM Microwave Imager (TMI), Visible

Infrared Scanner (VIRS), Clouds and Earth's Radiant Energy System (CERES), and the Lightning Imaging Sensor (LSI).

Among these instruments, TMI and PR are the primary tools used for precipitation measurement. The data collected from these sensors are processed through an algorithm that generates the TRMM Combined Instrument (TCI) calibration dataset (TRMM 2B31). This dataset plays a crucial role in the TRMM Multi-satellite Precipitation Analysis (TMPA), which produces precipitation estimates at different temporal scales.

The most widely used TRMM precipitation products for climate studies are:

- TMPA 3B43, which provides monthly precipitation averages
- TMPA 3B42, which offers daily and sub-daily (3-hourly) precipitation estimates

Both datasets are available at a 0.25° spatial resolution (~25 km) and cover latitudes between 50°N and 50°S from 1998 to the present.

For this study, the dataset utilized consists of precipitation estimates with a 3-hour temporal resolution and a 0.25° spatial resolution. These estimates are generated by integrating data from active and passive microwave sensors, further enhanced by infrared observations to improve accuracy. This dataset is well-suited for understanding precipitation dynamics in tropical and subtropical regions.

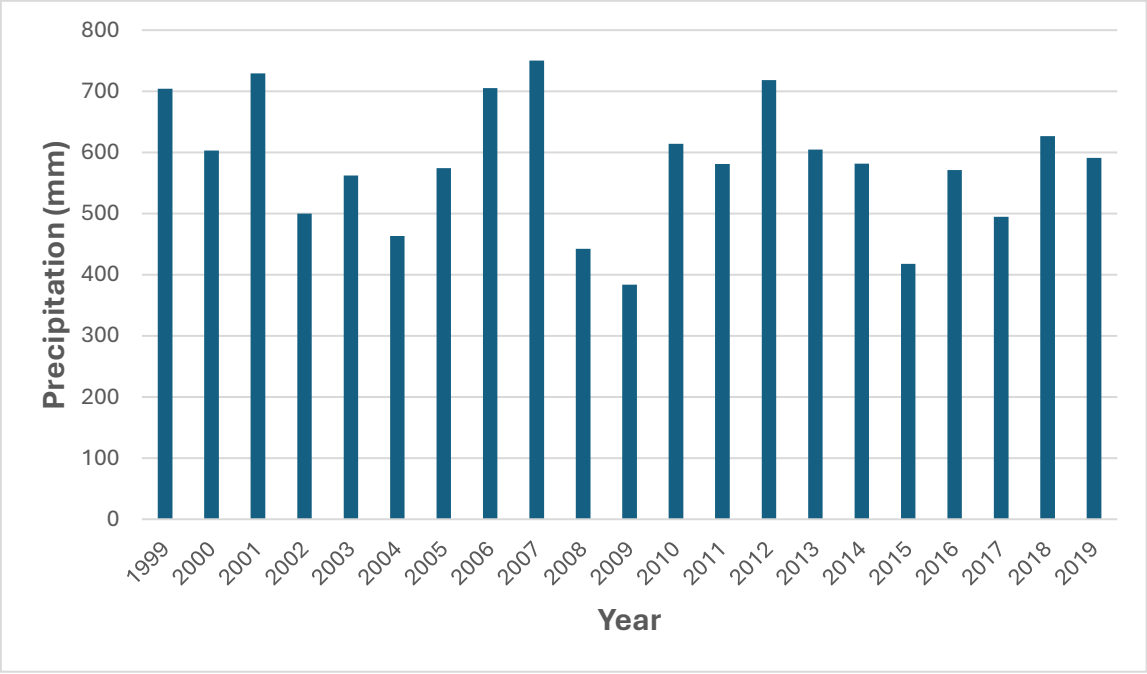

Figure 18. TRMM Annual precipitation over Gheba basin 1999-2019

4.1.6.3. CHIRPS DAILY PRECIPITATION DATA

The Climate Hazards group Infrared Precipitation with Stations (CHIRPS) dataset provides high-resolution precipitation estimates by combining satellite infrared Cold Cloud Duration (CCD) observations with in-situ station data. CHIRPS operates at a spatial resolution of 0.05° (~5 km) and includes daily, pentadal, and monthly precipitation estimates from 1981 to the present. The dataset is particularly designed to represent sparsely gauged locations using advanced interpolation techniques.

While the dataset is often applied in tropical and subtropical regions, its robust blending algorithm and validation results make it highly effective for analysing precipitation trends in semi-arid and arid regions, including the Greater Horn of Africa. In this context, CHIRPS has been shown to support hydrologic forecasting and trend analyses in areas with limited ground observations, making it an invaluable resource for assessing the hydrologic impacts of changing precipitation and rising air temperatures in the region [26].

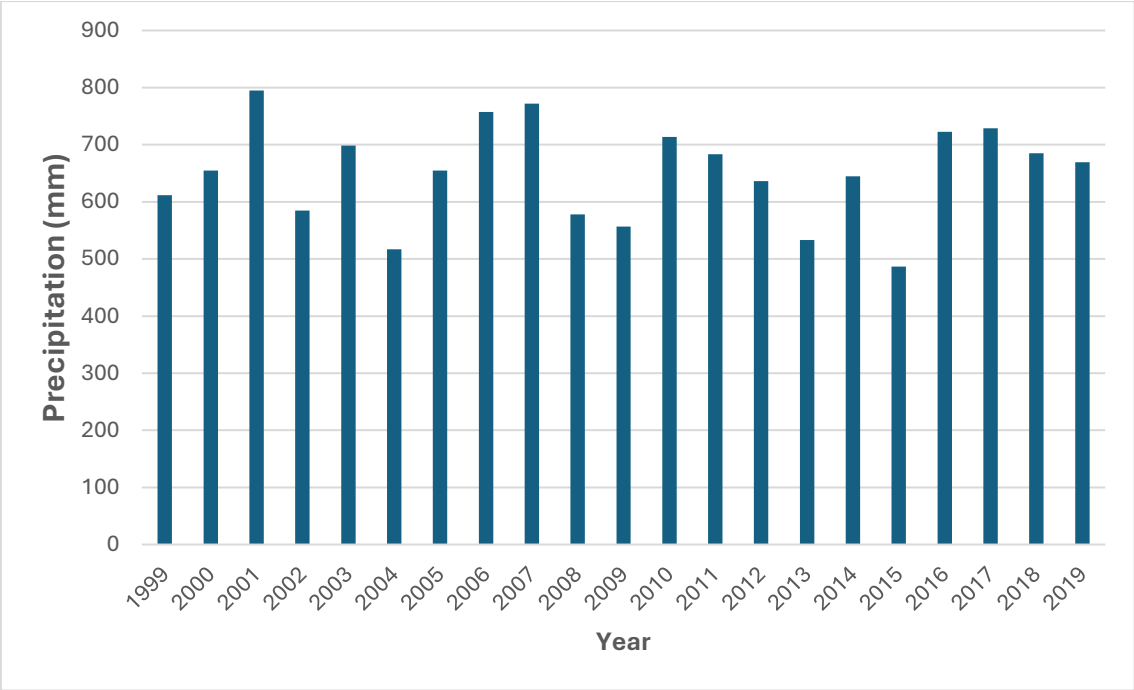

Figure 19. CHIRPS Annual precipitation over Gheba basin 1999-2019

4.1.6.4. TERRACLIMATE MONTHLY PRECIPITATION DATA

TerraClimate, developed by the University of Idaho, is a monthly global dataset that provides climate and climatic water balance data for terrestrial surfaces at a 4 km spatial resolution. It integrates high-resolution climate observations with interpolated data, making it well-suited for long-term climate trend analyses and hydrological modeling. The dataset is generated using a climate-based assisted interpolation approach, which combines high-spatial-resolution climate normals from WorldClim with time-varying data from CRU Ts4.0 and the Japanese 55-year reanalysis (JRA55). This methodology applies interpolated temporal anomalies from CRU Ts4.0/JRA55 to WorldClim's high-resolution climatology, producing a dataset that maintains both fine spatial detail and long-term temporal coverage. This dataset integrates high-resolution climate observations with interpolated data, making it ideal for long-term climate trend analyses and water balance modeling [27].

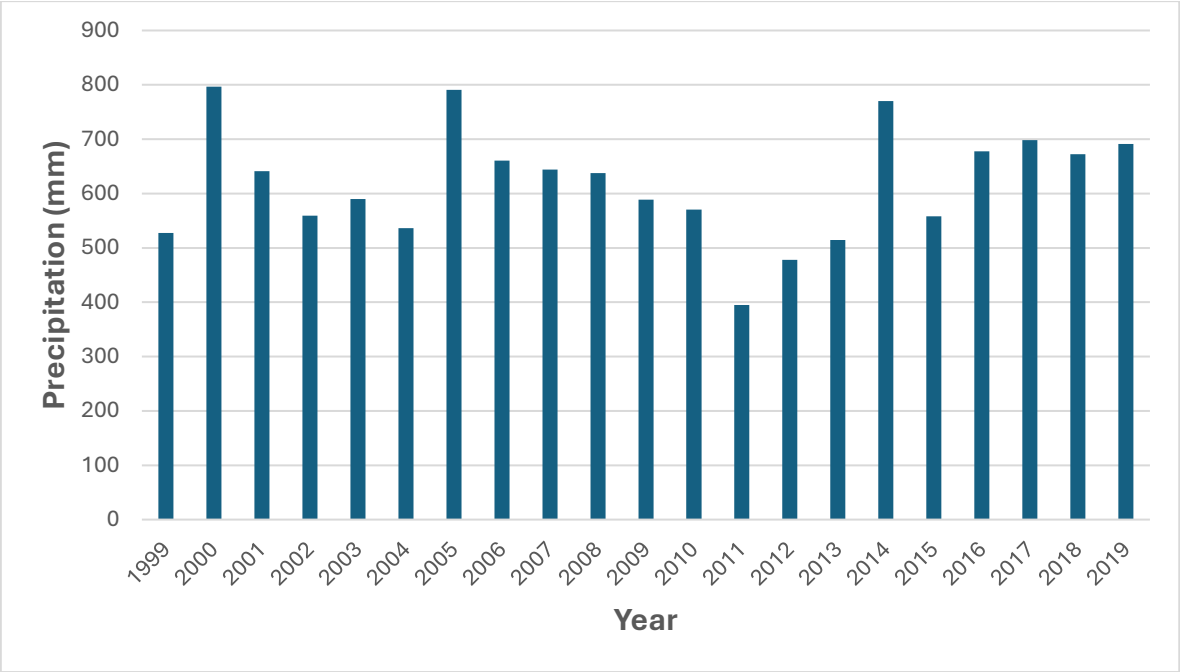

Figure 20. TERRACLIMATE Annual precipitation over Gheba basin 1999-2019

4.2. METHODS

4.2.1. STATISTICAL AND PERFORMANCE EVALUATION METRICS

To assess the accuracy and reliability of global precipitation datasets (CHIRPS, TRMM, ERA5-LAND, and TerraClimate) against ground-based observations from the Mekele Airport, Adigudom, and Edaga-Hamus stations, several statistical evaluation metrics were employed. These metrics provide insight into the datasets' performance in terms of bias, error magnitude, and correlation with observed values. The following statistical measures were used:

4.2.2. MEAN BIAS ERROR (MBE)

The Mean Bias Error (MBE) quantifies the average difference between estimated and observed precipitation values. It helps determine whether a dataset systematically overestimates (positive bias) or underestimates (negative bias) precipitation levels.

$$MBE = (1/N) * \Sigma (P\_model - P\_obs) \quad (18)$$

Where: *P_model is the modelled (satellite-derived) precipitation, P_obs is the observed precipitation, N is the total number of observations.*

A low absolute MBE value indicates better agreement between the dataset and observations, while large positive or negative values indicate systematic over- or underestimation [28]

4.2.3. ROOT MEAN SQUARE ERROR (RMSE)

The Root Mean Square Error (RMSE) measures the magnitude of the overall errors in the dataset without distinguishing between over- and underestimation. It gives higher weight to larger errors, making it particularly useful for detecting extreme deviations.

$$RMSE = sqrt((1/N) * \sum_{i=1}^{n} (P\_model - P\_obs)\text{^}2) \quad (19)$$

RMSE is always positive and has the same unit as precipitation (mm),

Lower RMSE values indicate better dataset accuracy, while higher values suggest greater deviation from observed precipitation [29].

In this study, RMSE is used for two primary purposes. First, it serves as a statistical measure to evaluate the accuracy of precipitation data by comparing observed and modelled values. Second, in the HEC-HMS hydrological model, RMSE is a key performance evaluation metric, applied over the entire simulation period to quantify overall model error. By capturing the magnitude of prediction errors, RMSE provides a reliable indicator of both precipitation accuracy and model performance in representing hydrological dynamics within the basin.

4.2.4. MEAN ABSOLUTE ERROR (MAE)

The Mean Absolute Error (MAE) measures the absolute differences between estimated and observed values. Unlike RMSE, it does not emphasize extreme errors but provides an overall average deviation.

$$MAE = (1/N) * \Sigma |P\_model - P\_obs| \quad (20)$$

MAE is useful for evaluating general performance, as it gives a direct interpretation of average error magnitude without being overly sensitive to large errors [29,30].

4.2.5. PEARSON CORRELATION COEFFICIENT (R)

The Pearson Correlation Coefficient (R) quantifies the strength and direction of the linear relationship between modelled and observed precipitation values.

$$R = [\Sigma (P\_model - P*\_model)(P\_obs - P*\_obs)] / [sqrt(\Sigma (P\_model - P*\_model)\text{^}2) * sqrt(\Sigma (P\_obs - P*\_obs)\text{^}2)] \quad (21)$$

Where: $P*\_model$ *and* $P*\_obs$ *are the mean values of modelled and observed precipitation, respectively.*

A higher value suggests a stronger agreement between observed and modelled precipitation [31].

The statistical metrics outlined in the previous section will be used to evaluate the performance of different global precipitation datasets (CHIRPS, TRMM, ERA5-LAND, TerraClimate) against observed station data in the Gheba Basin.

4.2.6. NASH-SUTCLIFFE EFFICIENCY (NSE)

The Nash-Sutcliffe Efficiency (NSE) is a widely used metric that measures the degree of agreement between simulated and observed discharge values, providing an overall indication of model performance. It is defined as:

$$NSE = 1 - [\Sigma (Q\_obs,i - Q\_sim,i)\text{^}2] / [\Sigma (Q\_obs,i - Q*\_obs)\text{^}2] \quad (22)$$

Where $Qobs,i$ is the observed discharge at time step i, Q_sim,i is the simulated discharge at time step i, Q*obs is the mean observed discharge and Σ sums the total number of observations.

An NSE value of 1.0 indicates a perfect match between the observed and simulated values, while values below zero suggest that the model predictions are less accurate than using the mean of the observed data as a predictor. In this study, the NSE is applied in event-scale evaluation and long term and annual evaluation.

4.3. SPATIAL ANALYSIS OF PRECIPITATION DISTRIBUTION

To analyze the spatial variability of precipitation across the Gheba Basin, annual precipitation maps were generated using CHIRPS and TRMM datasets for the period 1999–2002. The precipitation data was obtained in TIFF format from Google Earth Engine (GEE) and processed using QGIS.

The spatial distribution of precipitation was analysed at a high-resolution scale, ensuring that regional differences in rainfall patterns could be visualized. The downloaded raster datasets were projected into the Universal Transverse Mercator (UTM) coordinate system to maintain consistency with hydrological modeling inputs.

To assess the accuracy of the precipitation datasets, the locations of three ground-based rain gauges (Mekele Airport, Adigudom, and Edaga-Hamus) were overlaid onto the precipitation maps. This integration allowed for a visual and spatial comparison between observed and satellite-derived precipitation estimates, helping identify discrepancies across different parts of the basin

4.4. STOCHASTIC MODEL AND SCENARIOS

For this study, a stochastic weather generator was used to simulate precipitation patterns in the GHEBA basin**.** The model is based on the Bartlett-Lewis Stochastic Model (described in 2.2), which represents rainfall as a series of clustered storm events occurring according to a Poisson process. This model was selected due to its ability to capture the intermittent and highly variable nature of precipitation in semi-arid regions.

The primary parameters considered in this study include:

- Mean 24-hours precipitation
- Variance of 24-hours and 48-hours precipitation
- Correlation of 24-hours precipitation
- Dry fraction (24-hours and 48-hours periods)

The GHEBA basin's historical precipitation data was utilized for calibrating the stochastic weather generator and ensuring its reliability in representing observed climatic conditions. Precipitation records from three meteorological stations, spanning the period 1999–2002, served as the primary dataset. To enhance spatial representation, an interpolated precipitation dataset derived from the HEC-HMS model calibration was integrated into the analysis.

Initially, the stochastic generator was calibrated using the observed daily precipitation data from the 1999–2002 period. Upon successful calibration, a 100-year hourly precipitation dataset was generated to serve as the baseline climate scenario. The statistical properties of the original observational dataset were then systematically compared against those of the generated baseline dataset to assess the model's accuracy.

Once the baseline simulation demonstrated statistical agreement with observed precipitation characteristics, various climate change scenarios were applied. The hydrological responses under different climate conditions were evaluated by analysing changes in precipitation partitioning and hydrological components. This approach provided insights into the basin's hydrological behaviour under shifting climatic conditions, allowing for a comprehensive assessment of potential future impacts.

The generated precipitation dataset consists of a 100-year hourly precipitation series, allowing for detailed hydrological modeling and extreme event analysis. To assess potential changes in precipitation patterns and their impact on the partitioning of precipitation and the overall water balance over the Gheba Basin, four distinct climate scenarios were generated using a stochastic weather generator:

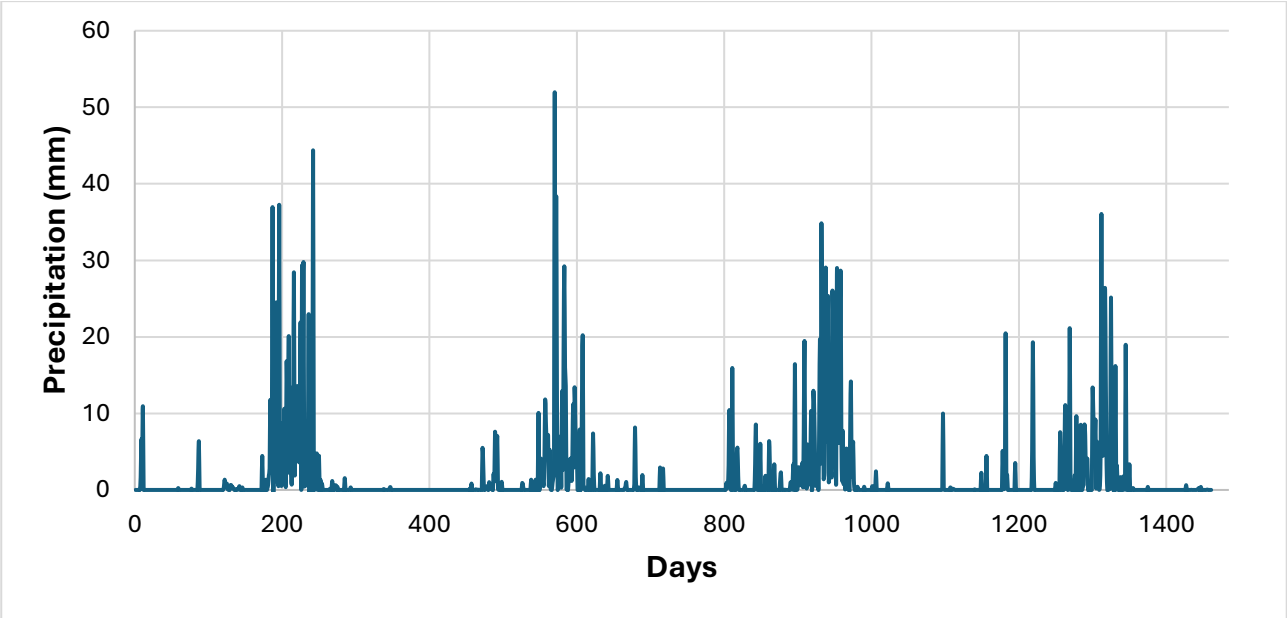

Figure 21. Observed Daily Precipitation over Gheba basin (1999–2002)

4.4.1. BASELINE (CURRENT-CLIMATE) SCENARIO:

The daily precipitation dataset (1999–2002) from HEC-HMS interpolations (based on three stations in the Gheba Basin) was used to calibrate the stochastic precipitation generator (HYDRO-GEN). The process began by running the generator's Calibration of Precipitation Model function, selecting the option for calibration using daily data, and inputting the properly formatted historical precipitation data. This step produced the observed precipitation statistics, including mean, variance, correlation, and dry fraction values (see appendix A1).

After obtaining the observation-based statistics, the next step involved generating a 100-year precipitation dataset, which serves as the baseline scenario. The statistical properties of this simulated 100-year baseline dataset were then compared against the historical observation statistics to assess the model's ability to reproduce real-world precipitation patterns. This comparison process constitutes the model calibration, ensuring that the generator accurately represents the baseline climate conditions.

Once the model was validated through this statistical agreement, it was then used to generate different climate change scenarios, applying predefined precipitation modifications to assess potential future climate impacts.

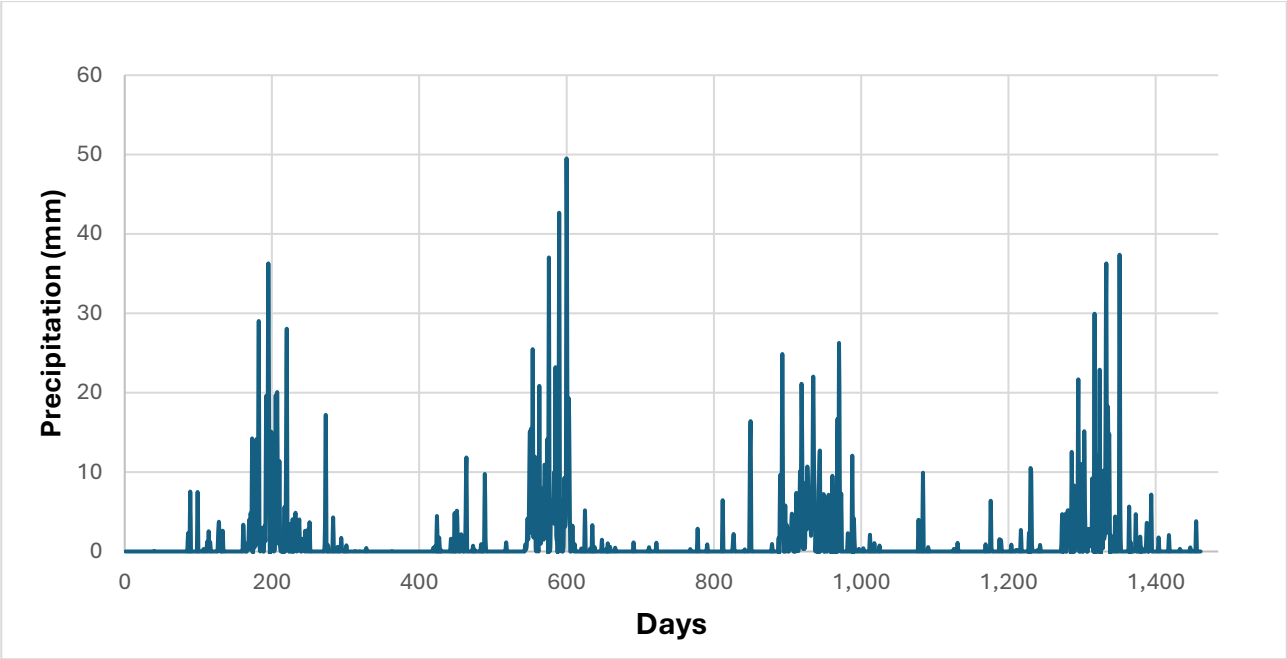

Figure 22. Stochastically Generated Daily Precipitation (First 4 Years)

4.4.2. SCENARIO-1: MODERATE INCREASE SCENARIO

This scenario is derived from climate projections specific to Northern Ethiopia, particularly the Tigray region which includes Gheba Basin, as presented in recent climate studies. The projections were generated using five Global Climate Models (GCMs) from CMIP5, downscaled using the delta downscaling method, and analysed under two Representative Concentration Pathways (RCP4.5 and RCP8.5) [1]. The study found that under RCP8.5, annual precipitation in the region is projected to increase by up to 10%, with the Kiremt (main rainy season: June–September) experiencing a more pronounced increase of up to 17% [1].These projections align with broader climate model findings that suggest a wetter future climate in Ethiopia, particularly during the peak rainy season.

Applied Adjustments:

To implement these projections in the stochastic weather generation process:

- The 24-hour mean precipitation was increased by 10% for all months except the wet season.
- During the wet season (June–September), the mean precipitation was increased by 17%, reflecting the projected peak seasonal increase.
- Variance and dry fraction values were not altered, as this scenario focuses on a moderate and steady increase in precipitation rather than intensification of extreme rainfall events.

Table 1.Precipitation adjustments for Scenario-1 (Moderate Increase Scenario) based on CMIP5 projections.

Month Category	Baseline Mean 24hr (μ)	Baseline Variance 24hr (σ^2)	Scenario-1 Mean 24hr	Scenario-1 Variance 24hr
Non-Wet Season	μ_n	σ^2_n	$\mu_n \times (1 + 0.10)$	σ^2_n (unchanged)
Wet Season (Jun–Sep)	μw	$\sigma^2 w$	$\mu w \times (1 + 0.17)$	$\sigma^2 w$ (unchanged)

These adjustments ensure that the scenario remains consistent with CMIP5 climate projections while maintaining natural precipitation variability. Thus, this scenario is designed to simulate a plausible

near-future climate for the region based on scientific projections, providing a foundation for hydrological and agricultural impact assessments.

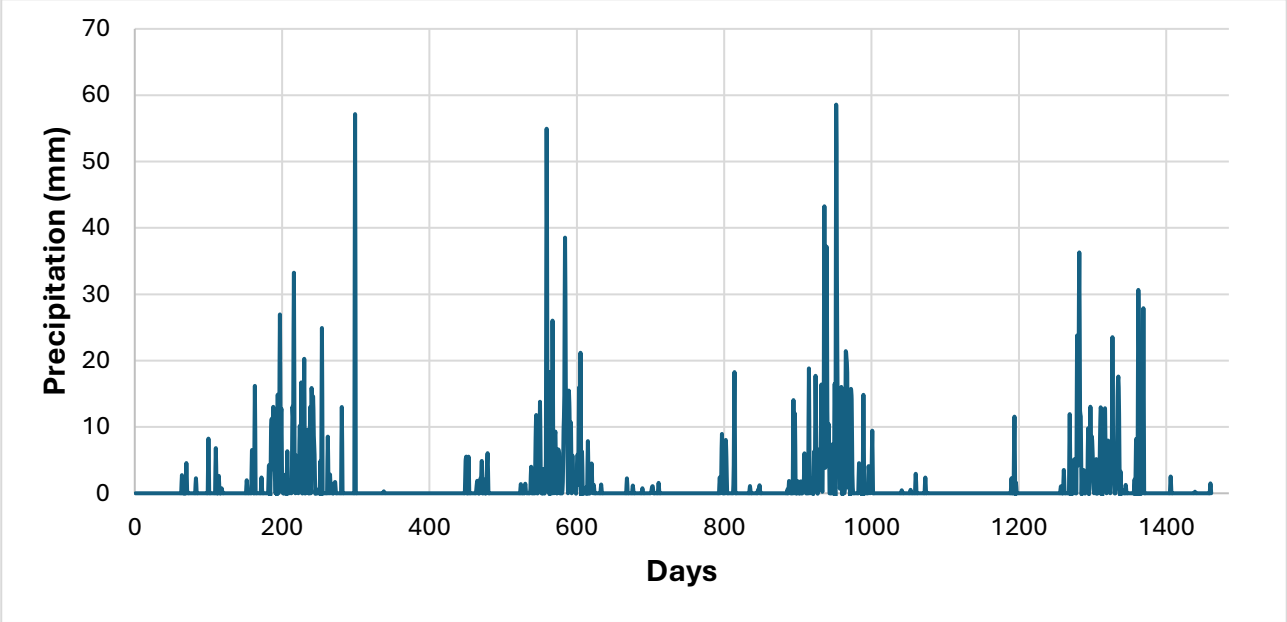

Figure 23. Scenario 1: Climate-Adjusted Stochastic daily Precipitation (First 4 Years)

4.4.3. SCENARIO-2: INTENSIFIED RAINFALL SCENARIO

This scenario is designed to simulate a future climate characterized by more extreme precipitation events. To achieve this, modifications were applied consistently across all months, ensuring a uniform shift toward wetter conditions with higher variability in rainfall patterns.

Specifically, the 24-hour mean precipitation was increased by 30% for all months, reflecting a general rise in precipitation levels throughout the year. Additionally, the 24-hour variance was increased by 50% across all months, amplifying the intensity and unpredictability of extreme rainfall events. This adjustment means that not only does the total precipitation increase, but rainfall events become more erratic, with a greater likelihood of short but intense downpours. These changes were applied uniformly rather than seasonally differentiated, based on the assumption that climate change could lead to a systematic intensification of precipitation patterns, rather than only affecting specific seasons. This assumption aligns with studies suggesting that a warming atmosphere holds more moisture, increasing the potential for extreme rainfall events regardless of seasonal timing.

It is important to note that this scenario-2 represents a hypothetical experiment rather than a precise prediction. The goal is to explore the potential hydrological impacts of a more extreme precipitation regime, helping to assess vulnerabilities related to flash floods, surface runoff, and infrastructure resilience under intensified rainfall conditions.

By maintaining consistency in adjustments across all months, this scenario provides a clear and reproducible framework for analysing these potential climate-driven changes.

Table 2.Precipitation adjustments for Scenario-2 (Intensified Rainfall Scenario).

Month Category	Baseline Mean 24hr (μ)	Baseline Variance 24hr (σ^2)	Scenario-2 Mean 24hr	Scenario-2 Variance 24hr
All Seasons	μ_n	$\sigma^2{}_n$	$\mu_n \times (1 + 0.30)$	$\sigma^2{}_n \times (1 + 0.50)$

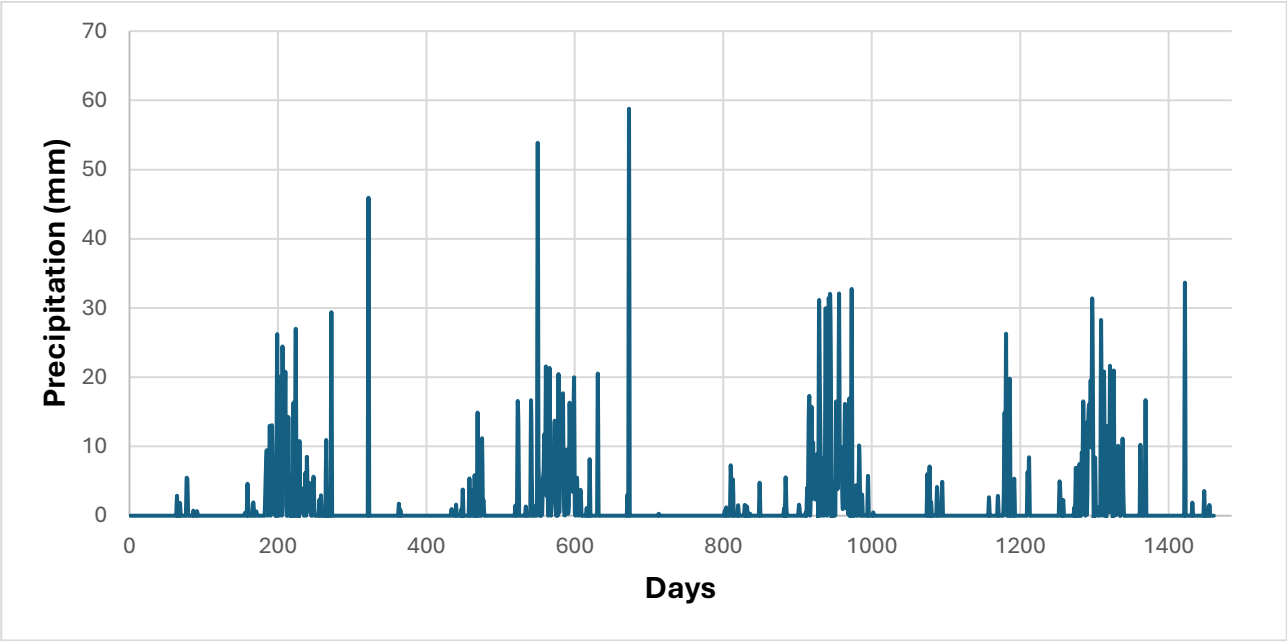

Figure 24. Climate-Adjusted Stochastic daily Precipitation (First 4 Years)

4.4.4. SCENARIO-3: PROLONGED DRY SCENARIO

This scenario was designed to simulate a future with more dominant drought conditions. To achieve this, the mean 24-hour precipitation was uniformly reduced by 30% across all months, ensuring a general decline in precipitation levels throughout the year. Additionally, modifications were made to the dry fraction to reflect seasonal variations in drought intensity. Specifically, during the wet season (June–September), the dry fraction was increased by 20%, leading to fewer rainy days and longer consecutive dry periods in these critical months. In contrast, for the remaining months (October–May), the dry fraction was left unchanged to preserve the baseline seasonality. These targeted adjustments create a scenario where overall precipitation declines while the wet season experiences more pronounced dry periods. This approach ensures a realistic representation of prolonged drought conditions, extended dry spells, and reduced wet season recovery periods. The detailed methodology allows for full reproducibility of the scenario.

Table 3.Precipitation adjustments for Scenario-3 (Prolonged Dry Scenario)

Month Category	Baseline Mean 24hr (μ)	Baseline Variance 24hr (σ^2)	Baseline Dry Fraction 24hr (Pdry)	Scenario-3 Mean 24hr	Scenario-3 Dry Fraction 24hr
Non-Wet Season	μ_n	$\sigma^2{}_n$	$Pdry_n$	$\mu_n \times (1 - 0.30)$	$Pdry_n$ (unchanged)
Wet Season (Jun–Sep)	μw	$\sigma^2 w$	$Pdry w$	$\mu w \times (1 - 0.30)$	$Pdry w + 0.20$

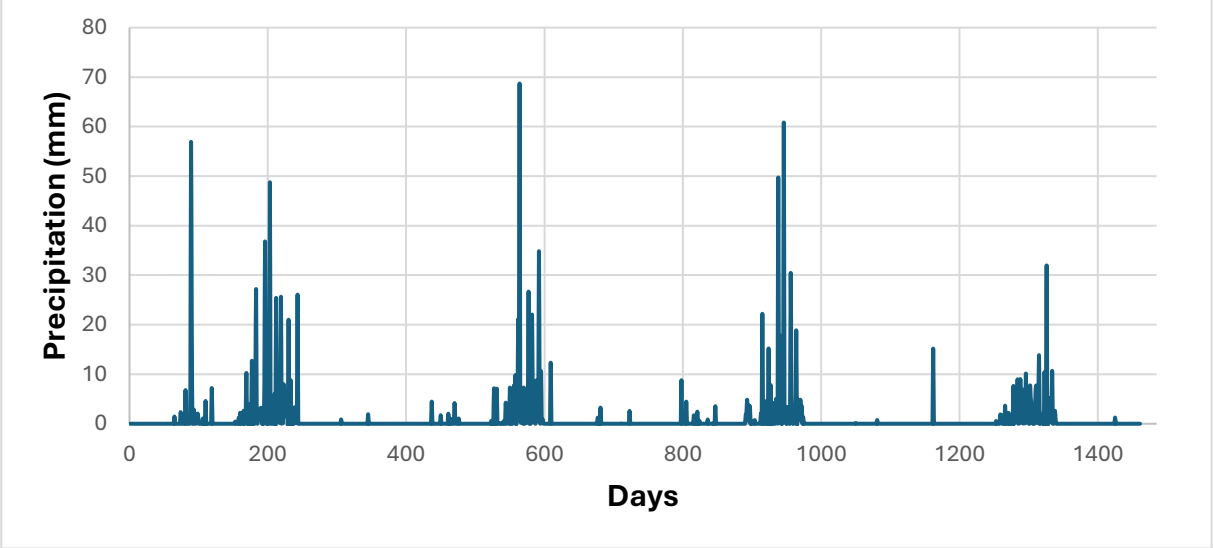

Figure 25. Climate-Adjusted Stochastic daily Precipitation (First 4 Years)

The impact of these modifications will be analysed in the results section, where we will evaluate how precipitation partitioning and water balance components respond to these climate shifts over the Gheba Basin. The differences between scenarios will help identify potential risks and adaptation strategies under future climate conditions.

The plots illustrate the daily precipitation over a 4-year period for different scenarios. The first plot represents observed precipitation from 1999 to 2002, serving as the reference dataset. The Baseline Scenario was generated using a stochastic weather generator calibrated on this historical data. Since the stochastic model produces 100 years of hourly precipitation, only the first 4 years were extracted for direct comparison with the observed dataset. Similarly, for Scenarios 1–3, the first 4 years of stochastically generated data under different climate change conditions were extracted to analyze potential variations in precipitation patterns.

This does not imply that the analysis is limited to only 4 years; rather, this period is chosen to provide an initial comparative view against the observed dataset. The long-term dataset (100 years) remains available for further analysis to assess trends over extended periods. While a 4-year segment alone is not sufficient to fully capture the magnitude of long-term precipitation trends, it is still valuable for observing patterns, identifying shifts in rainfall distribution, and evaluating how precipitation characteristics evolve under different climate scenarios. This approach helps validate the model's ability to replicate observed conditions before extending the analysis to longer time scales. Please see the result section for details of the precipitation patterns in different scenarios.

Since the stochastically generated dataset represents a hypothetical 100-year period, we could not assign specific years to the generated data. Instead, the x-axis is labelled in days, maintaining a consistent time representation across all scenarios. This allows for direct pattern comparison without implying specific calendar years.

4.5. MODEL SETUP IN HEC-HMS

4.5.1. HEC-HMS MODEL CONFIGURATION

Model simulation involves utilizing a calibrated hydrological model to predict the system's response under specific conditions, such as precipitation, temperature, or land-use changes. The objective of this setup was to configure the model using available topographical, meteorological, and hydrological datasets, followed by calibration and validation against observed streamflow data.

The setup of the HEC-HMS model for the Gheba Basin followed a systematic approach to ensure accurate representation of the basin's hydrological processes. Initially, basin delineation was performed using a Digital Elevation Model (DEM) to define watershed boundaries and stream networks. Sub-basin and river reach segmentation were then established to enhance model accuracy. However, initial simulations showed discrepancies between observed and simulated discharge.

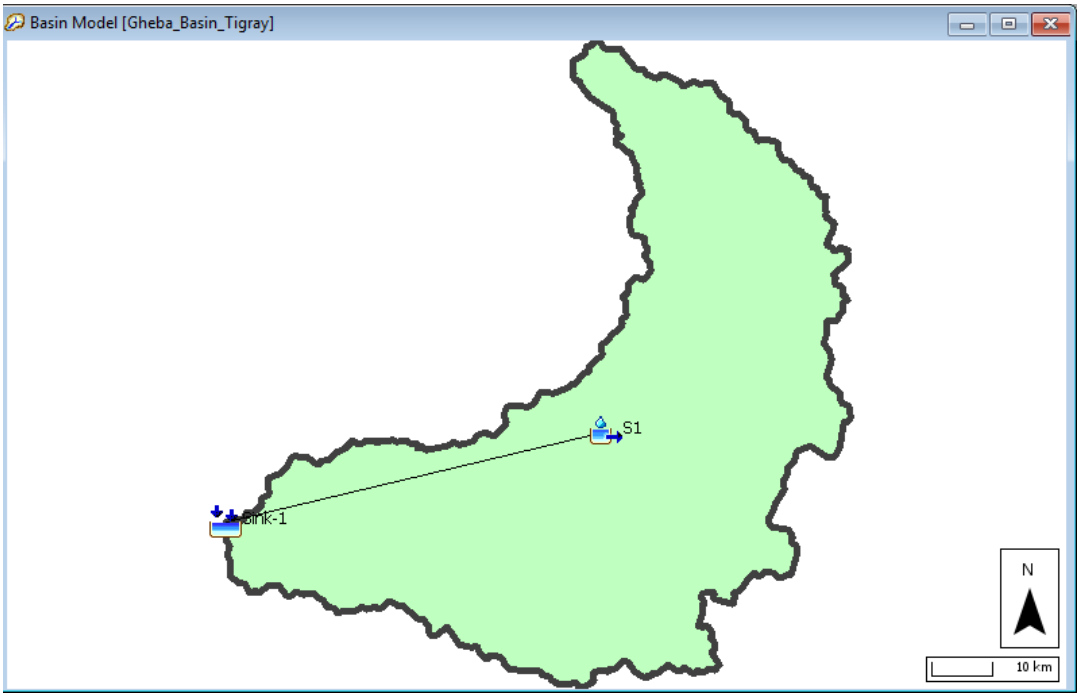

Figure 26. Gheba basin watershed established on HEC-HMS model

Basin Characteristics

Table 4. Gheba Basin Characteristics

Area KM2	Longest Flow path Length (KM)	Longest Flow path Slope (M/M)	Centroidal Flow path Length (KM)	Flow path Length (KM)	Flow path Slope (M/M)	Basin Slope (M/M)	Basin Relief (M)	Relief Ratio
4720	207.2981	0.00984	112.58468	155.4736	0.00624	0.18771	2039	0.00984

The model configuration incorporated various components tailored to the basin's characteristics. The Soil Moisture Accounting (SMA) method was applied to estimate infiltration and storage, while runoff transformation was conducted using the Clark Unit Hydrograph.

Baseflow contributions were simulated through the Linear Reservoir method. Once the model was structured, simulation periods were defined to align with available streamflow data for calibration and validation. The simulation results were analysed to assess peak flows, runoff volumes, and overall hydrological response, allowing for iterative adjustments to improve model performance.

Using HEC-HMS, the Basin was delineated based on the DEM, allowing for the extraction of key hydrological parameters such as basin area (4719.9 km^2), longest flow path (207.3 km), centroidal flow path length (112.6 km), flow path slope (0.00624 m/m), basin relief (2039 m), and relief ratio (0.00984). These parameters provided a foundation for defining the hydrological behaviour of the basin. Sub-basins and river reaches were initially defined within HEC-HMS to establish appropriate hydrological connectivity between different units. However, due to low model performance, the basin was treated as a single sub-basin, which significantly improved the match between observed and simulated discharge. Hydrological parameters were adjusted iteratively based on calibration results to optimize runoff representation and minimize errors.

Loss Method: The Soil Moisture Accounting (SMA) method (described in section 2.3.2) is used to distribute precipitation among different hydrological components, such as infiltration, surface runoff, evapotranspiration, and groundwater recharge. As a continuous loss model, it monitors soil moisture fluctuations over time, making it effective for simulating annual variations and accounting for prior moisture conditions. This approach is designed to capture both short-term and long-term hydrological processes.

Key parameters of the SMA method include: Maximum Soil Storage Capacity (mm): Defines the soil's total water retention capability, Initial Soil Moisture Content (% of storage): Represents the soil's moisture level at the start of the simulation, Impervious Area (%): Indicates the portion of the sub-basin covered by impervious surfaces, which directly contributes to surface runoff, Maximum Percolation Rate (mm/hr): Specifies the rate at which water moves from the soil into the groundwater system.

Transform Method: Clark Unit Hydrograph Method is used in this study; the Clark Unit Hydrograph method is used to transform excess precipitation into direct runoff at the outlet of sub-basin. This method combines Time of Concentration (Tc) and Storage Coefficient (R)

The model simulation incorporated Digital Elevation Model (DEM), daily precipitation, daily discharge and monthly potential evapotranspiration data as a main input. The SMA algorithm processed these inputs by calculating infiltration, evapotranspiration, surface runoff, and groundwater flow. The simulated flow was then compared to observed data at the Gheba Nr. Adi Kumsi station for the year 1999-2002 to calibrate and validate the model's accuracy.

Simulated hydrographs provided detailed information on the timing, magnitude, and distribution of runoff within the watershed. The outputs highlighted seasonal variability, with higher flows during the rainy season and reduced baseflows during dry periods. The integration of surface and subsurface hydrological processes allowed the model to capture the interplay between precipitation and streamflow effectively.

Overall, the simulation results will confirm the model's capability to represent the hydrological processes of the Gheba watershed. This simulation serves as a foundation for further analyses, including scenario testing under different climate and land-use conditions.

4.5.2. MODEL CALIBRATION

Model calibration is the process of adjusting model parameters within acceptable ranges to align simulated results with observed data. This step is crucial to ensure that the hydrological model accurately represents the physical processes of the watershed and can reliably predict future scenarios. Calibration provides confidence in the model's ability to replicate real-world conditions, enhancing its utility for water resource planning and management.

For this study, the calibration process focused on matching simulated streamflow to observed discharge data recorded at the Gheba Nr. Adi Kumsi station during the year 1999-2000. The observed stream discharge data served as a reference for iterative parameter adjustments, ensuring that the model output closely mirrored the measured flows. The selection of 1999-2000 as the calibration period was based on the availability of reliable daily precipitation and streamflow data, which are essential for parameter fine-tuning.

The calibration involved comparing observed and simulated hydrographs, paying special attention to baseflow dynamics and peak flow patterns. Summary statistics, including Nash-Sutcliffe efficiency (NSE) and percent bias (PBIAS), were used to evaluate the performance of the calibrated model. While challenges such as overestimating peak flows were encountered, iterative adjustments to parameters, such as soil storage and groundwater routing coefficients, improved the fit between simulated and observed flows.

The manual calibration process highlighted the importance of observed data quality and its role in constraining parameter values. By using stream discharge observations from the Gheba Nr. Adi Kumsi station, the calibrated model offers a reasonable representation of the watershed's hydrological response for the basin for the year 1999-2000, providing a solid foundation for further analyses.

4.5.3. MODEL VALIDATION

The validation of the HEC-HMS model was conducted using the same model setup, but with a different simulation period to assess its performance in an independent dataset. Following the calibration phase (1999–2000), the model was validated against observed streamflow data from 2001–2002 at the Gheba Nr. Adi Kumsi station. This approach ensures that the model's ability to simulate hydrological processes is tested on an unseen dataset, providing confidence in its predictive performance.

The CHIRPS and TRMM datasets were retained for further water balance analysis, allowing for an independent assessment of these satellite-derived precipitation products in estimating the overall hydrological response of the basin. By decoupling the precipitation dataset evaluation from model validation, we maintain the integrity of the calibration-validation framework while still exploring the applicability of CHIRPS and TRMM for broader hydrological assessments in the Gheba Basin.

4.5.4. PRECIPITATION PARTITIONING IN HEC-HMS

Precipitation partitioning is a crucial step in hydrological modeling that helps determine how precipitation is distributed into different hydrological components within a watershed. In the HEC-HMS model, precipitation undergoes partitioning into surface runoff, infiltration, evapotranspiration, and groundwater recharge. This process is essential to accurately simulate the hydrological response of the Gheba Basin.

In this study, precipitation partitioning was analysed by assessing the outputs of the HEC-HMS model during simulation. The primary components of precipitation partitioning considered include:

- Direct Runoff: The portion of rainfall that immediately contributes to surface flow, influenced by land cover, slope, and soil saturation.
- Infiltration: The amount of rainfall absorbed into the soil, which later contributes to baseflow and groundwater recharge.
- Evapotranspiration: The loss of water through evaporation from soil and plant transpiration, significantly affected by climatic factors such as temperature and wind speed.
- Baseflow Contribution: The delayed portion of infiltrated water that sustains river flow during dry periods.

The precipitation partitioning analysis helps evaluate the efficiency of the HEC-HMS model in representing the hydrological processes of the Gheba Basin. By comparing the partitioned precipitation components across the basin, insights into water balance dynamics and hydrological responses under various precipitation scenarios can be derived. The results from this partitioning analysis will be further examined in the results section to assess the performance of the model in capturing seasonal and inter-annual variations in the hydrological cycle.

One key parameter used in evaluating precipitation partitioning is the Runoff Coefficient, which represents the fraction of total precipitation that is converted into runoff. The volumetric runoff coefficient is calculated as:

$$C_r = \frac{V_{runoff}}{V_{precipitation}} \quad (23)$$

Where: Cr is the runoff coefficient, V_{runoff} is the total runoff volume, $V_{precipitation}$ is the total precipitation volume.

A higher runoff coefficient indicates that a greater proportion of rainfall contributes to surface flow, whereas a lower coefficient suggests more infiltration and evapotranspiration. This metric helps assess the efficiency of the HEC-HMS model in representing hydrological processes within the Gheba Basin, particularly in differentiating between wet and dry periods.

5. RESULT AND DISCUSSION

5.1. PRECIPITATION (GLOBAL AND OBSERVATION)

The comparison between global precipitation datasets (CHIRPS, TRMM, ERA5-LAND, and TerraClimate) and ground-based observations was conducted using three key metrics: mean and standard deviation differences, correlation, and mean absolute differences. These metrics were chosen to evaluate the datasets' alignment with observed precipitation values in terms of central tendency, variability, and trend consistency.

Even though there are three ground observation stations in the study area—Adigudom, Edaga-Hamus, and Mekele Airport—Mekele Airport was selected as the primary reference station. This decision was based on the availability of long-term rainfall records, as Mekele Airport has over 20 years (1999–2019) of continuous precipitation data, making it a more robust dataset for comparison. In contrast, the other two stations (Adigudom and Edaga-Hamus) only have four years of continuous records (1999–2002), which was insufficient for a comprehensive assessment. Given the need for a longer temporal record to evaluate the accuracy and consistency of global precipitation datasets, Mekele Airport was chosen as the baseline for assessing the dataset that best aligns with observed precipitation trends.

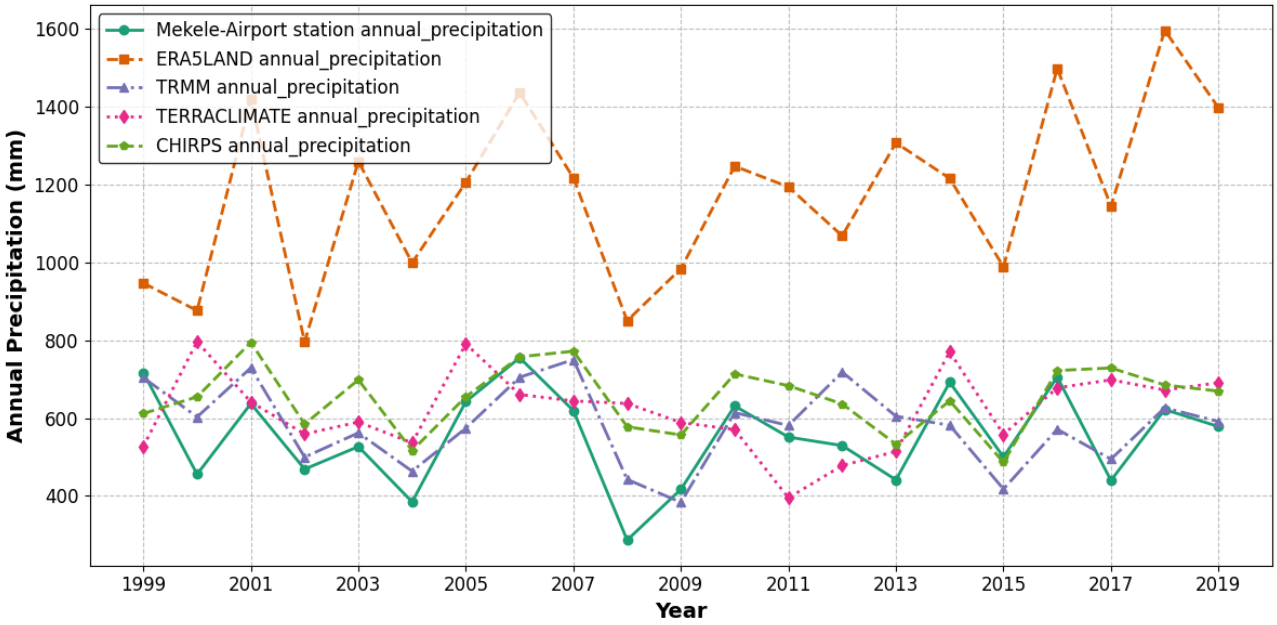

Figure 27. Annual Precipitation comparison: Global precipitation vs Observation 1999-2019

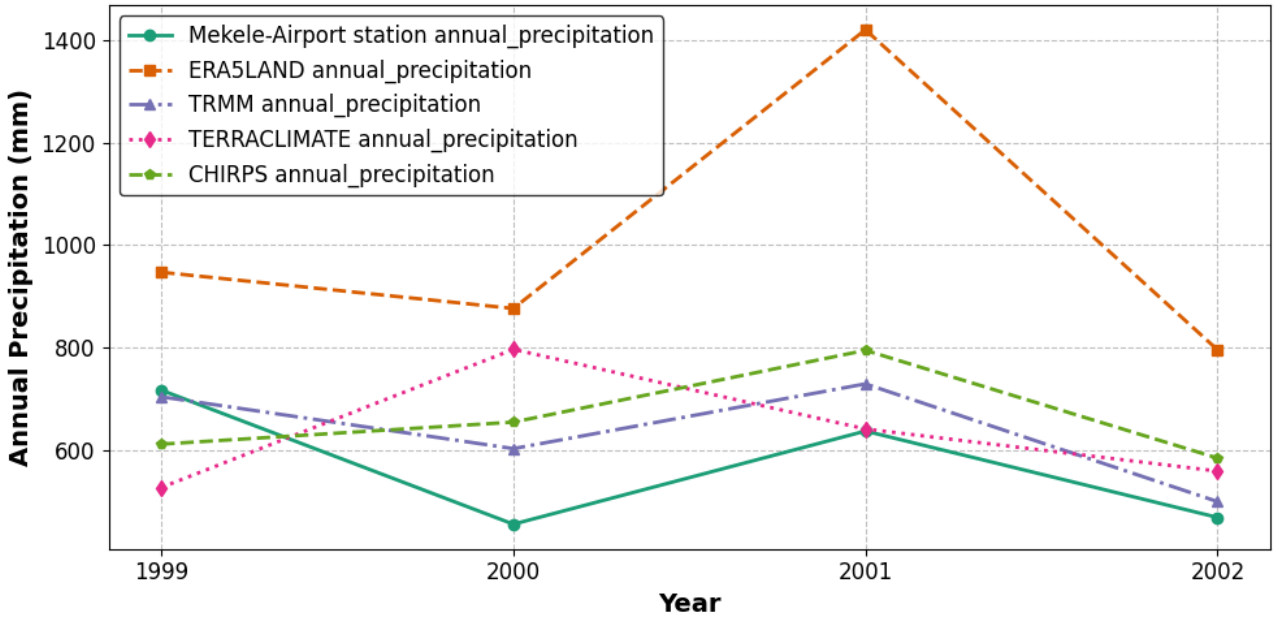

Figure 28. Annual Precipitation comparison: Global precipitation vs Observation 1999-2002

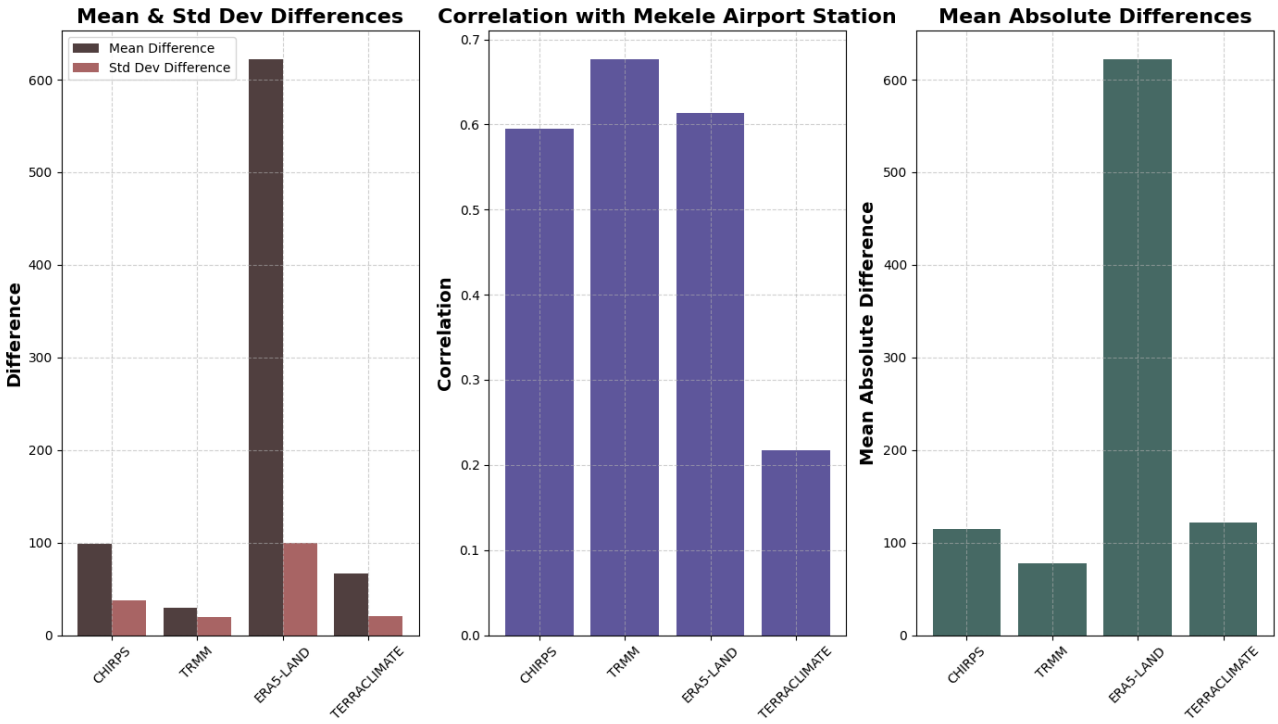

Figure 29.Statistical Comparison of Global Precipitation Datasets vs Mekele-station Observations

The first metric, mean and standard deviation differences, highlights the degree to which each dataset matches Mekele's annual precipitation observations. CHIRPS and TRMM demonstrated the smallest mean and standard deviation differences, indicating strong alignment in both average precipitation levels and variability. Conversely, ERA5-LAND exhibited the largest mean difference, suggesting significant overestimation of precipitation compared to Mekele. TerraClimate showed moderate differences, performing better than ERA5-LAND but not as well as CHIRPS and TRMM.

Correlation analysis provided insight into the datasets' ability to replicate Mekele-station's precipitation patterns over time. TRMM achieved the highest correlation with Mekele, closely followed by CHIRPS, indicating their strong agreement in tracking annual trends. TerraClimate and ERA5-LAND exhibited weaker correlations, implying that their annual precipitation patterns diverged more from Mekele's observations.

The mean absolute difference (MAD) metric further confirmed CHIRPS and TRMM's alignment with Mekele. Both datasets had the smallest MAD values, demonstrating consistent agreement with the observation dataset. In contrast, ERA5-LAND displayed the largest MAD, reinforcing its tendency to overestimate precipitation. TerraClimate, while better than ERA5-LAND, had moderate MAD values, reflecting some inconsistencies in its alignment with Mekele.

Table 5.Statistical Comparison of CHIRPS and TRMM (1999–2002

Mean and Standard Deviation Differences:

Dataset	Mean difference	Std Dev	Correlation	Mean Absolute
CHIRPS	99.1	38.1	0.59	115
TRMM	29.4	19.2	0.67	77.9
ERA5-LAND	621.6	100.1	0.61	621.6
TERRACLIMATE	66.5	20.5	0.21	121.8

Overall, TRMM emerged as the most reliable dataset, demonstrating the highest correlation with Mekele observations while maintaining minimal differences in both mean and mean absolute difference (MAD). CHIRPS followed closely, exhibiting comparable performance, making it another strong candidate for precipitation estimation.

In contrast, ERA5-LAND significantly overestimated precipitation, as evidenced by its large mean and MAD differences, making it less suitable for accurate hydrological modeling in the Gheba Basin. TerraClimate was excluded from further analysis due to its monthly temporal resolution, which is insufficient for basin-scale hydrological modeling requiring finer temporal granularity.

These findings emphasize the importance of selecting an appropriate precipitation dataset for hydrological studies in data-scarce regions. Given their high correlation and lower mean absolute differences, TRMM and CHIRPS were chosen for further hydrological modeling of the Gheba Basin.

5.1.1. TEMPORAL ANALYSIS

Following the statistical evaluation against Mekele Airport Station, TRMM and CHIRPS emerged as the most reliable global precipitation datasets, demonstrating higher correlation and lower mean absolute differences compared to other datasets. To further assess their applicability at the basin scale, precipitation estimates from these datasets were spatially aggregated across the Gheba Basin and compared with available ground observations.

This comparison ensures that the selected datasets effectively represent precipitation variability at a regional scale, which is critical for hydrological modeling. The analysis aims to validate the consistency of TRMM and CHIRPS in capturing precipitation dynamics within the basin and their suitability for subsequent hydrological simulations

To further evaluate the performance of TRMM and CHIRPS at the basin scale, scatter plots were generated comparing daily precipitation observations from the three ground stations (Mekele Airport, Adigudom, and Edaga-Hamus) against the basin-wise average daily precipitation derived from both datasets. This analysis aims to assess how well the global datasets capture daily precipitation variability across the Gheba Basin, providing insights into their reliability for hydrological applications. The scatter plots illustrate the relationship between observed and estimated precipitation, highlighting potential biases and deviations in dataset performance

SCATTER PLOT FOR DAILY DATA

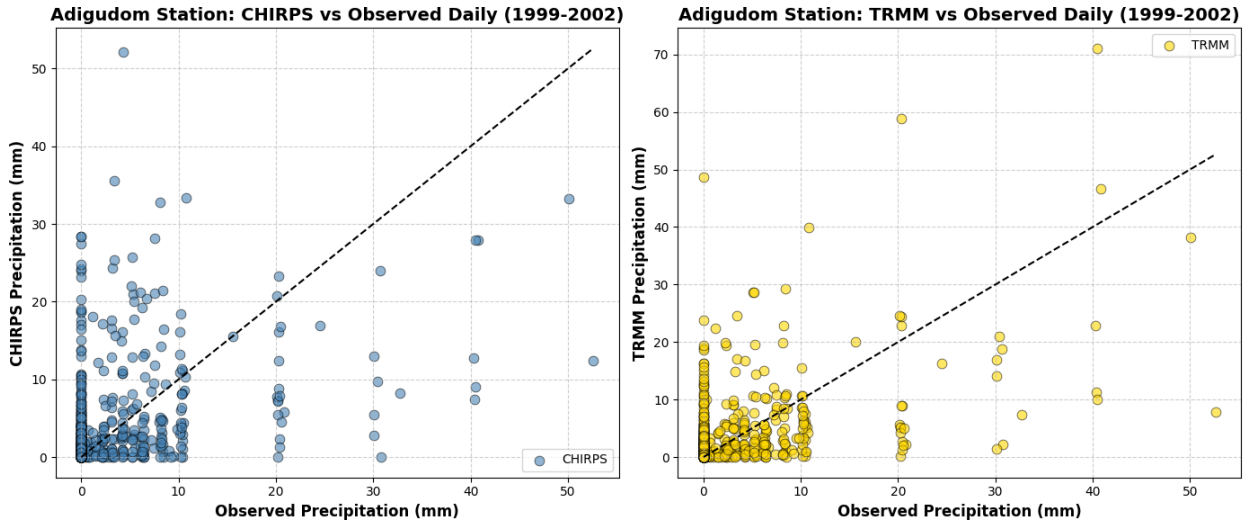

Figure 30. Comparison between observation vs two global datasets at Adigudom station

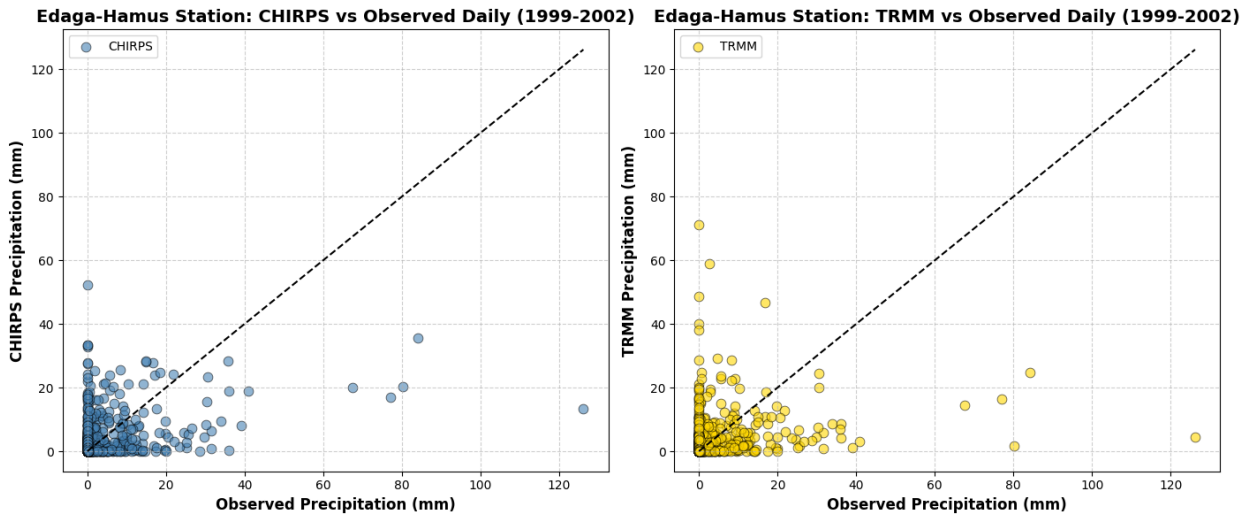

Figure 31. Comparison between observation vs two global datasets at Edaga-Hamus station

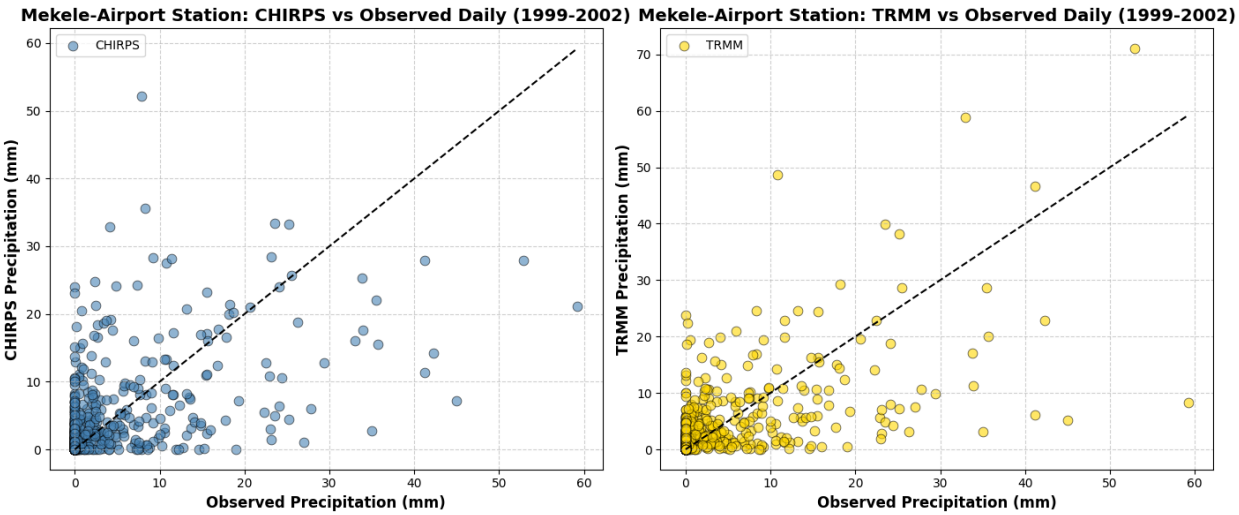

Figure 32.Comparison between observation vs two global datasets at Mekele-Airport station

The scatter plots in (*Figures 23–25)* compare CHIRPS and TRMM against observed rainfall. A 1:1 reference line is included to indicate perfect agreement between datasets.

Both CHIRPS and TRMM tend to underestimate high rainfall events (>30 mm), with most data points clustering at low values (0–10 mm). CHIRPS exhibits a tighter spread around the 1:1 line, indicating a better match with observed data. TRMM shows higher variability, with greater overestimation of light rainfall and underestimation of heavy rainfall.

The performance varies by station, with Mekele and Adigudom showing better alignment between satellite data and observations, while Edaga-Hamus exhibits larger discrepancies.

To complement the scatter plot analysis, **Bias, RMSE, MAD, and Pearson Correlation (R)** were computed (*Table 2*).

Table 6.Statistical Comparison of CHIRPS and TRMM (1999–2002) Daily

Daily Overall Statistical Comparison (1999-2002)- All Years Combined:

Station	Dataset	Bias (mm)	RMSE (mm)	MAD (mm)	Correlation
Adigudom	CHIRPS	-1.1	6.2	2.9	0.74
Adigudom	TRMM	-2.7	7.5	4.1	0.63
Edaga-Hamus	CHIRPS	-1.5	7.1	3.5	0.68
Edaga-Hamus	TRMM	-3.2	8.3	4.7	0.60
Mekele Airport	CHIRPS	-1.2	5.8	3.1	0.72
Mekele Airport	TRMM	-2.4	6.9	4.3	0.65

CHIRPS consistently exhibits lower bias and RMSE values across all stations, indicating a more accurate estimation of daily precipitation trends. Higher correlation coefficients (0.68–0.74) for CHIRPS suggest a stronger relationship with observed rainfall compared to TRMM (0.60–0.65). The mean absolute difference (MAD) is also lower for CHIRPS, indicating its estimates are closer to observed values.

However, both CHIRPS and TRMM show significant underestimation of high rainfall events, with TRMM exhibiting greater variability and error. Overall, CHIRPS outperforms TRMM, making it a more reliable dataset for hydrological applications.

TEMPORAL ANALYSIS (MONTHLY ANALYSIS)

In addition to the daily-scale analysis, the study also examines monthly and seasonal precipitation patterns, focusing on the rainy season (July to September) in the Gheba Basin. This seasonal evaluation helps assess the datasets' ability to capture longer-term precipitation trends essential for hydrological modeling. The comparison provides insights into how well CHIRPS and TRMM represent both short-term and cumulative rainfall dynamics in the region.

The following figures from 27-30 shows monthly and seasonal comparison between observations and basin scale global datasets for the year 1999-2002.

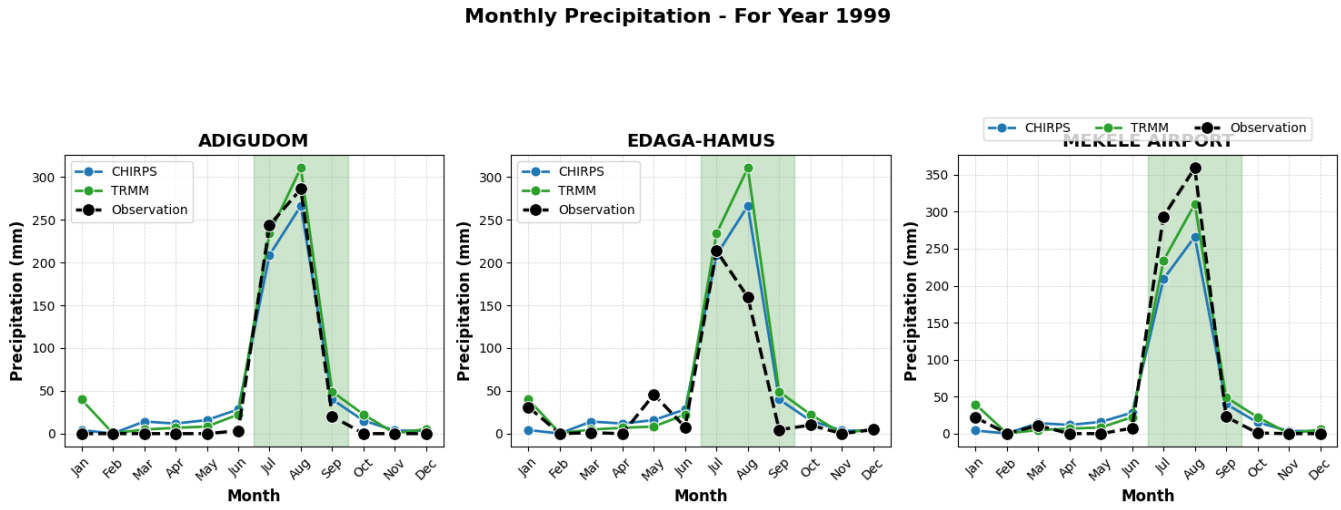

Figure 33. Temporal analysis at all three stations with the basin-wise global datasets (TRMM and CHIRPS) for the year 1999

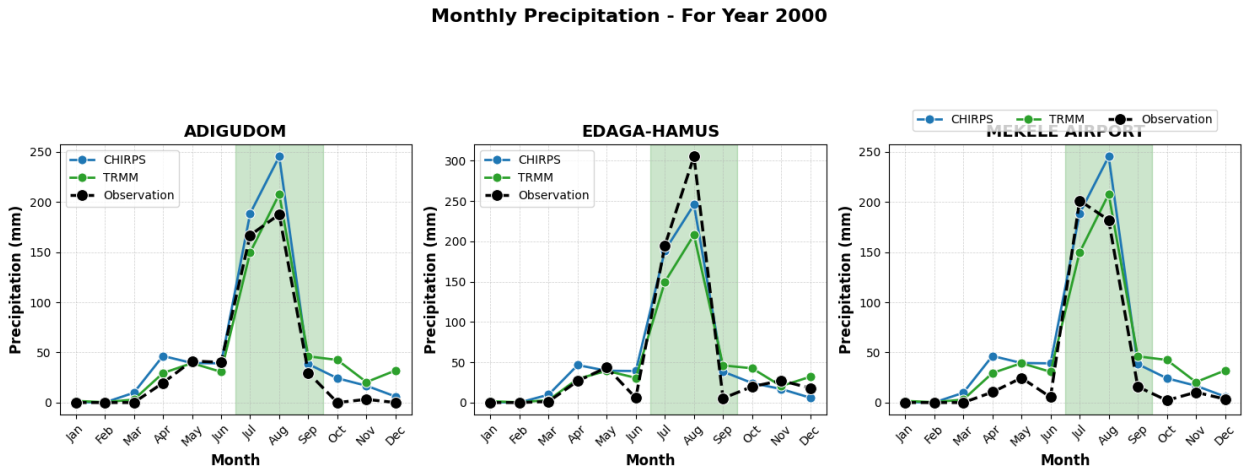

Figure 34. Temporal analysis at all three stations with the basin-wise global datasets (TRMM and CHIRPS) for the year 2000

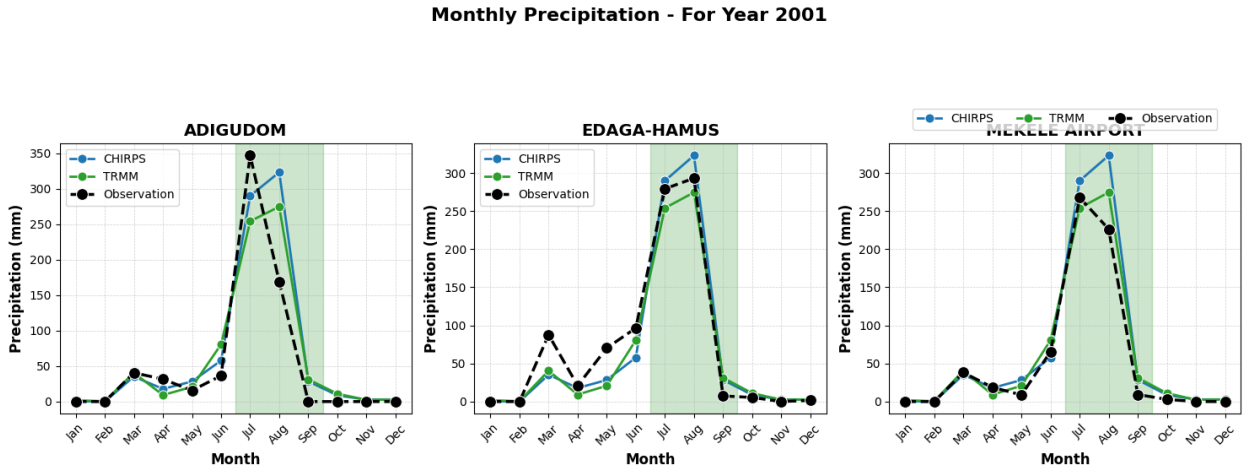

Figure 35. Temporal analysis at all three stations with the basin-wise global datasets (TRMM and CHIRPS) for the year 2001

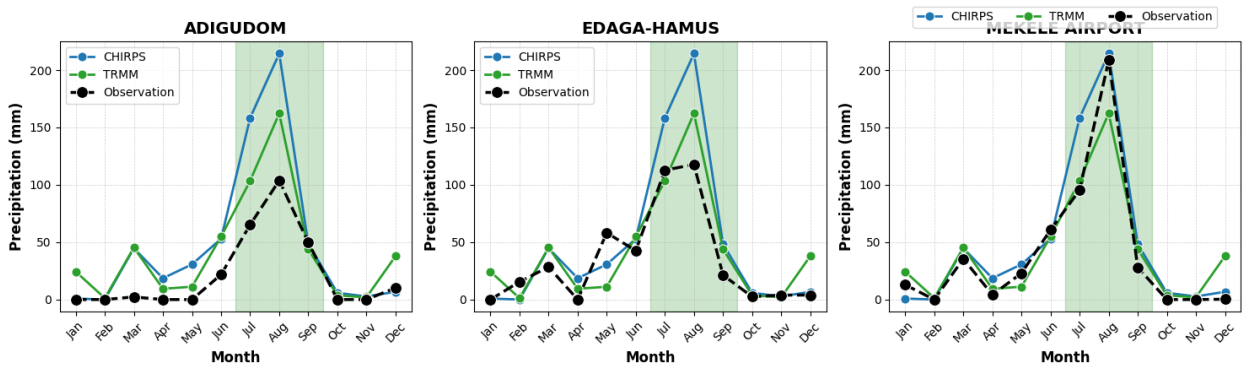

Figure 36. Temporal analysis at all three stations with the basin-wise global datasets (TRMM and CHIRPS) for the year 2002

The performance of CHIRPS and TRMM precipitation datasets was assessed against station-based observations at Adigudom, Edaga-Hamus, and Mekele Airport stations for the period 1999–2002. The evaluation was conducted at multiple temporal scales, including overall performance, yearly variations, and seasonal (rainy season) trends.

Table 7. Statistical Comparison of CHIRPS and TRMM (1999–2002) Monthly

Monthly Overall Statistical Comparison (1999-2002)

Station	Dataset	Bias (mm)	RMSE (mm)	MAD (mm)	Correlation
Adigudom	CHIRPS	14.82	36.14	20.57	0.92
Adigudom	TRMM	12.52	29.29	19.16	0.94
Edaga-Hamus	CHIRPS	5.24	29.95	19.25	0.94
Edaga-Hamus	TRMM	2.95	34.03	20.93	0.91
Mekele Airport	CHIRPS	7.65	29.30	17.64	0.95
Mekele Airport	TRMM	5.35	22.22	15.92	0.97

Table 8. Statistical Comparison of CHIRPS and TRMM (1999–2002) Seasonal

Seasonal (JAS) (Rainy Season - All Years Combined) Statistical Comparison:

Station	Dataset	Bias (mm)	RMSE (mm)	MAD (mm)	Correlation
Adigudom	CHIRPS	28.63	59.47	42.82	0.88
Adigudom	TRMM	17.80	44.43	34.64	0.92
Edaga-Hamus	CHIRPS	22.58	46.21	36.29	0.93
Edaga-Hamus	TRMM	11.75	52.27	38.17	0.88
Mekele Airport	CHIRPS	11.18	48.15	36.93	0.91
Mekele Airport	TRMM	0.35	33.04	28.63	0.97

Overall Performance (1999–2002)

Table X presents the statistical comparison between CHIRPS, TRMM, and observed precipitation for the entire period from 1999 to 2002. The key observations are:

- Bias Analysis: CHIRPS exhibited a higher bias at Adigudom (14.82 mm) and Edaga-Hamus (5.24 mm), while TRMM showed relatively lower bias values, particularly at Mekele Airport (5.35 mm).
- Error Metrics: TRMM demonstrated lower RMSE (22.22 mm) and MAD (15.92 mm) at Mekele Airport, suggesting better agreement with observations compared to CHIRPS.
- Correlation: TRMM consistently achieved higher correlation coefficients (0.94–0.97) across all stations, indicating a stronger relationship with observed precipitation.

Overall, TRMM outperformed CHIRPS in terms of lower RMSE and MAD, while both datasets exhibited strong correlations with observations

Yearly Performance Analysis

The performance of CHIRPS and TRMM varied significantly across different years:

- 1999: CHIRPS and TRMM exhibited the highest correlations (~0.99) across all stations. However, Edaga-Hamus had the largest biases (18.85 mm for TRMM), indicating an overestimation of precipitation.
- 2000: CHIRPS had a significant positive bias at Mekele Airport (16.59 mm), whereas TRMM performed better in reducing bias at Edaga-Hamus (-3.71 mm).
- 2001: TRMM and CHIRPS showed lower biases at Edaga-Hamus and Mekele Airport, but Adigudom had a notably high RMSE (~48.88 mm for CHIRPS and 44.06 mm for TRMM).
- 2002: Biases increased significantly at Adigudom (27.62 mm for CHIRPS and 20.53 mm for TRMM), indicating potential overestimation by both datasets during this year.

The year-wise analysis suggests that 1999 and 2000 showed the best agreement, whereas 2001 and 2002 had larger errors and deviations from observed values.

Seasonal Analysis (Rainy Season: June–September):

Since the rainy season (June–September) is hydrologically significant in the Tigray region, the performance of CHIRPS and TRMM was specifically analyze during these months.

Overall Rainy Season Performance (1999–2002)

- Bias Analysis: CHIRPS had the highest bias at Adigudom (28.63 mm), while TRMM exhibited lower bias across all stations, particularly at Mekele Airport (0.35 mm).
- RMSE & MAD: Both datasets showed the highest RMSE at Adigudom (59.47 mm for CHIRPS and 44.43 mm for TRMM), indicating greater uncertainty in satellite estimates at this location.
- Correlation: TRMM achieved the strongest correlation at Mekele Airport (0.97), confirming its superior agreement with observed precipitation during the rainy season.

Annual Rainy Season Analysis:

- 1999: CHIRPS and TRMM had the highest correlation values (~1.00) at all stations, but TRMM overestimated precipitation at Edaga-Hamus (bias = 57.61 mm).
- 2000: CHIRPS performed well, showing minimal bias at Edaga-Hamus (0.12 mm), while TRMM underestimated rainfall at this station (bias = -19.16 mm).
- 2001: Both datasets showed higher biases at Adigudom (36.74 mm for CHIRPS, 22.06 mm for TRMM), indicating overestimation in this region.
- 2002: The largest seasonal biases were observed at Adigudom (CHIRPS = 58.42 mm, TRMM = 30.97 mm), suggesting strong overestimation of rainfall events.

These findings highlight that TRMM generally performs better than CHIRPS during the rainy season, but biases increase in extreme rainfall years (e.g., 1999 and 2002)

Summary and Implications

- TRMM consistently outperforms CHIRPS in terms of lower RMSE and higher correlation.
- Biases are highest at Adigudom, particularly during the rainy season, suggesting overestimation.
- Both datasets perform best in 1999 and 2000 but show larger errors in 2001 and 2002.
- TRMM is more reliable for estimating precipitation trends, especially at Mekele Airport.

5.1.2. SPATIAL ANALYSIS

The spatial analysis of TRMM and CHIRPS datasets for the 1999–2002 period revealed distinct precipitation patterns across the Gheba Basin. Figures 31 and 40 display the average annual precipitation derived from the two datasets.

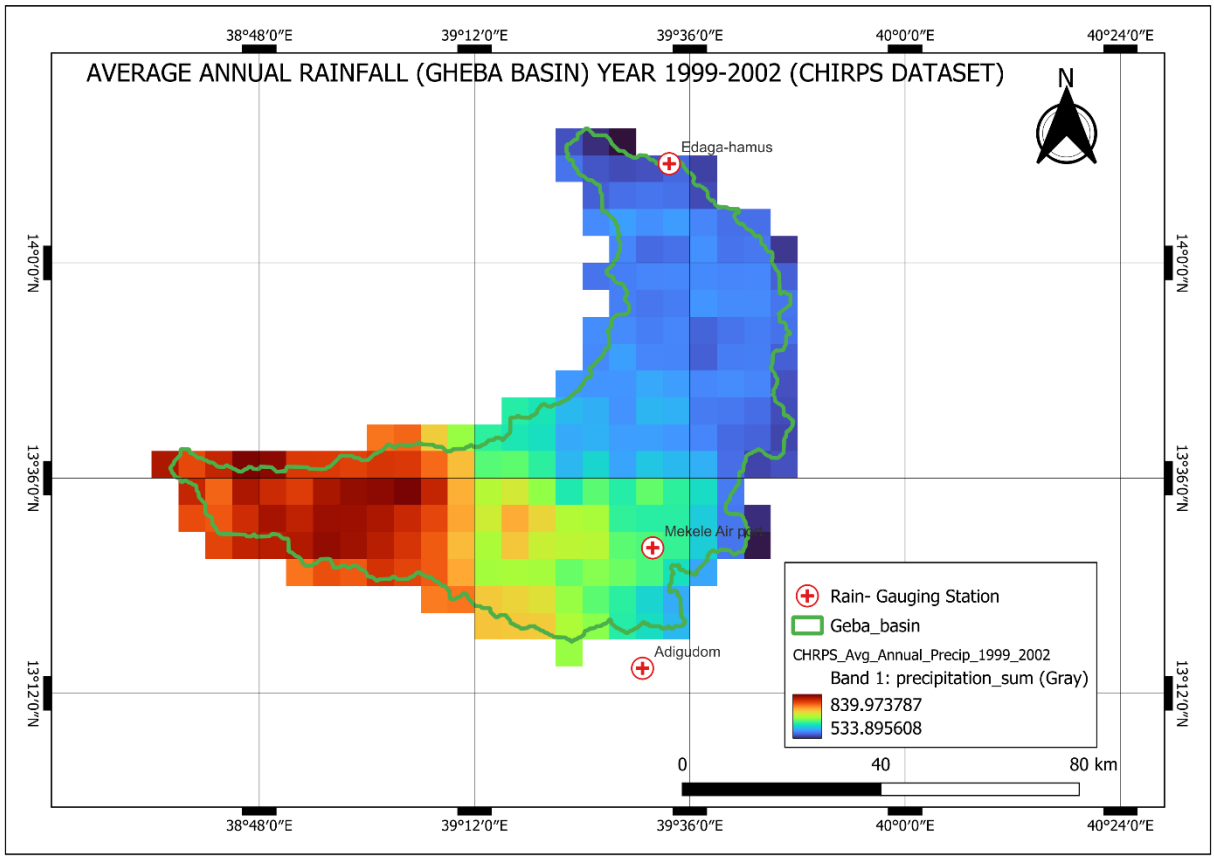

Figure 37. Average annual precipitation over Gheba basin (CHIRPS dataset) 1999-2002

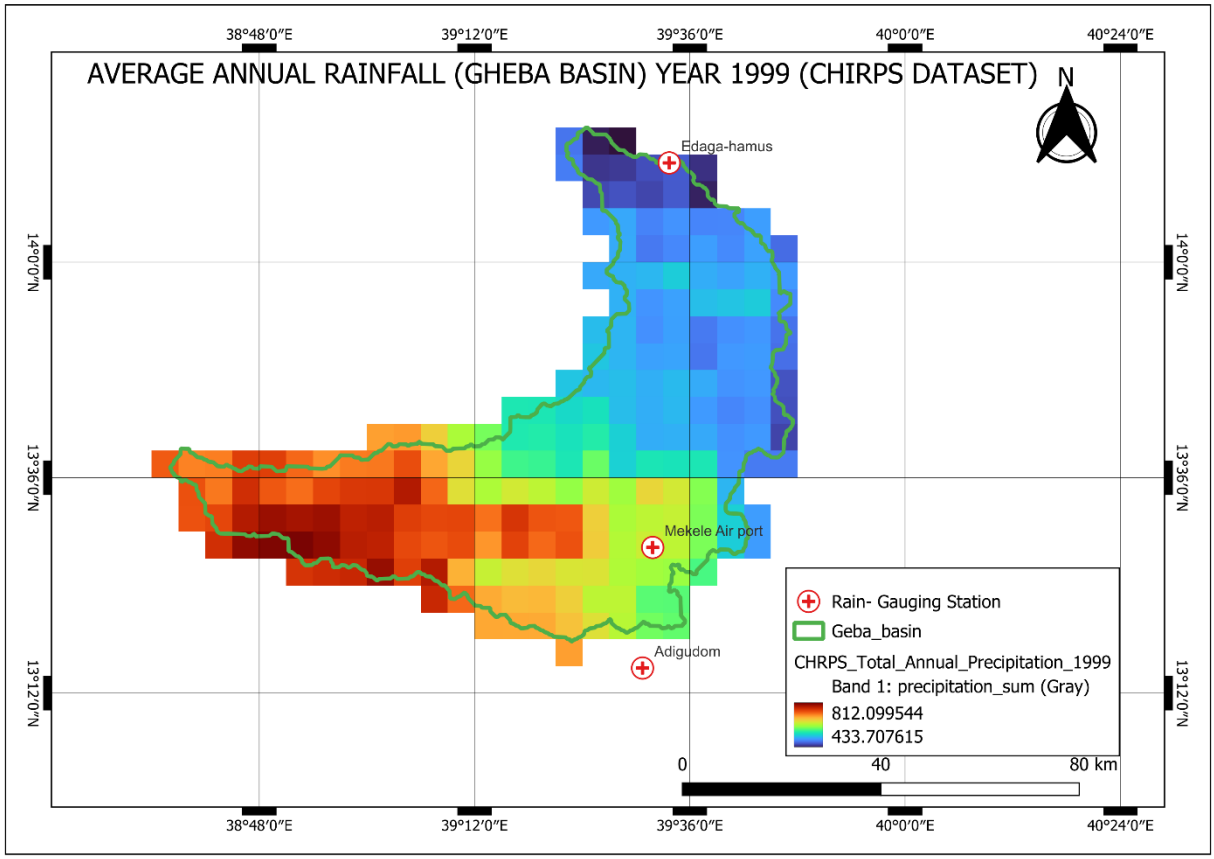

Figure 38. Average annual precipitation over Gheba basin (CHIRPS dataset) 1999

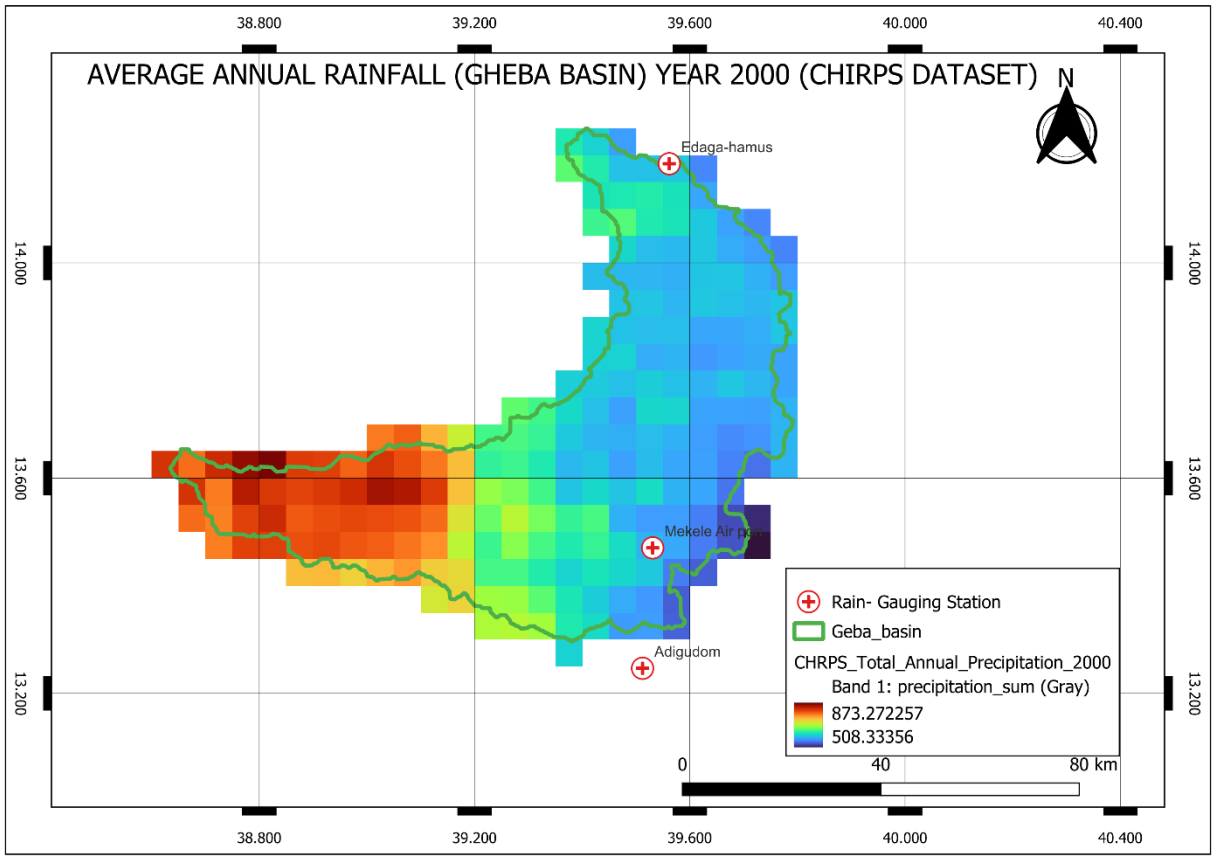

Figure 39. Average annual precipitation over Gheba basin (CHIRPS dataset) 2000

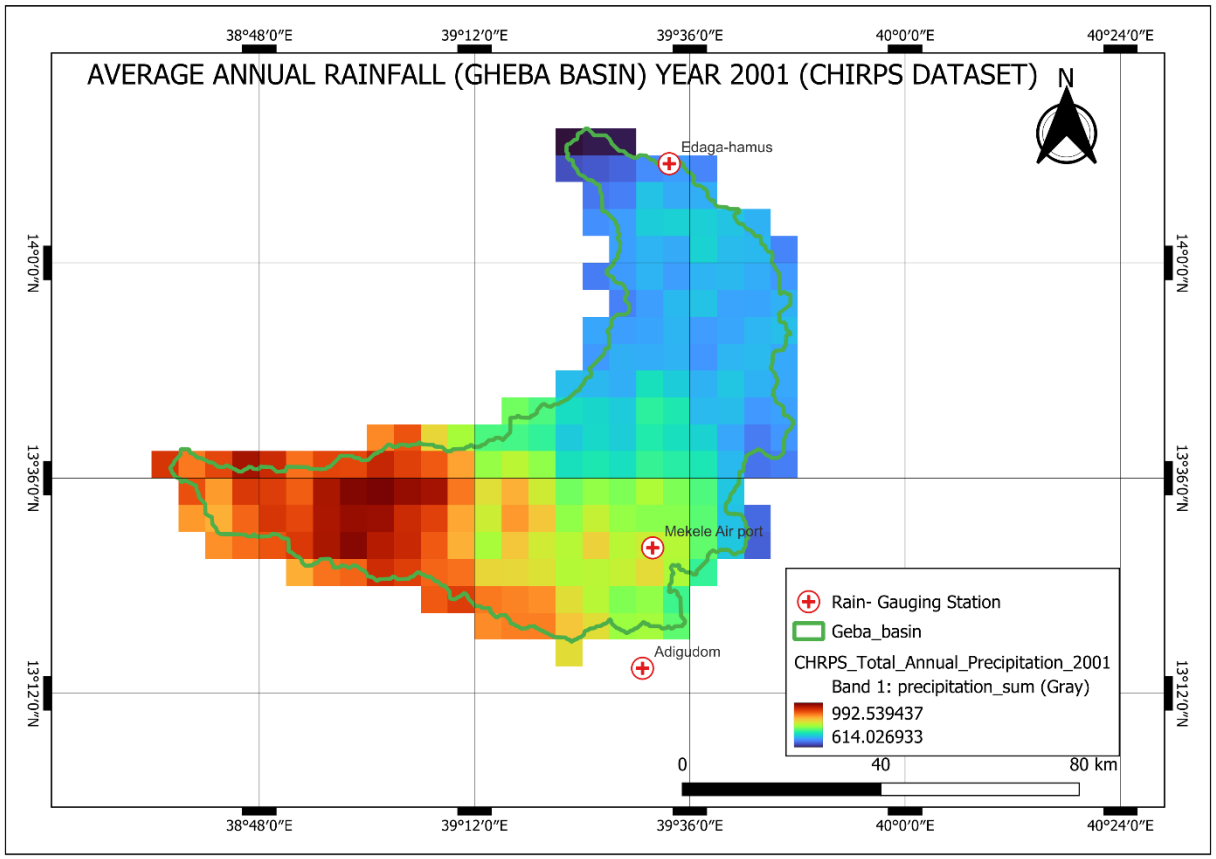

Figure 40. Average annual precipitation over Gheba basin (CHIRPS dataset) 2001

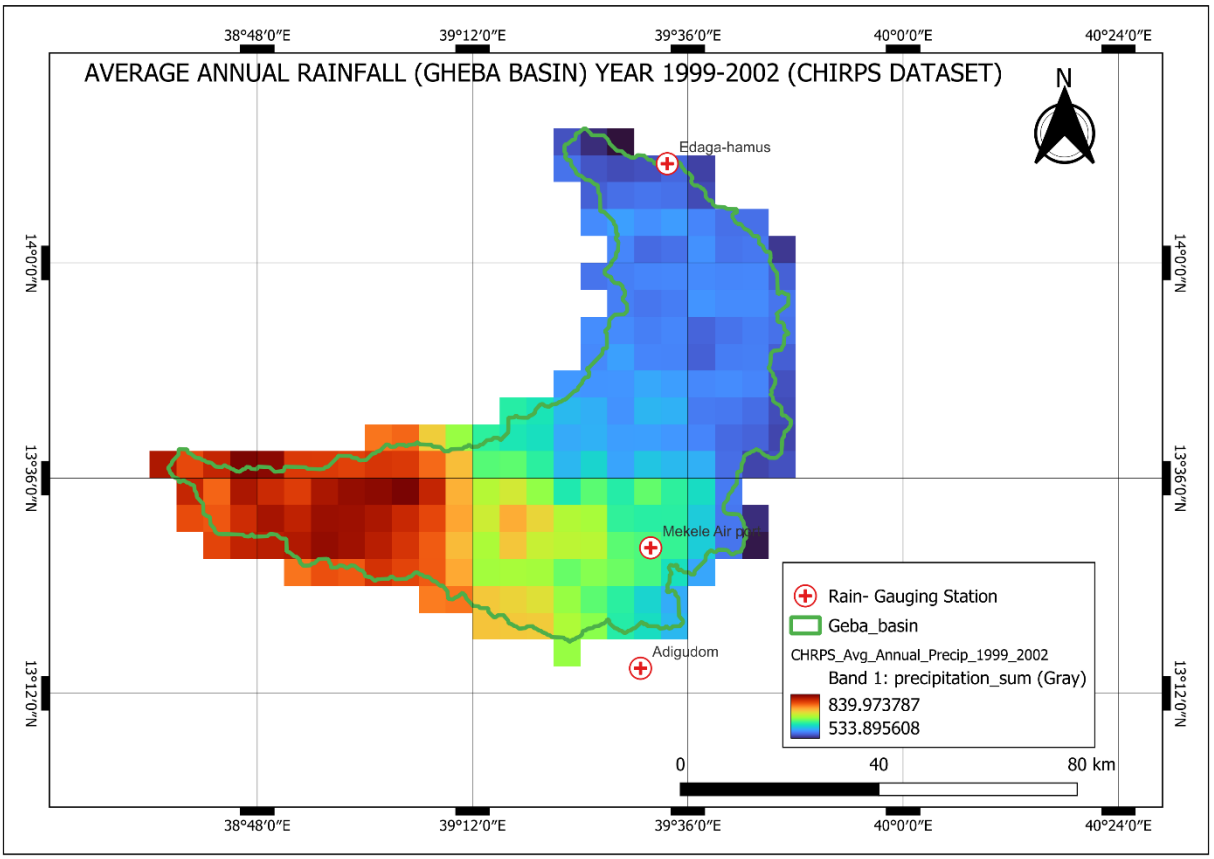

Figure 41. Average annual precipitation over Gheba basin (CHIRPS dataset) 2002

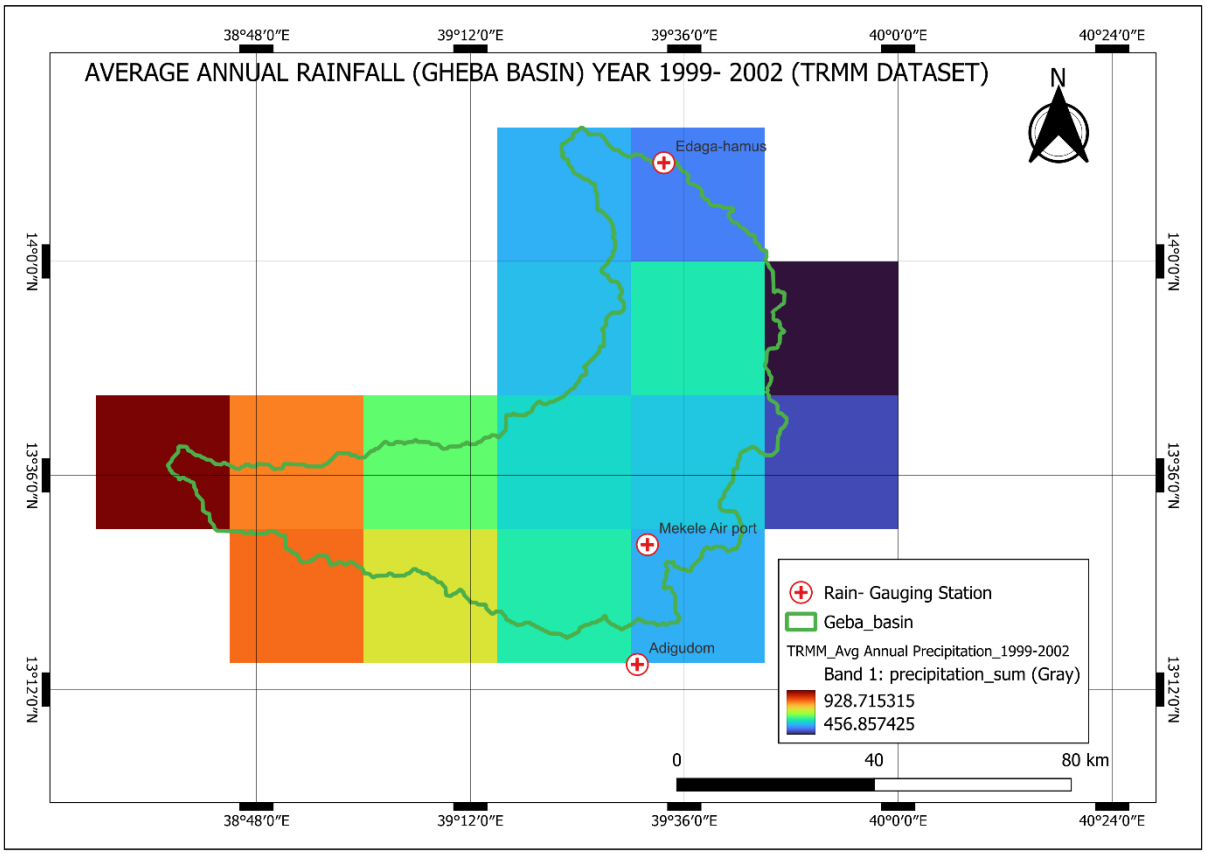

Figure 42. Average annual precipitation over Gheba basin (TRMM dataset) 1999-2002

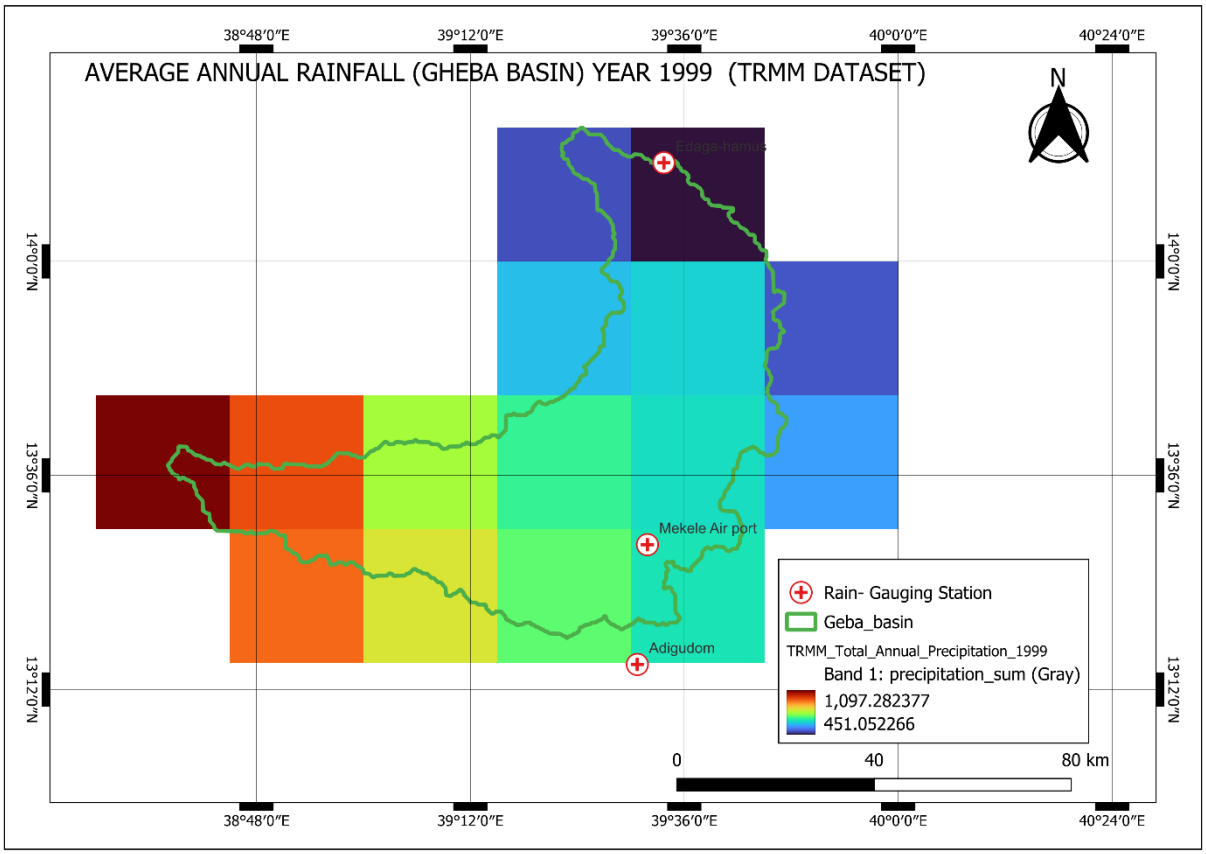

Figure 43. Average annual precipitation over Gheba basin (TRMM dataset) 1999

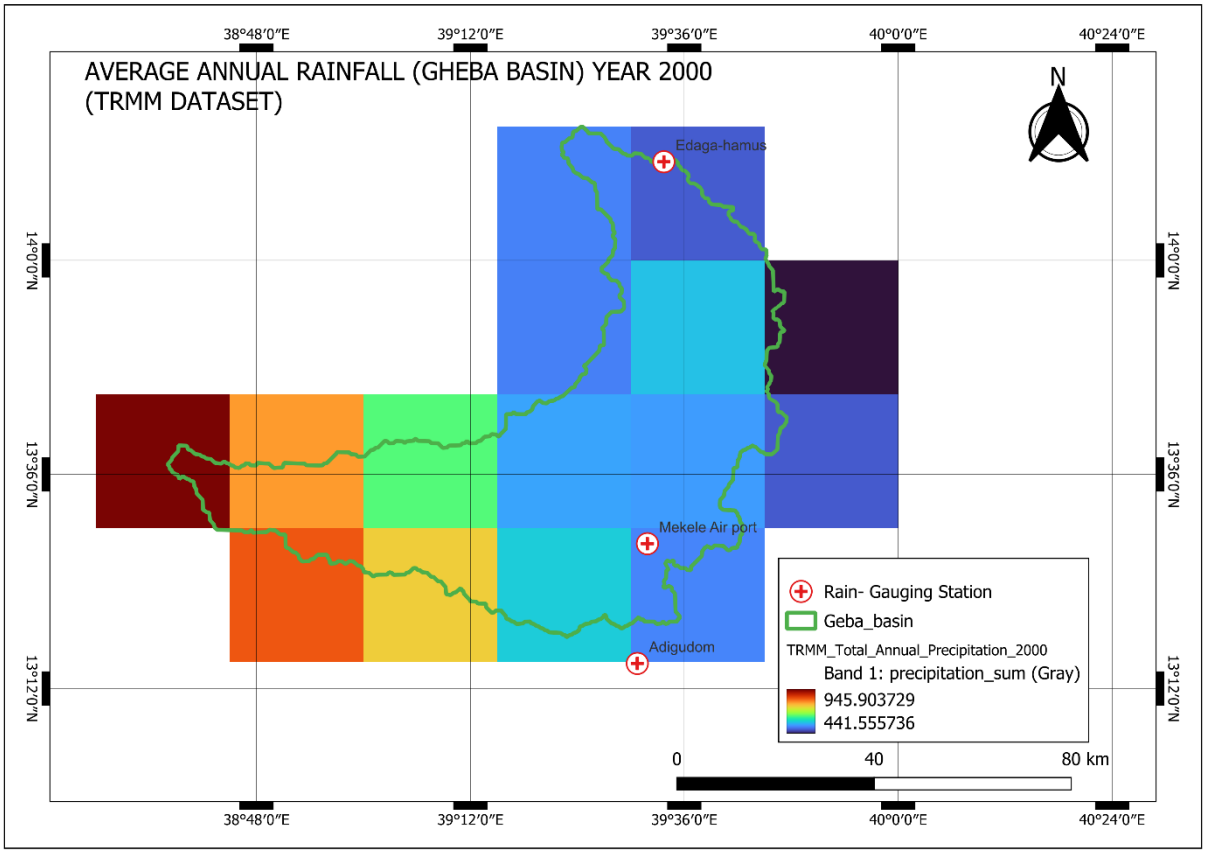

Figure 44. Average annual precipitation over Gheba basin (TRMM dataset) 2000

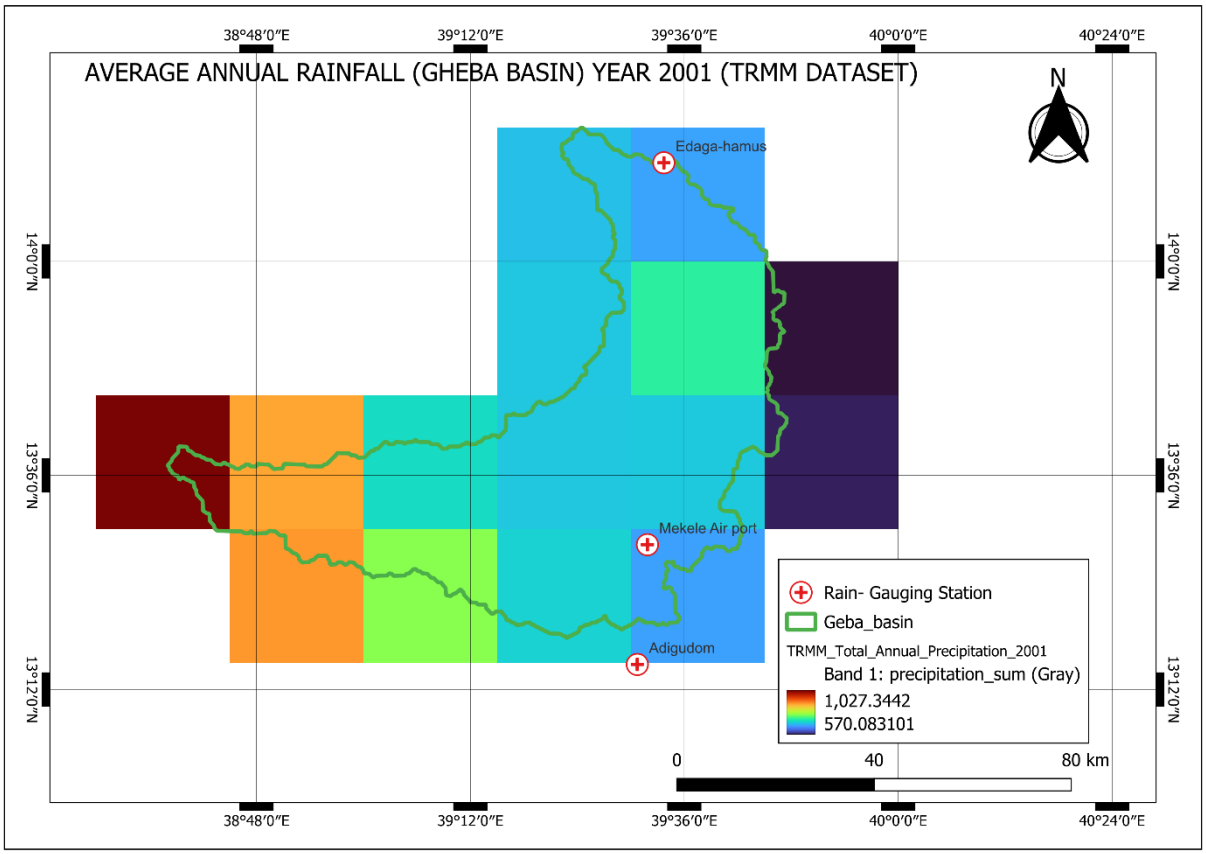

Figure 45. Average annual precipitation over Gheba basin (TRMM dataset) 2001

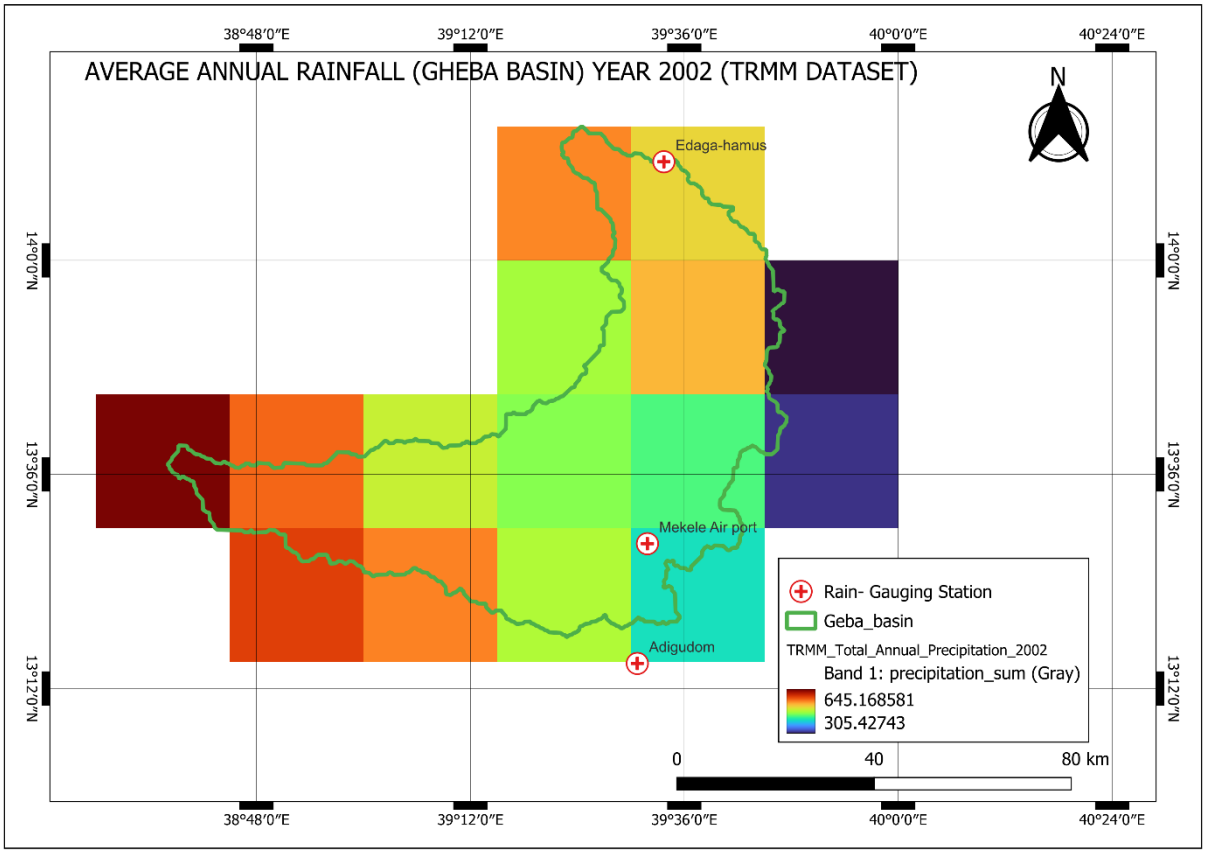

Figure 46. Average annual precipitation over Gheba basin (TRMM dataset) 2002

The annual spatial analysis of TRMM and CHIRPS datasets for the period 1999–2002 revealed distinct precipitation patterns across the Gheba Basin. The TRMM dataset exhibited a broader range of precipitation values, with estimates varying from 451 mm to 1097 mm in 1999, 441 mm to 945 mm in 2000, 570 mm to 1027 mm in 2001, and 305 mm to 645 mm in 2002. In contrast, CHIRPS consistently showed slightly lower precipitation values, ranging from 433 mm to 812 mm in 1999, 508 mm to 873 mm in 2000, 614 mm to 992 mm in 2001, and 471 mm to 775 mm in 2002. These variations highlight the influence of spatial resolution on precipitation estimations.

When compared to observed precipitation from the three ground stations (Adigudom, Edaga-Hamus, and Mekele Airport), CHIRPS aligned more closely with field measurements, particularly at Mekele Airport and Adigudom. The recorded observations for 1999 ranged from 477 mm at Edaga-Hamus to 717 mm at Mekele Airport, while in 2000, values ranged between 456 mm and 648 mm. In 2001, there was significant variation, with Edaga-Hamus reaching 862 mm while the other two stations recorded between 637 mm and 640 mm. By 2002, a decline in precipitation was observed, with values between 406 mm and 468 mm. TRMM consistently overestimated precipitation, especially in high-altitude regions, whereas CHIRPS provided a more refined representation of the rainfall distribution.

5.2. STATISTICS FOR STOCHASTICALLY GENERATED DATA

The Statistics like mean of 24hrs, var of 24hrs&48hrs, Corr for 24hr, prop. Dry for 24hrs^48hrs were compared to accept the Generator. And the following are the results

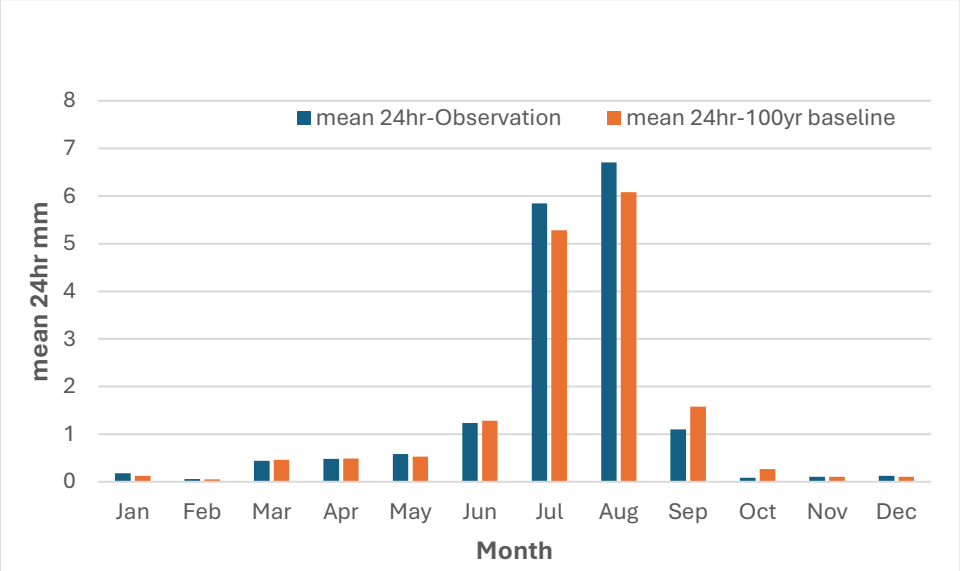

Figure 47. Mean for 24hrs precipitation Statistics for baseline and observation

The mean 24-hour precipitation (Figure 47) aligns well with observations, particularly during the wet season (June–September), demonstrating the model's capability to capture seasonal rainfall trends. Minor overestimation in August and underestimation in September are present, but these discrepancies are expected given the arid nature of the study area, where localized rainfall variability is high.

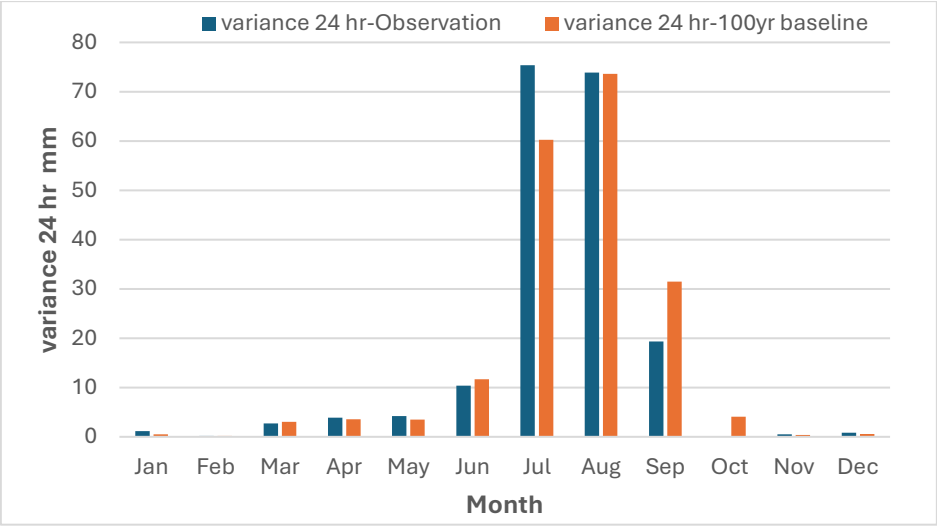

Figure 48. Variance for 24hrs precipitation Statistics for baseline and observation

The variance of 24-hour precipitation (Figure 48) shows that while observed variance is higher during peak rainfall months, the stochastic model successfully represents seasonal variability. The underestimation of extreme values is common in such models, particularly in arid regions where rainfall events are more sporadic, but it still provides a reasonable approximation of rainfall distribution.

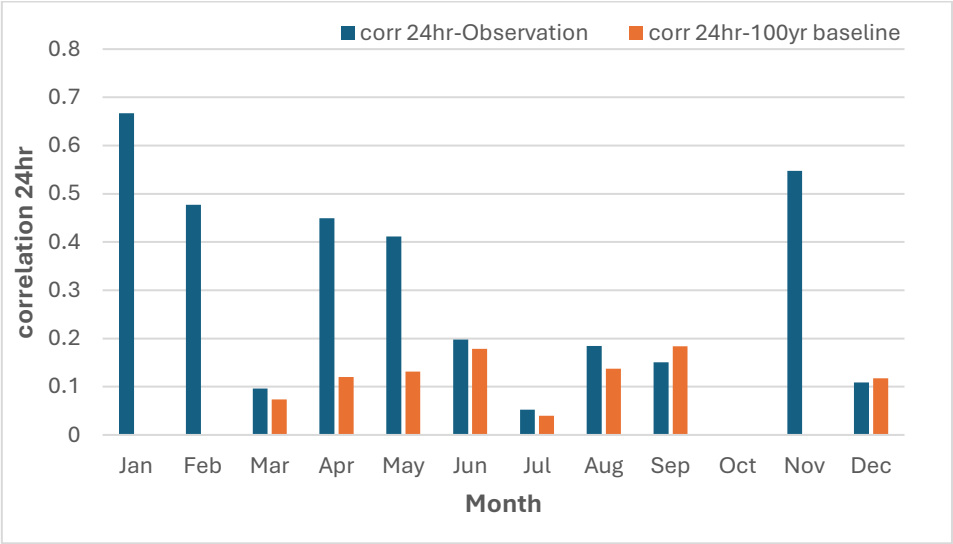

Figure 49. Correlation for 24hrs precipitation Statistics for baseline and observation

The correlation of 24-hour precipitation (Figure 49) is generally lower in the baseline dataset compared to observations, suggesting slightly weaker rainfall persistence.

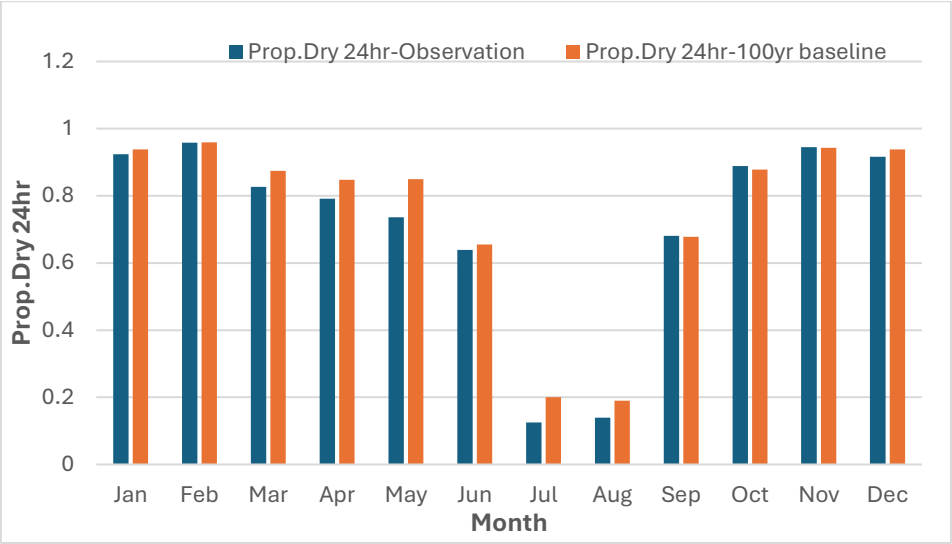

Figure 50. prop. Dry for 24hrs for precipitation Statistics for baseline and observation

The proportion of dry days (24-hour) (Figure 50) is well represented, with only slight deviations. The model slightly overestimates wet conditions in the wet season and underestimates dryness in drier months, but overall, it effectively captures the arid region's high-frequency dry spells.

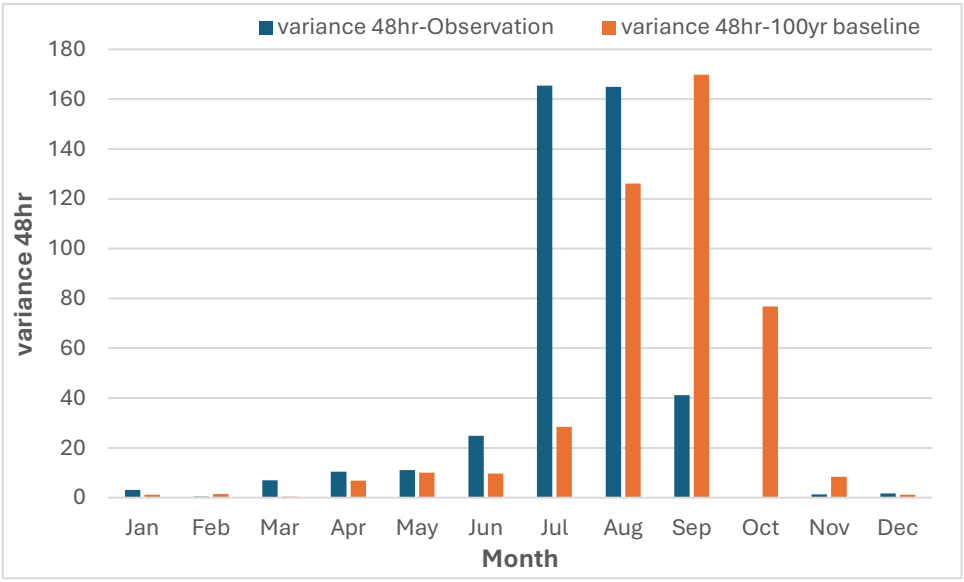

Figure 51. Variance for 48hrs precipitation Statistics for baseline and observation

For 48-hour precipitation variance (Figure 51), observed values are higher in peak months, indicating more extreme rainfall events than what the baseline captures. However, this is an expected limitation, as stochastic weather generators typically perform better in humid regions, and despite this, the model still provides a reliable representation of long-term rainfall characteristics.

The proportion of dry days (48-hour) (Figure 52) follows observed trends closely, with minor overestimations of dry periods in August and September. Given that the study area is arid, the model's ability to reflect prolonged dry conditions is a strong indicator of its applicability.

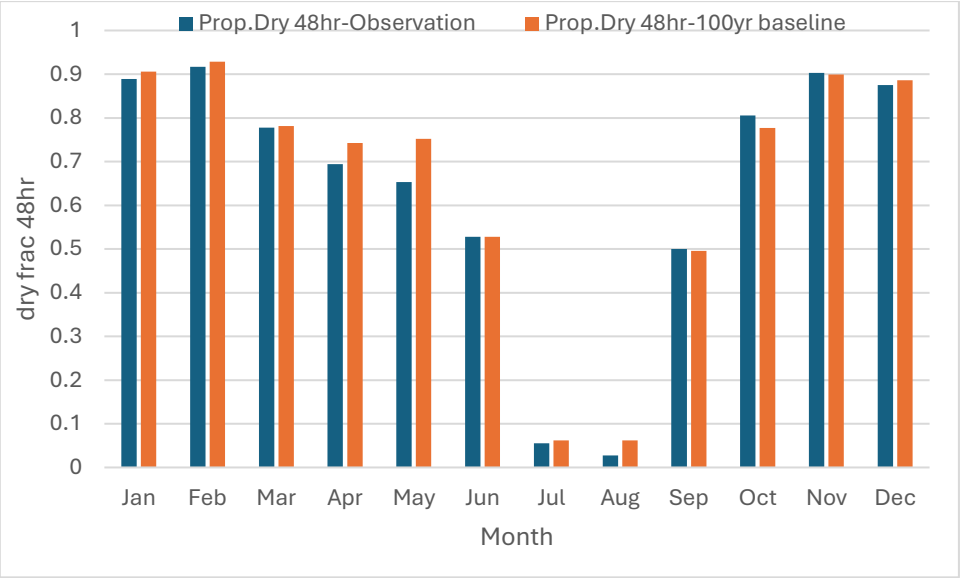

Figure 52. prop. Dry for 48hrs for precipitation Statistics for baseline and observation

Overall, despite some underrepresentation of extreme events, the model successfully simulates seasonal precipitation trends and dry-wet cycles, making it a valuable tool for long-term hydrological assessments in arid environments. While originally designed for wetter climates, its performance in this arid region is acceptable and useful for hydrological modeling.

5.3. STOCHASTICALLY GENERATED 100-YEAR ANNUAL PRECIPITATION TRENDS

The 100-year annual precipitation data, generated using a stochastic weather model, provides insight into long-term precipitation variability under different climate scenarios. The purpose of generating these scenarios was to explore how different assumed climatic changes.

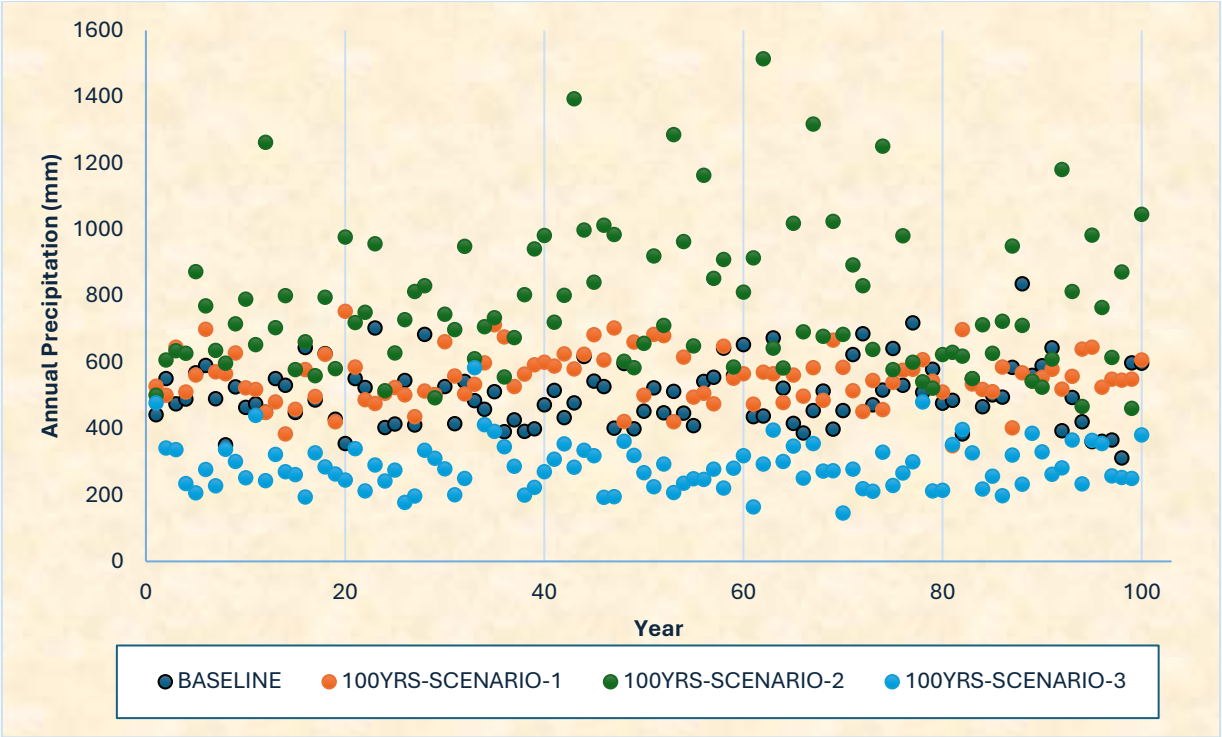

Figure 53. Stochastically Generated 100-Year Annual Precipitation Trends Under Different Climate Scenarios

As shown in Figure 53 above, the baseline scenario exhibits relatively stable annual precipitation trends, reflecting historical climate characteristics. Scenario 1, which was designed to introduce a moderate increase in precipitation intensity, follows a slightly higher trajectory than the baseline, though it remains within a comparable range.

In Scenario 2, where precipitation was set to be more intense and variable, the results align with this expectation. The annual precipitation shows significant fluctuations, with pronounced peaks and troughs, indicating a more extreme hydrological regime. This pattern suggests a future where wet years become wetter and dry years become drier, potentially increasing the risk of both flooding and drought periods.

Conversely, Scenario 3, which was constructed to represent a drying climate, demonstrates a clear reduction in total annual precipitation over time. The trend suggests a more prolonged dry period compared to the baseline, which could have implications for water resource availability and hydrological stress.

These results highlight how different assumed climate trajectories translate into long-term precipitation behaviour. The stochastic approach allows for a probabilistic assessment of potential future conditions, reinforcing the importance of climate-adaptive water management strategies.

5.4. HEC-HMS SIMULATION RESULTS

In this section, the result of the simulated are compared with the Gheba station serving as the outlet for comparison and validation

5.4.1. DISCHARGE SIMULATIONS RESULTS USING OBSERVED DATA 1999-2002

The simulated peak discharge is 83.5 m^3/s on 27 July 2000, while the observed peak discharge is 104.5 m^3/s on 2 August 2001. The mean annual total simulated volume is 50.13 mm/yr, slightly higher than the observed 48.77 mm/, showing a good match in overall water balance. The Nash-Sutcliffe

efficiency (NSE) of 0.719 indicates a strong model performance, capturing the general flow dynamics well.

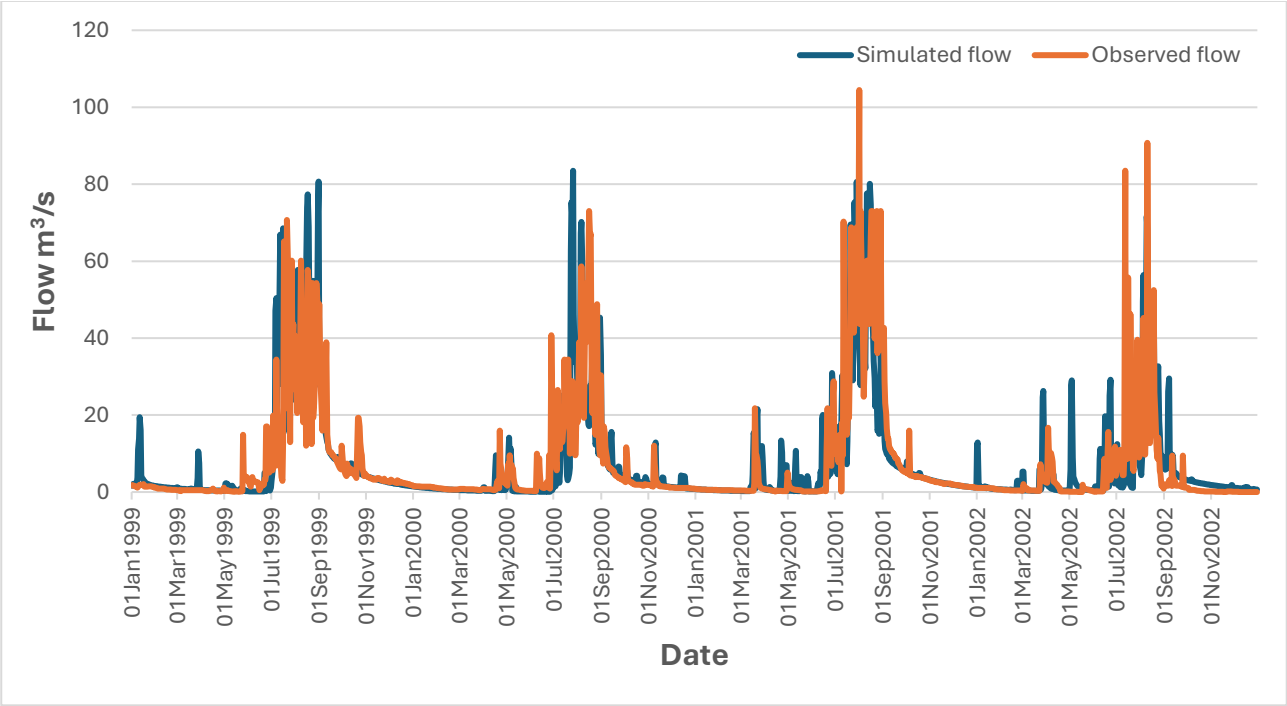

Figure 54. Observed and Simulated flow hydrograph using Observed precipitation over Gheba basin 1999-2002

The percent bias (-12.36%) suggests a slight underestimation of total flow but given the availability of only four years of daily flow data, achieving a perfect match, especially for peak flows, is challenging. Since daily data makes it difficult to capture exact peak discharges, the primary objective is to approximate the overall water balance, which the model does effectively.

The hydrograph shows a comparison of simulated and observed flow over time from 1999 to 2002. The model effectively captures the seasonal patterns and general trend of the observed discharge, especially during low and moderate flows. It successfully represents the timing of flow peaks and recessions, demonstrating a good overall performance in simulating the basin's hydrological response. However, during high-flow events, the observed discharge tends to be higher than the simulated values, indicating some underestimation of extreme flows.

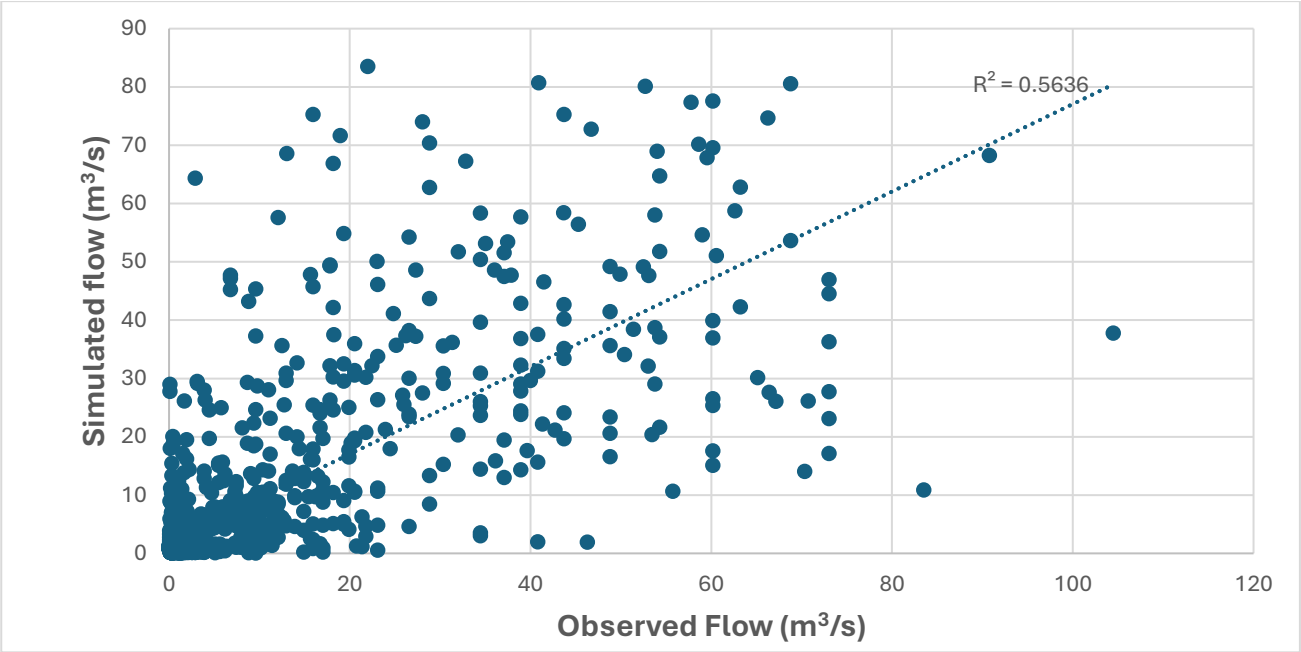

Figure 55. Scatter Plot of Observed Discharge and Simulated Discharge Using Observed precipitation data 1999-2002

The scatter plot compares simulated and observed discharge values, showing a moderate correlation ($R^2 = 0.5636$). While the model aligns well with lower flow values, there is greater scatter at higher discharge levels, indicating higher uncertainty in extreme flow conditions. The trend line suggests a general agreement, but significant deviations occur during peak flow events.

5.4.2. DISCHARGE SIMULATIONS RESULTS USING CHIRPS DATA 1999-2002

The simulated peak discharge is 94.5 m³/s on 28 July 2002, while the observed peak discharge is 104.5 m³/s on 2 August 2001. The mean annual total simulated volume is 54.86 mm, slightly higher than the observed 48.77 mm, showing a reasonable match in water balance. The Nash-Sutcliffe efficiency (NSE) is 0.557, and it indicates a moderate model performance, capturing the overall trend but with some deviations. The percent bias (12.49%) suggests a slight overestimation of total flow.

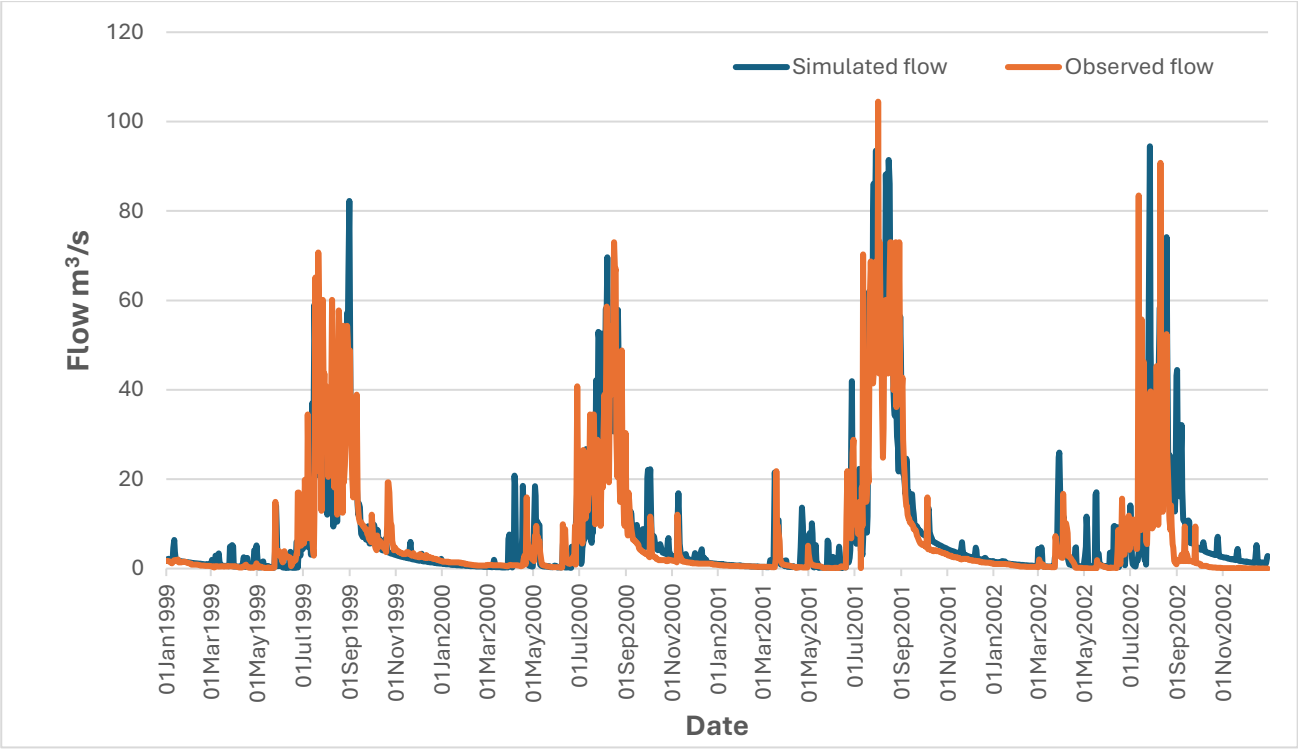

Figure 56. Observed and Simulated flow hydrograph using CHIRPS precipitation over Gheba basin 1999-2002

The hydrograph compares simulated and observed flow over time from 1999 to 2002. The model effectively captures the seasonal flow patterns and general discharge trends, closely following observed values during low and moderate flows. The timing of peak flows is well represented, demonstrating the model's ability to simulate the basin's hydrological response.

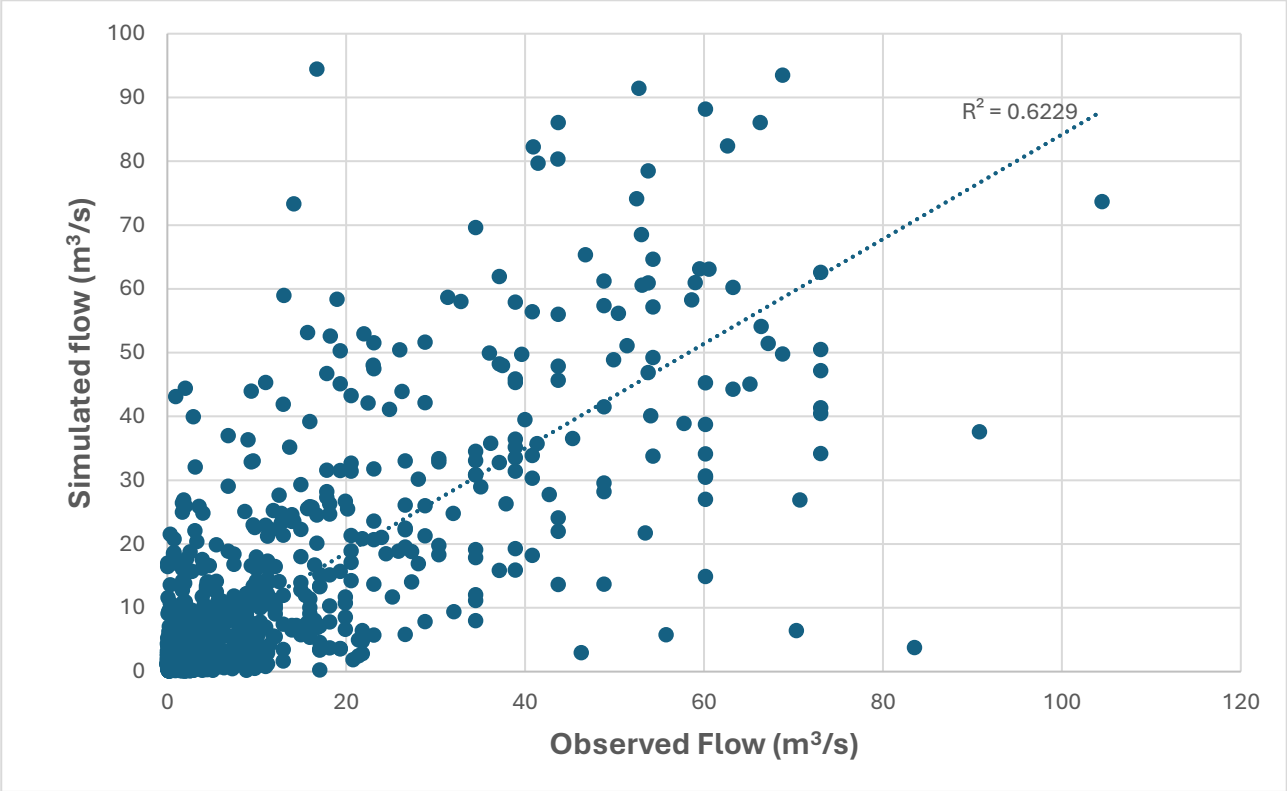

Figure 57. Scatter Plot of Observed Discharge and Simulated Discharge Using CHIRPS precipitation data 1999-2002

The scatter plot compares simulated and observed discharge, showing an R^2 value of 0.6229, which indicates a moderate correlation and better than the observation data condition. The model performs well in simulating lower flow values, aligning closely with observed data, though some scatter is present at higher discharges. The general trend suggests a good representation of flow variations, though some deviations occur, especially for extreme events.

5.4.3. DISCHARGE SIMULATIONS RESULTS USING TRMM DATA 1999-2002

The simulated peak discharge is 116.6 m^3/s on 12 August 2001, while the observed peak discharge is 104.5 m^3/s on 2 August 2001. The mean annual total simulated volume is 49.64 mm, which closely matches the observed 48.77 mm, indicating a strong representation of the water balance. The Nash-Sutcliffe efficiency (NSE) of 0.578 suggests a moderate model performance, with reasonable accuracy in simulating flow dynamics. The percent bias (1.76%) shows a minimal deviation, meaning the model does well in preserving overall flow volume.

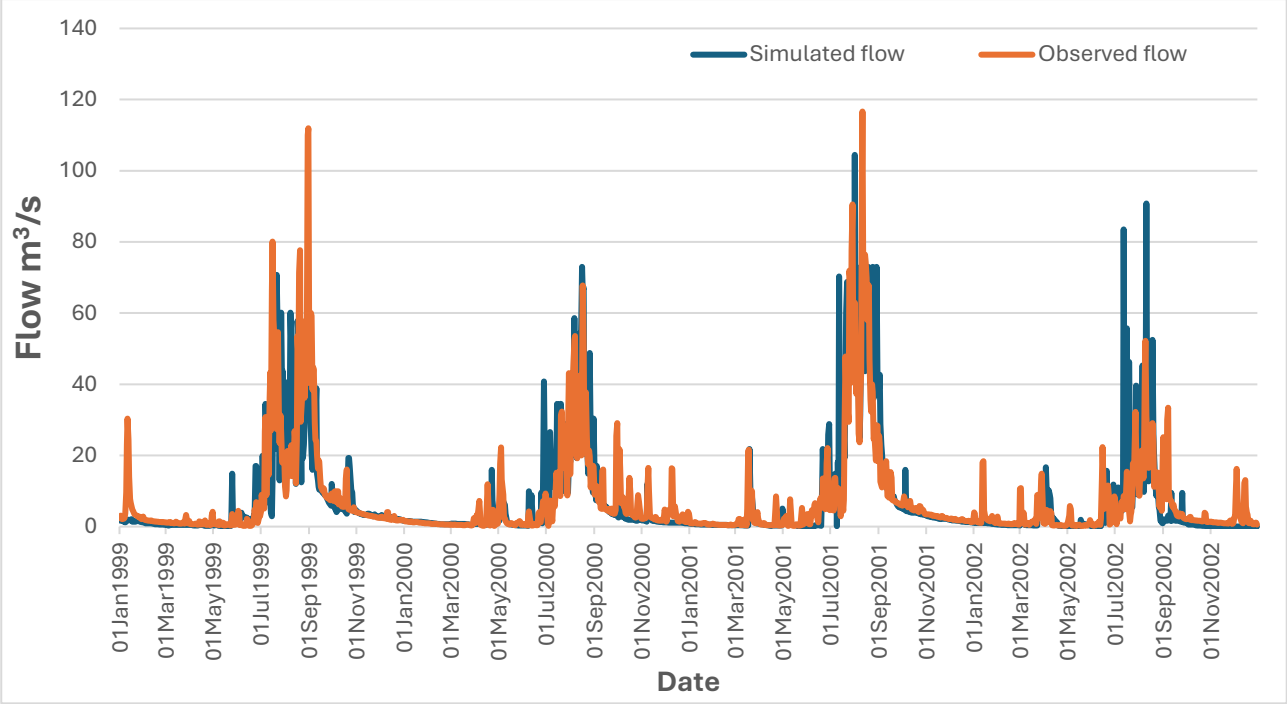

Figure 58. Observed and Simulated flow hydrograph using TRMM precipitation over Gheba basin 1999-2002

The model effectively captures seasonal variations, maintaining good alignment with observed trends, especially in low and moderate flows. The timing and magnitude of peak flows are well-represented, with some overestimations in certain high-flow events. Considering the four-year daily dataset, which poses challenges in perfectly capturing individual peak discharges, the model still provides a reliable simulation of the basin's overall hydrological response.

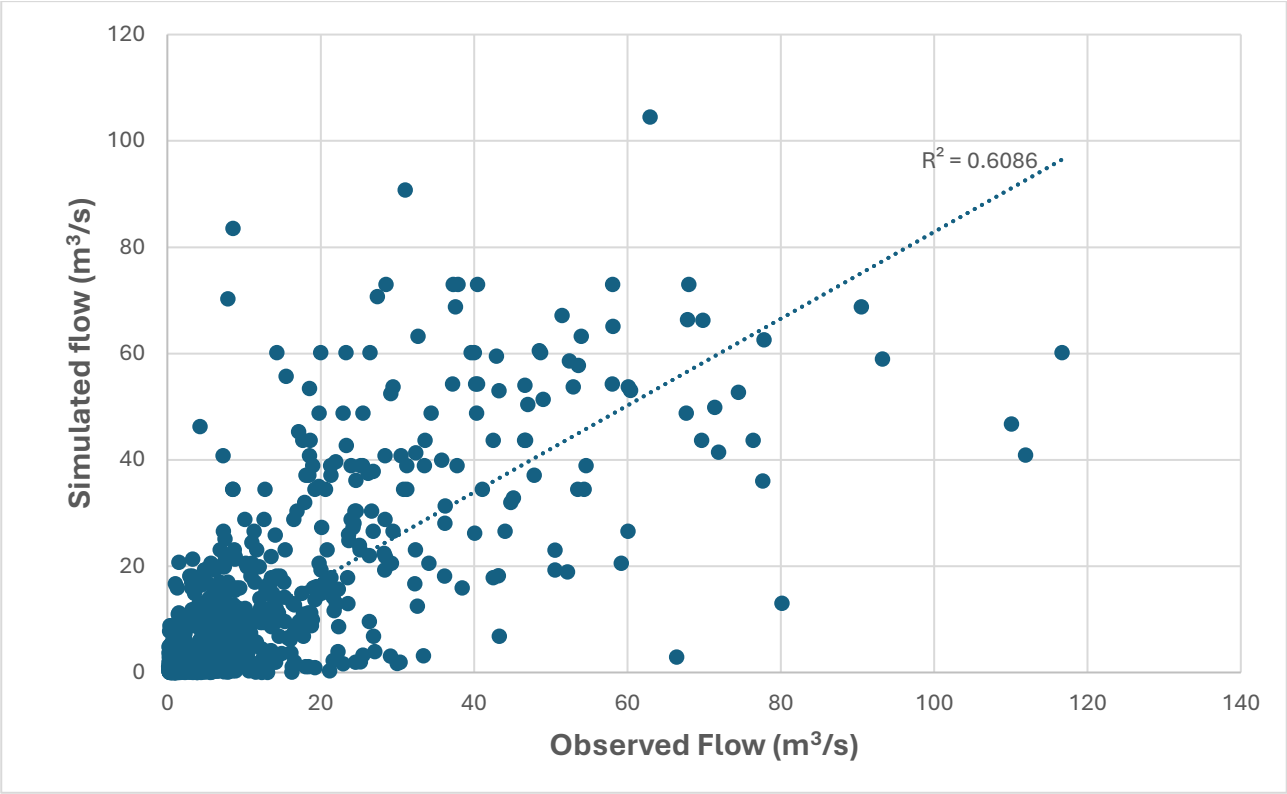

Figure 59. Scatter Plot of Observed Discharge and Simulated Discharge Using TRMM precipitation data 1999-2002

R^2 value of 0.6086, indicating a moderate correlation. The model performs well in simulating lower and moderate flow values, with a clear trend along the observed discharge line. While some scatter exists at higher discharge levels, this is expected given the limited four-year dataset, which makes it harder to capture extreme flow events precisely.

Overall, the model demonstrates a reasonable performance across all three datasets (Observed, CHIRPS, and TRMM), effectively capturing seasonal flow variations and maintaining a good representation of the overall water balance. While there are some discrepancies in peak discharge estimations, particularly in extreme flow events, the model still provides a moderate to strong correlation (NSE between 0.55 - 0.72, R^2 around 0.56 - 0.62) with observed data. Given the limited four-year daily dataset, the model performs well in approximating the basin's hydrological response, making it a useful tool for streamflow simulation.

5.4.4. STREAM FLOW ANALYSIS

MEAN STREAM FLOW ANALYSIS (MONTHLY)

This section presents the mean monthly streamflow analysis based on observed and simulated results using HEC-HMS with different precipitation datasets, including ground-observed precipitation,

TRMM, and CHIRPS. The comparison evaluates how well each dataset represents streamflow variability in the Gheba Basin. The shaded section in the table highlights the rainy season (June to September), the period of highest streamflow contributions in the basin.

Table 9. Mean monthly stream flow analysis of simulation based on observed against the global dataset 1999-2002

	Mean streamflow OBSERVED (m^3/s)				Simulated Mean streamflow based on GROUND OBSERVED precipitation (m^3/s)				Simulated Mean streamflow based on TRMM precipitation (m^3/s)				Simulated Mean streamflow based on CHIRPS precipitation (m^3/s)			
	Year															
Month	1999	2000	2001	2002	1999	2000	2001	2002	1999	2000	2001	2002	1999	2000	2001	2002
Jan	1.5	1.4	0.6	1.0	3.9	1.1	0.6	1.8	6.0	1.2	0.9	3.1	1.4	0.7	0.6	0.9
Feb	0.8	0.8	0.5	0.5	1.2	0.7	0.4	0.8	1.5	0.7	0.5	0.8	0.9	0.4	0.4	0.6
Mar	0.5	0.7	2.4	1.5	1.4	0.4	4.1	3.1	1.2	0.6	3.6	3.7	0.5	0.2	0.3	0.4
Apr	0.4	2.2	0.5	3.3	0.4	1.2	1.8	1.0	0.9	2.4	1.0	1.1	0.3	0.2	0.3	0.5
May	1.4	2.1	0.7	0.3	0.8	2.1	1.5	3.3	1.0	3.5	1.6	1.0	0.2	0.3	0.2	0.4
Jun	4.3	4.7	5.1	4.0	0.7	0.4	6.0	5.5	1.8	2.1	6.3	4.2	0.1	0.2	0.1	0.3
Jul	26.7	19.2	31.6	16.1	33.6	21.8	30.3	9.5	28.6	13.9	25.3	9.1	3.1	1.0	3.1	0.5
Aug	36.2	35.4	54.6	18.6	47.3	29.5	40.8	27.5	35.5	29.9	48.1	18.4	9.4	15.2	21.7	12.8
Sep	16.5	7.1	13.1	2.3	15.6	8.0	8.9	6.8	22.7	7.8	10.9	8.2	5.6	4.8	7.6	4.4
Oct	7.4	2.7	4.4	0.4	5.8	3.3	4.5	2.5	7.1	7.1	5.4	1.9	3.1	2.9	4.4	2.6
Nov	3.4	2.2	2.4	0.1	3.3	2.7	2.5	1.5	3.2	3.3	2.9	1.1	1.8	1.8	2.6	1.5
Dec	2.4	1.1	1.5	0.0	2.0	1.4	1.5	0.9	2.3	3.8	1.8	3.8	1.1	1.0	1.6	1.0

The results show a distinct seasonal trend, with streamflow increasing from May, peaking during the rainy season (June to September), and gradually decreasing towards the end of the year. Observed streamflow values reflect this pattern, with mean values of 4.3 m^3/s (June 1999), 26.7 m^3/s (July 1999), 36.2 m^3/s (August 1999), and 16.5 m^3/s (September 1999), showing significant variation across the years. In 2001, for example, August recorded the highest observed streamflow at 54.6 m^3/s, while in 2000, the highest value was in July at 31.6 m^3/s.

The simulated streamflow using ground-observed precipitation generally follows the observed trend but with some underestimations. For instance, in August 1999, the simulated streamflow was 47.3 m^3/s, slightly overestimated compared to the observed 36.2 m^3/s, while in July 2001, it was 21.8 m^3/s, lower than the observed 31.6 m^3/s.

The TRMM-based simulations capture the seasonal variation but show inconsistencies in magnitude. For example, in July 1999, the simulated streamflow is 28.6 m^3/s, which is higher than the observed 26.7 m^3/s, while in September 2000, it underestimates with 7.8 m^3/s compared to the observed 13.1 m^3/s.

The CHIRPS-based simulations consistently produce lower streamflow estimates than observed values. In August 1999, CHIRPS-based simulation resulted in 15.2 m^3/s, significantly lower than the observed 36.2 m^3/s. Similarly, in July 2001, the CHIRPS model estimated 9.1 m^3/s, much lower than the observed 31.6 m^3/s.

PEAK FLOW ANALYSIS (MONTHLY)

This section presents the monthly peak streamflow analysis based on observed and simulated results using HEC-HMS with different precipitation datasets, including ground-observed precipitation,

TRMM, and CHIRPS. The results compare observed peak flows with simulated values to evaluate the accuracy of different precipitation datasets in capturing high-flow events.

Table 10. Peak monthly stream flow analysis of simulation based on observed against the global dataset 1999-2002

	Peak streamflow OBSERVED (m^3/s)				Simulated Peak streamflow based on GROUND OBSERVED precipitation (m^3/s)				Simulated Peak streamflow based on TRMM precipitation (m^3/s)				Simulated Peak streamflow based on CHIRPS precipitation (m^3/s)			
	Year															
Month	1999	2000	2001	2002	1999	2000	2001	2002	1999	2000	2001	2002	1999	2000	2001	2002
Jan	2.1	1.6	0.8	1.1	19.5	1.5	12.9	1.8	30.3	1.6	2.3	18.4	6.4	1.6	1.0	1.6
Feb	1.2	1.1	0.5	0.6	1.5	0.9	3.0	0.8	2.1	0.9	0.8	1.7	1.3	0.6	0.6	0.9
Mar	0.5	0.8	21.8	7.3	10.6	0.5	26.3	3.1	3.2	2.4	21.6	14.9	5.3	7.7	21.5	25.9
Apr	1.2	15.9	5.1	16.7	0.5	9.6	4.6	1.0	4.1	11.9	8.5	4.8	5.2	20.8	13.6	11.5
May	14.9	9.6	3.3	1.9	2.3	14.1	29.0	3.3	3.5	22.2	7.6	5.8	14.1	18.5	10.1	17.1
Jun	17.0	40.8	28.8	15.6	5.0	2.0	29.2	5.5	6.8	9.3	22.0	22.3	10.3	18.2	41.9	9.6
Jul	70.7	34.5	70.3	83.5	68.6	83.5	28.0	9.5	80.1	43.1	90.5	32.3	59.0	53.0	93.5	94.5
Aug	60.1	73.0	104.5	90.8	80.7	70.2	71.6	27.5	111.9	67.8	116.6	52.2	82.3	69.6	91.4	74.1
Sep	48.8	17.0	42.7	9.4	35.6	16.0	29.5	6.8	60.1	29.1	25.5	33.4	57.4	22.1	36.4	44.4
Oct	19.3	11.6	15.9	1.0	7.7	5.7	3.3	2.5	16.1	21.7	8.5	3.9	9.9	22.2	13.4	7.1
Nov	4.3	12.0	3.1	0.2	4.1	12.9	1.8	1.5	4.0	16.5	3.5	1.7	5.9	16.8	5.9	4.4
Dec	3.3	1.2	1.9	0.1	2.7	4.3	1.3	0.9	4.1	16.4	2.2	16.2	3.3	4.3	4.7	5.3

The observed peak streamflow shows significant variation across months and years, with higher values recorded during the rainy season (June to September). For instance, in July 1999, the peak observed streamflow reached 70.7 m^3/s, while in August 2001, it recorded 104.5 m^3/s, the highest value in the dataset. Similarly, high peaks were observed in August 2000 (73.0 m^3/s) and July 2002 (83.5 m^3/s).

The simulated peak streamflow using ground-observed precipitation captures seasonal trends but underestimates extreme peaks in several cases. For instance, in August 2001, the observed peak was 104.5 m^3/s, while the simulation produced 71.6 m^3/s. Similarly, in July 1999, the observed peak was 70.7 m^3/s, whereas the simulation estimated 68.6 m^3/s, showing a closer approximation.
TRMM-Based Simulation:

TRMM-based simulations show inconsistencies, with some cases of overestimation and underestimation. For example, in August 1999, the observed peak was 60.1 m^3/s, while the TRMM-based simulation resulted in 111.9 m^3/s, significantly overestimating the actual value. However, in July 2001, the TRMM simulation recorded 43.1 m^3/s, much lower than the observed 70.3 m^3/s.

CHIRPS-based simulations generally underestimate peak flows compared to observed values. In August 2001, the observed peak was 104.5 m^3/s, while CHIRPS estimated 91.4 m^3/s. Similarly, in July 2000, the observed peak was 34.5 m^3/s, while CHIRPS simulated 53.0 m^3/s, indicating an overestimation.

During the dry months, peak streamflow values remain significantly lower across all datasets. For instance, in December 1999, the observed peak was 3.3 m^3/s, while simulated values from ground precipitation, TRMM, and CHIRPS were 2.7 m^3/s, 3.4 m^3/s, and 3.3 m^3/s, respectively, showing relatively smaller differences.

5.4.5. PRECIPITATION PARTITIONING

In this section, the precipitation partitioning was done for all the datasets and the pie charts along with the percentage of the hydrological components explain in depth the partitioning over the basin.

5.4.5.1. PARTITIONING USING OBSERVATION DATA 1999-2002

Over the four-year period, mean annual total observed precipitation in the Gheba Basin amounted to 574.3 mm/yr, of which 50.14 mm/yr (≈8.73%) was converted into streamflow close to the 48.77mm/yr mean flow recorded at the Adi-Kumsi streamflow station. A significant portion of the precipitation was lost through evapotranspiration (ET), with 301.6 mm/yr (52.5%) attributed to canopy interception and 1.95 mm/yr (0.34%) to surface evaporation. Aquifer recharge contributed 255 mm/yr (44.4%), emphasizing the dominance of infiltration-driven processes in the basin. The runoff coefficient (Cr), calculated as the ratio of total flow to precipitation, was 0.087 (8.7%), indicating that only a small fraction of rainfall contributes directly to runoff.

In 1999, total precipitation reached 678.57 mm/yr, with total simulated flow of 62.89 mm/yr, yielding a runoff coefficient of 0.093. Baseflow contributed 22.17 mm/yr, while direct runoff accounted for 15.43 mm/yr, indicating that groundwater recharge played a significant role in sustaining flows. Evapotranspiration was relatively high, reaching 213.99 mm/yr, while aquifer recharge was estimated at 430.18 mm/yr, emphasizing the infiltration-dominated hydrological response.

During 2000, precipitation decreased to 486.52 mm/yr, resulting in a simulated total flow of 33.72 mm/yr and a runoff coefficient of 0.069. Baseflow contribution was 12.13 mm/yr, while direct runoff was only 8.85 mm/yr, reinforcing the infiltration-driven nature of the basin. The evapotranspiration rate increased to 230.02 mm/yr, suggesting that most of the rainfall was lost through ET processes, while aquifer recharge was recorded at 230.80 mm/yr.

Precipitation levels increased again in 2001, reaching 683.48 mm/yr, with a corresponding increase in total simulated flow to 50.94 mm/yr and a runoff coefficient of 0.075. Baseflow increased to 18.62 mm/yr, while direct runoff was 13.24 mm/yr, highlighting an improved surface flow contribution compared to 2000. Evapotranspiration also peaked at 287.69 mm/yr, which was the highest in the four-year period. Aquifer recharge remained substantial at 346.84 mm/yr, maintaining the infiltration-dominated water balance.

In 2002, precipitation was at its lowest, with 448.80 mm/yr recorded. Consequently, total flow was also at a minimum (26.99 mm/yr), resulting in a runoff coefficient of 0.060, the lowest of all four years. Baseflow was 9.54 mm/yr, while direct runoff was 7.72 mm/yr, indicating extremely low surface water contribution. Evapotranspiration remained high at 260.17 mm/yr, while aquifer recharge was measured at 178.70 mm/yr, demonstrating that even in drier years, a significant proportion of precipitation infiltrates into the subsurface.

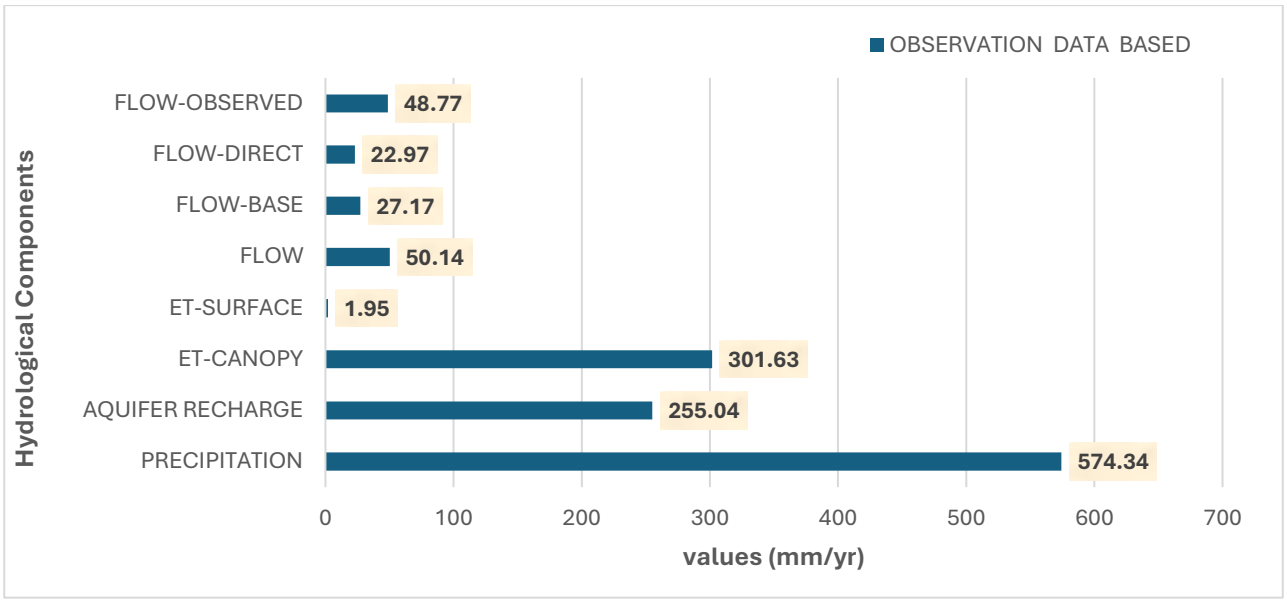

Figure 60. Mean Annual Water Balance for Gheba Basin for Observation Data 1999-2002

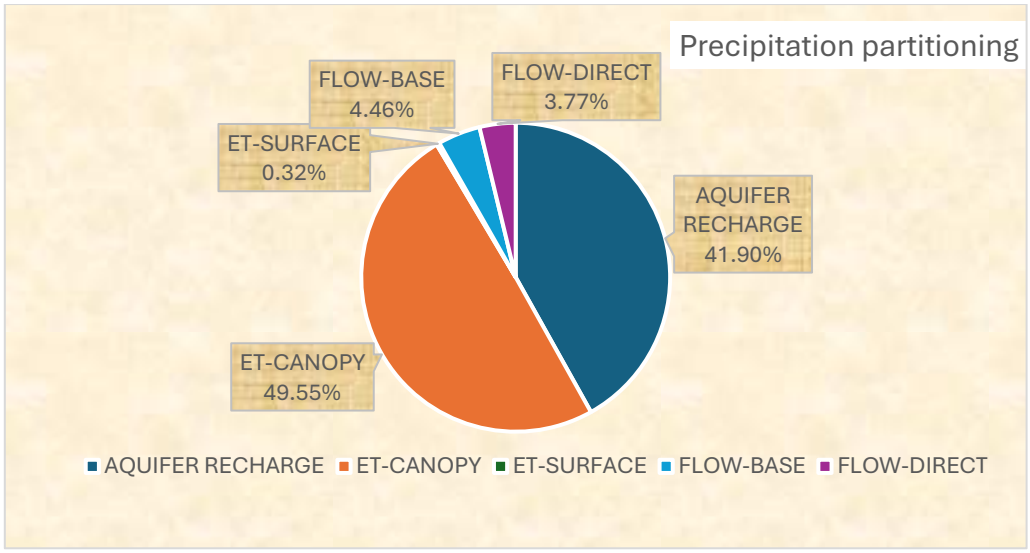

Figure 61. Mean Annual Precipitation partitioning (%) for Gheba Basin for Observation Data 1999-2002

5.4.5.2. PARTITIONING USING TRMM DATA 1999-2002

The HEC-HMS model was further tested using TRMM precipitation data to compare how satellite-based precipitation influences streamflow simulation in the Gheba Basin. The mean annual total precipitation recorded using TRMM data from 1999 to 2002 was 633.9 mm/yr, slightly higher than the observed precipitation dataset. The simulated total flow volume was 49.64 mm/yr slightly above, observed 48.77 mm/yr at Adi-Kumsi station, indicating a close match but with some discrepancies in flow partitioning.

For the year 1999, total precipitation from TRMM was 704.06 mm/yr, with total flow simulated at 62.85 mm/yr, resulting in a runoff coefficient of 0.089. Aquifer recharge accounted for 354.84 mm/yr, while evapotranspiration was 351.78 mm/yr, demonstrating an infiltration-dominated water cycle.

In 2000, precipitation dropped to 602.95 mm/yr, leading to a total flow of 43.09 mm/yr and a runoff coefficient of 0.071. Aquifer recharge decreased to 164.00 mm, while evapotranspiration (418.27 mm/yr) remained relatively high, indicating significant moisture loss through atmospheric processes.

Precipitation increased to 729.18 mm/yr in 2001, with a total flow of 61.02 mm/yr, yielding a runoff coefficient of 0.084. Aquifer recharge was measured at 298.10 mm/yr, and ET-canopy loss reached 383.99 mm/yr, showing a balanced distribution between infiltration and atmospheric loss.

In 2002, precipitation was at its lowest, with 499.42 mm/yr recorded, resulting in total simulated flow of 31.57 mm, corresponding to a runoff coefficient of 0.063. Aquifer recharge (100.13 mm/yr) and evapotranspiration (388.18 mm/yr) dominated the water balance, reinforcing the low runoff potential of the basin.

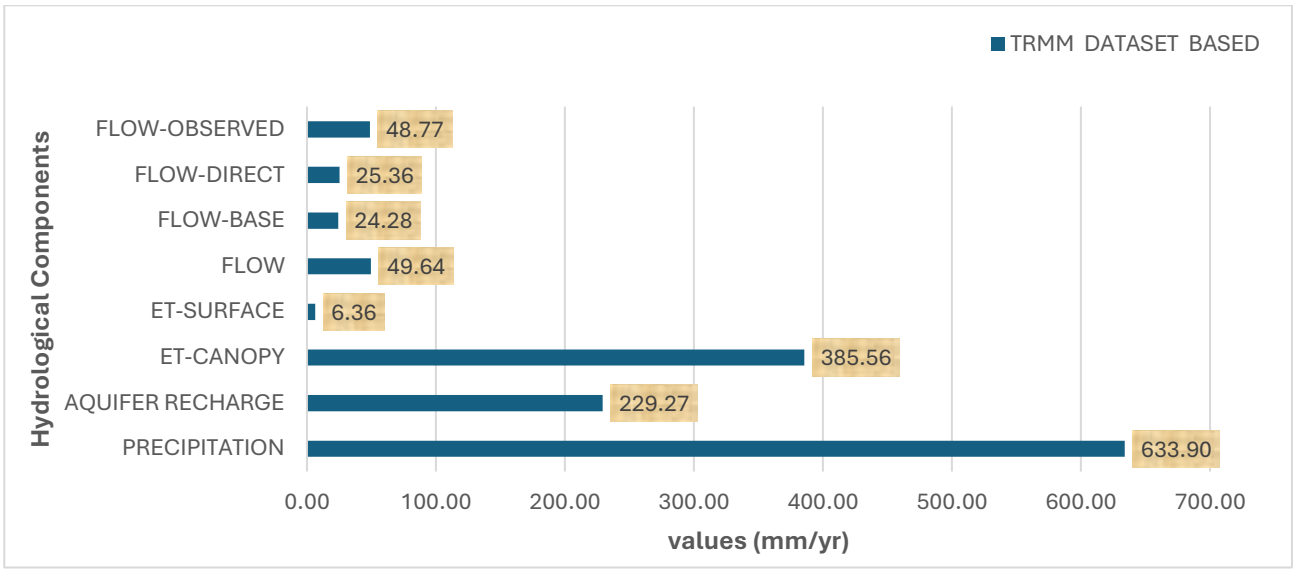

Figure 62. Mean Annual Water Balance for Gheba Basin for TRMM Data 1999-2002

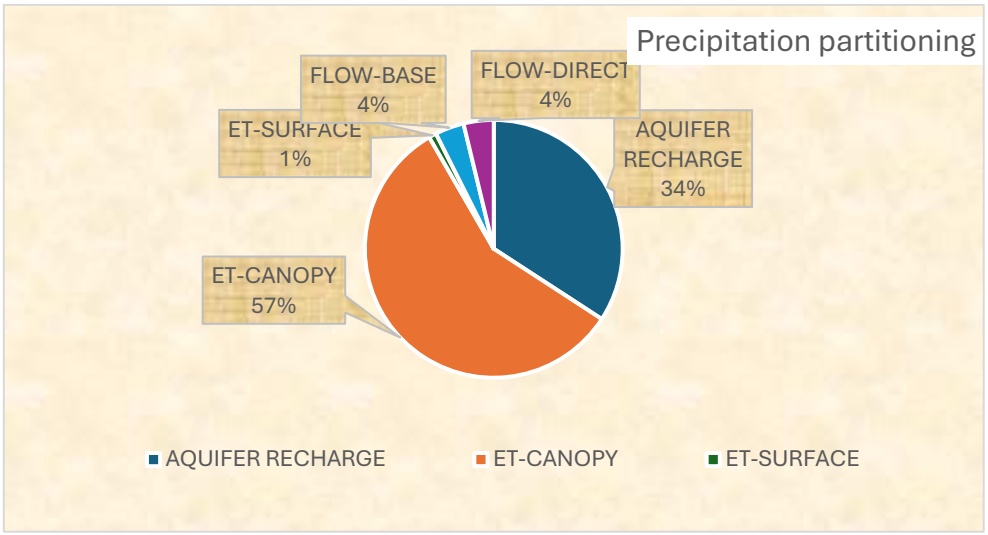

Figure 63. Mean Annual Precipitation partitioning (%) for Gheba Basin for Observation Data 1999-2002

5.4.5.3. PARTITIONING USING CHIRPS DATA 1999-2002

The mean annual total precipitation recorded using CHIRPS data from 1999 to 2002 was 661.46 mm/yr, which is slightly higher than the TRMM dataset and the observed precipitation dataset. The simulated total flow volume was 54.86 mm/yr, compared to the observed flow at station and also the simulated flow using TRMM data, indicating a slight overestimation but still within a reasonable range.

Annual Hydrological Breakdown Using CHIRPS Data For the year 1999, total precipitation from CHIRPS was 710.36 mm/yr, with total flow simulated at 65.34 mm/yr, resulting in a runoff coefficient of 0.092. Aquifer recharge accounted for 360.12 mm, while evapotranspiration was 354.90 mm/yr, demonstrating an infiltration-dominated hydrological cycle.

In 2000, precipitation decreased to 618.21 mm/yr, leading to a total flow of 45.11 mm/yr and a runoff coefficient of 0.073. Aquifer recharge dropped to 170.50 mm/yr, while evapotranspiration remained relatively high at 421.60 mm/yr, indicating significant moisture loss through atmospheric processes.

Precipitation increased to 748.75 mm/yr in 2001, with a total flow of 63.27 mm/yr, yielding a runoff coefficient of 0.085. Aquifer recharge was measured at 305.45 mm/yr, and evapotranspiration losses reached 390.03 mm/yr, showing a balance between infiltration and atmospheric moisture loss.

In 2002, precipitation was at its lowest, with 568.52 mm/yr recorded, resulting in total simulated flow of 38.22 mm/yr, corresponding to a runoff coefficient of 0.067. Aquifer recharge (120.75 mm/yr) and evapotranspiration (409.55 mm/yr) dominated the water balance, reinforcing the low runoff potential of the basin.

Overall, the CHIRPS data provided reasonable streamflow simulations, capturing the general hydrological dynamics of the basin.

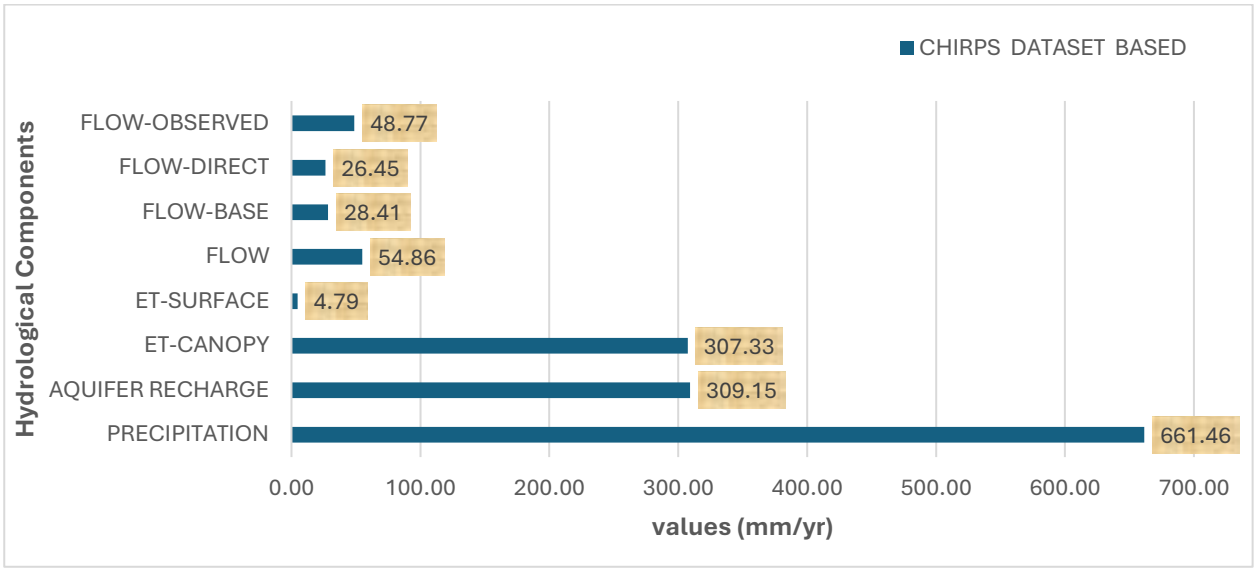

Figure 64. Mean Annual Water Balance for Gheba Basin for CHIRPS Data 1999-2002

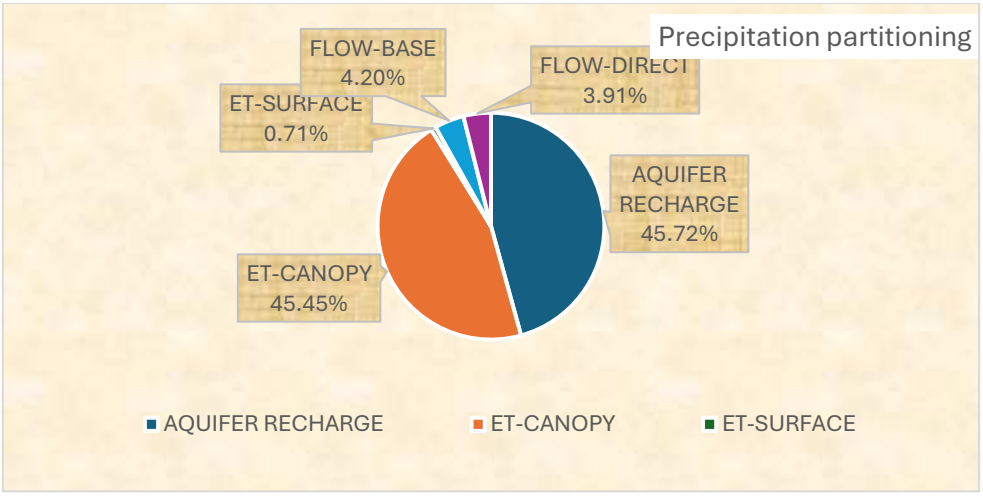

Figure 65. Mean Annual Precipitation partitioning (%) for Gheba Basin for Chirps Data 1999-2002

Generally, plotting the mean annual water balance for the simulation based on observed and global precipitation for Gheba basin presented in the figure 66.

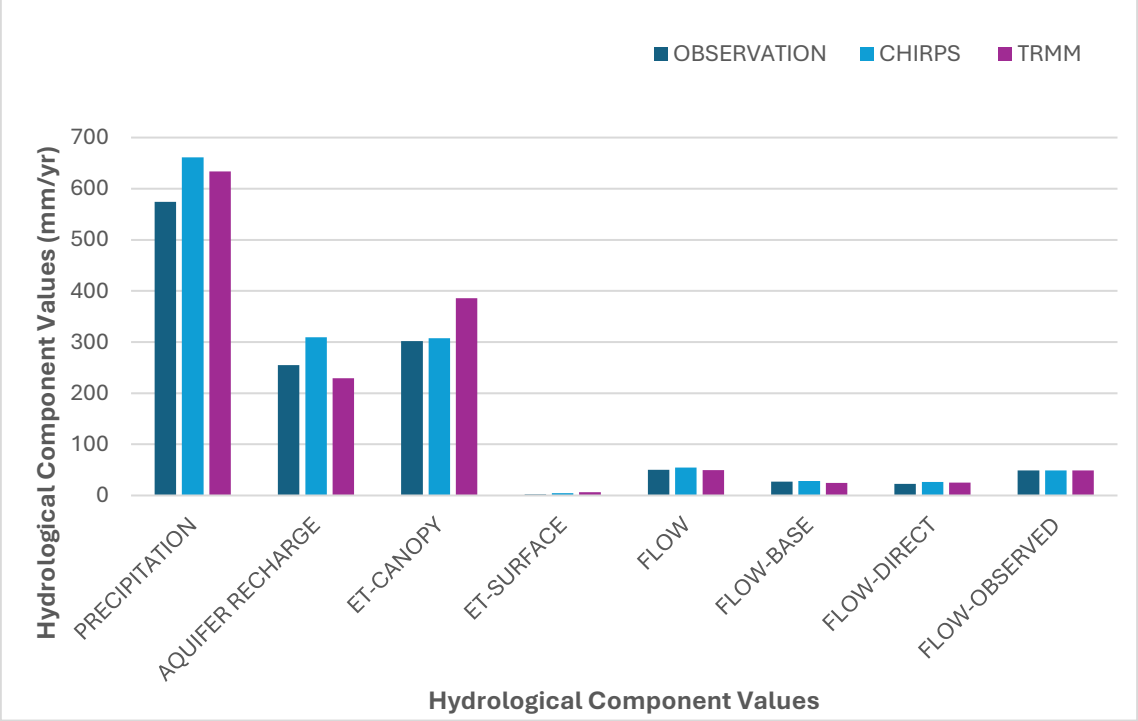

Figure 66. Mean Annual Water Balance for Gheba Basin for Observation and Global Datasets 1999-2002

5.5. MODEL SIMULATION FOR STOCHASTICALLY GENERATED DATA

5.5.1. SIMULATION FOR BASELINE CLIMATE (CURRENT CLIMATE)

The Baseline Climate Scenario represents the current precipitation conditions based on historical observations. The 100-year stochastic hourly rainfall dataset was generated and subsequently aggregated to daily values to align with the temporal resolution of the HEC-HMS hydrological model calibration. This approach ensures that the precipitation input accurately reflects observed climate variability while maintaining model consistency. The hydrological simulation under the baseline scenario provides a reference for comparing future climate change impacts. Key hydrological

components such as runoff generation, infiltration, evapotranspiration, and streamflow responses were assessed using the HEC-HMS model. The results from the simulation under baseline conditions see figure (67-68).

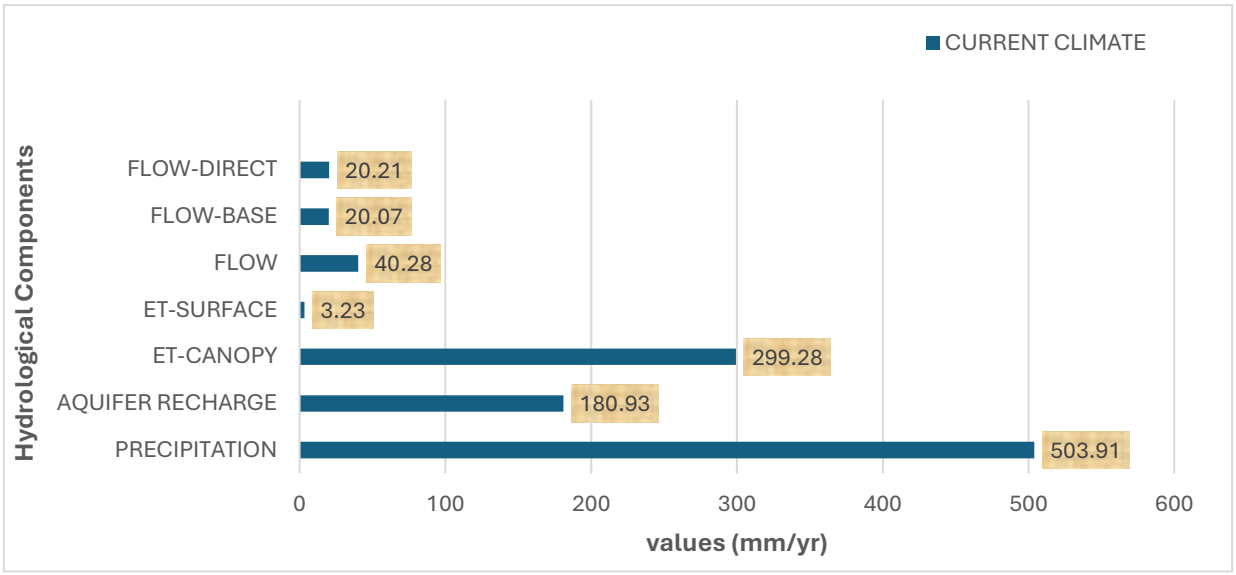

Figure 67. 100yrs Mean Annual Water Balance for Gheba Basin for Baseline Climate Scenario

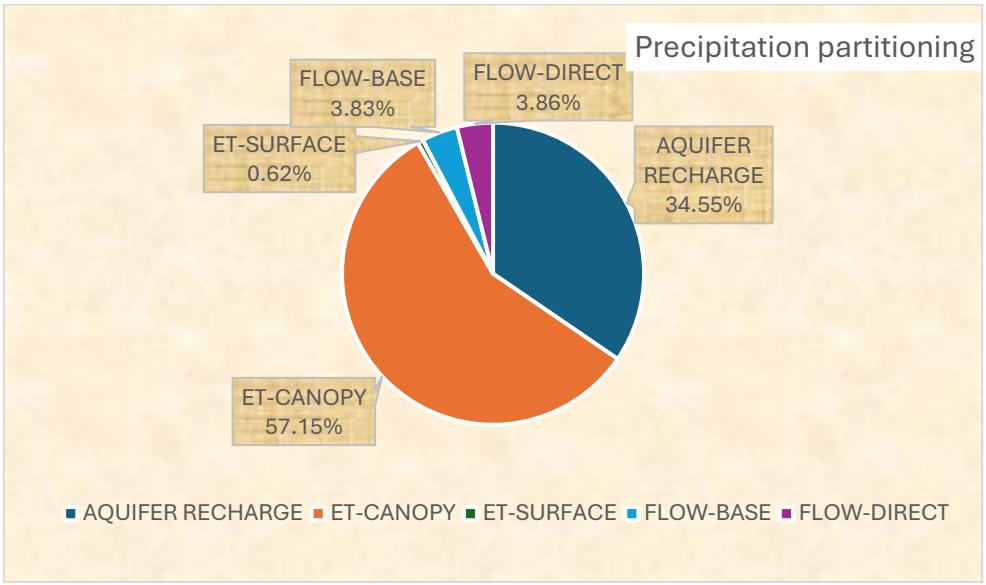

Figure 68. 100yrs Mean Annual Precipitation partitioning (%) for Gheba Basin for Baseline Climate Scenario

Under current climate conditions, mean annual total precipitation over the 100yrs is 503.91 mm/yr, partitioned primarily into evapotranspiration ET canopy 57% and aquifer recharge 34%, with direct flow 4% and base flow 4% contributing relatively small amounts. This indicates a balanced hydrological system, where most precipitation is either evaporated or percolates into groundwater, with minimal runoff.

5.5.2. SIMULATION FOR SCENARIO-1 (MODERATE INCREASE SCENARIO)

A 10% increase in mean annual precipitation and a 17% increase during the peak rainy season (July-September). The Moderate increased scenario results are presented in the following figures (69 -70)

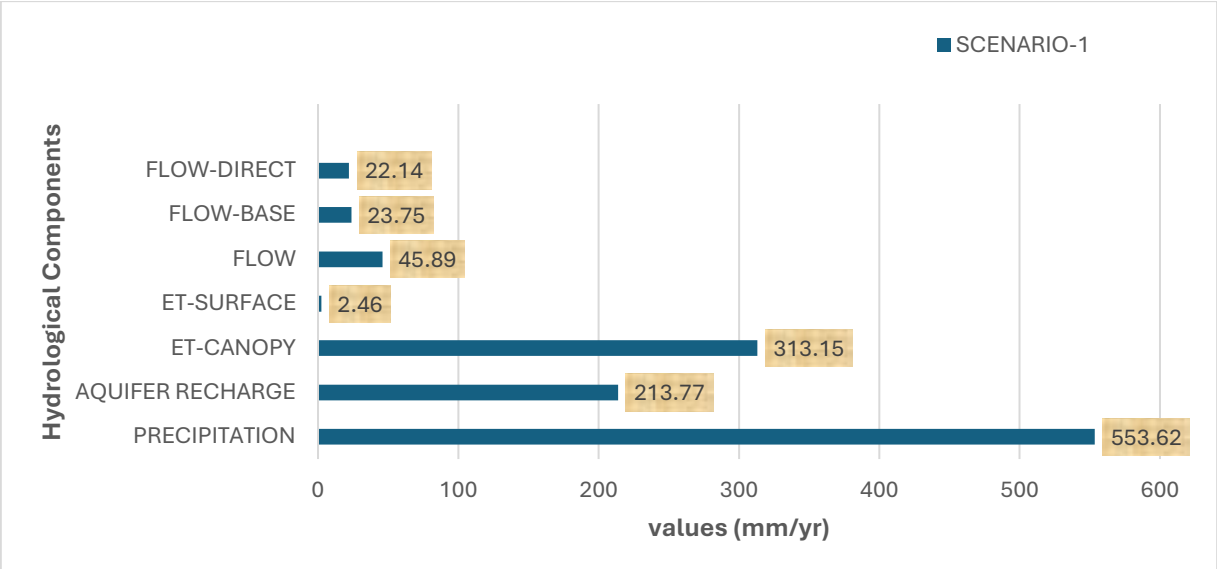

Figure 69. 100yrs Mean Annual Water Balance for Gheba Basin for Moderate Increase Scenario

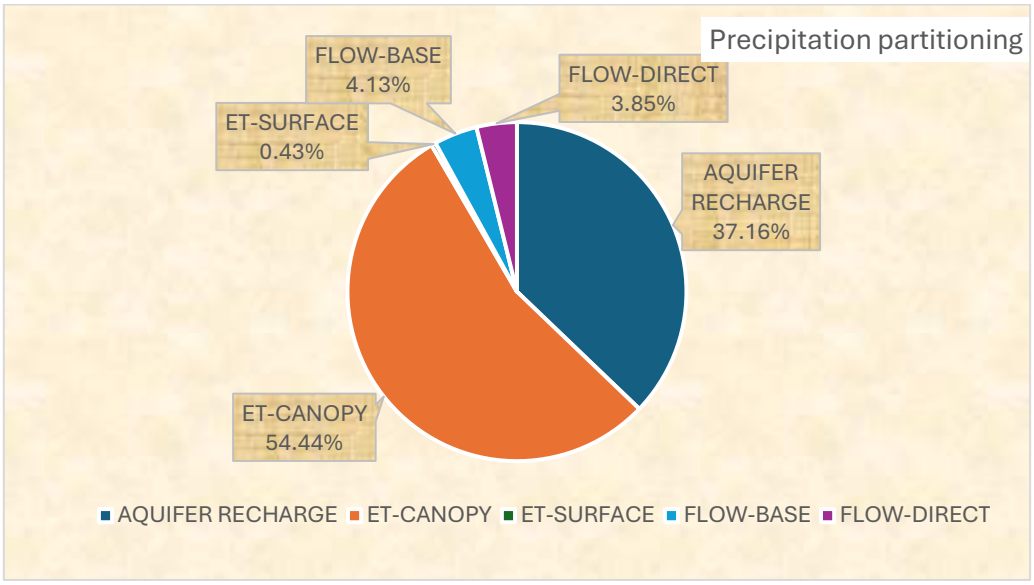

Figure 70. 100yrs Mean Annual Precipitation partitioning (%) for Gheba Basin for Moderate Increase Scenario

Scenario 1 applies a 10% increase in mean annual precipitation and a 17% increase during peak rainy months, leading to a 10% rise in mean annual total precipitation (553.62 mm/yr) compared to the baseline (503.91 mm/yr). This increase contributes to an 18% rise in aquifer recharge and a 5% increase in ET canopy. Flow components also see a moderate increase, with total flow rising by 14%, base flow increasing by 18%, and direct flow increasing by 10%. The ET surface component decreases by 24%, suggesting that additional precipitation is being absorbed into storage rather than evaporating directly. Overall, Scenario 1 maintains a similar partitioning structure to the baseline but enhances storage components, indicating a moderate but stable shift in hydrological balance without significantly altering the surface runoff response.

5.5.3. SIMULATION FOR SCENARIO-2 (INTENSIFIED RAINFALL SCENARIO)

The 24-hour mean precipitation was increased by 30%, reflecting a wetter future climate, while the 24-hour variance was increased by 50%, amplifying the intensity of extreme rainfall events. The Intensified rainfall scenario results are presented in the following figures (71 - 72)

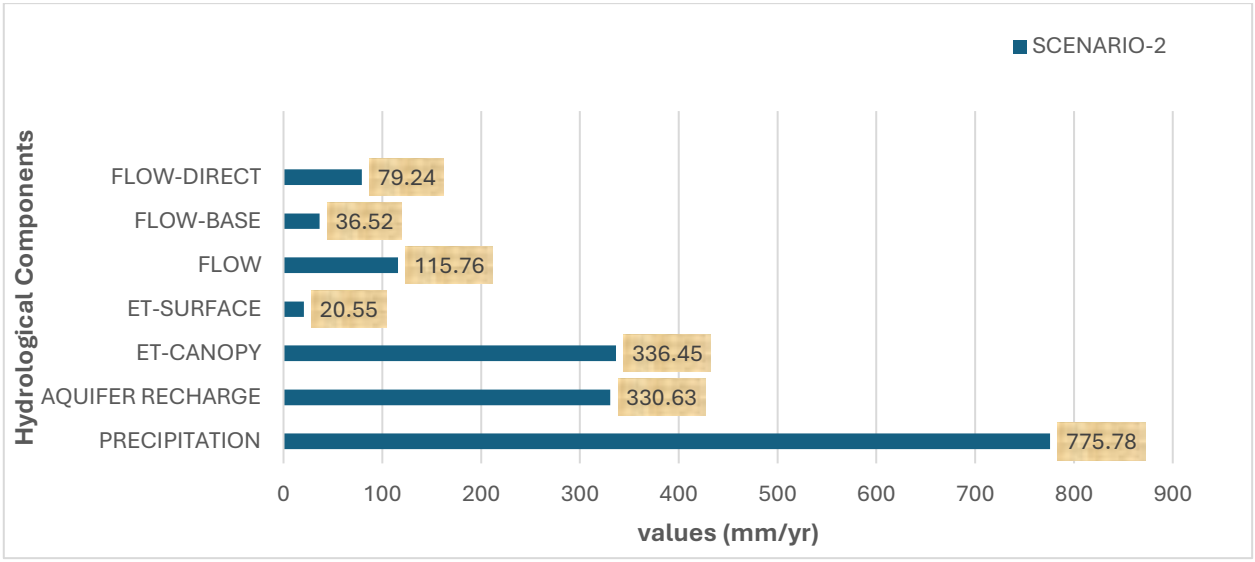

Figure 71. 100yrs Mean Annual Water Balance for Gheba Basin for Intensified Rainfall Scenario

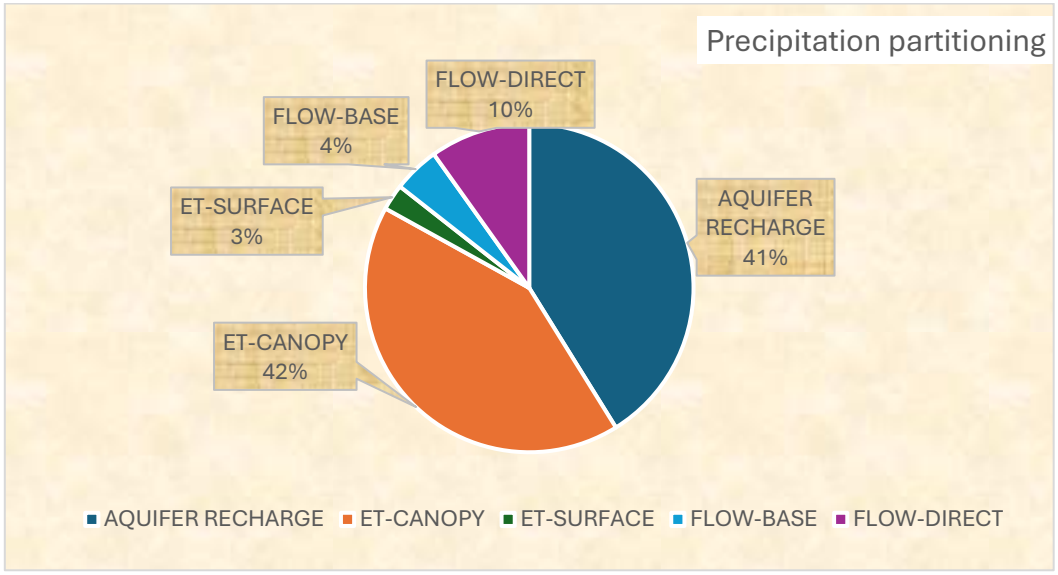

Figure 72. 100yrs Mean Annual Precipitation partitioning (%) for Gheba Basin for Intensified Rainfall Scenario

Scenario 2 represents a more extreme wet climate, with a 30% increase in mean precipitation and a 50% increase in variance, simulating intense and frequent rainfall bursts. The mean annual total precipitation increases to 775.78 mm/yr, a 54% increase compared to the baseline. This change compared to the current climate, significantly increase to a substantial rise in aquifer recharge (83% increase) and ET canopy (12% increase). Surface flow components experience the largest changes, with total flow increasing substantially (187% increase), base flow rising (82% increase), and direct flow surging to (292% increase). These shifts indicate a much greater proportion of precipitation contributing to runoff, increasing flood risks. ET surface increases significantly, from 3.23 mm/yr to 20.55 mm/yr, further confirming the presence of short-duration high-intensity storms that result in higher evaporation losses.

5.5.4. SIMULATION FOR SCENARIO-3 (PROLONGED DRY SCENARIO)

Scenario 3 introduces a 30% reduction in mean precipitation and increased dry fraction, leading to a 43% decrease in total precipitation (287.13 mm/yr) compared to the baseline. This reduction

translates into a 53% drop in aquifer recharge, severely limiting groundwater replenishment. ET canopy falls by 37% due to reduced moisture availability, further emphasizing the drying trend. Flow components are drastically reduced, with total flow dropping by 48%, base flow declining to 9.67 mm/yr (-52%), and direct flow decreasing to 11.49 mm/yr (-43%). These changes indicate a severe decline in available water resources, increased risk of hydrological drought, and reduced streamflow sustainability

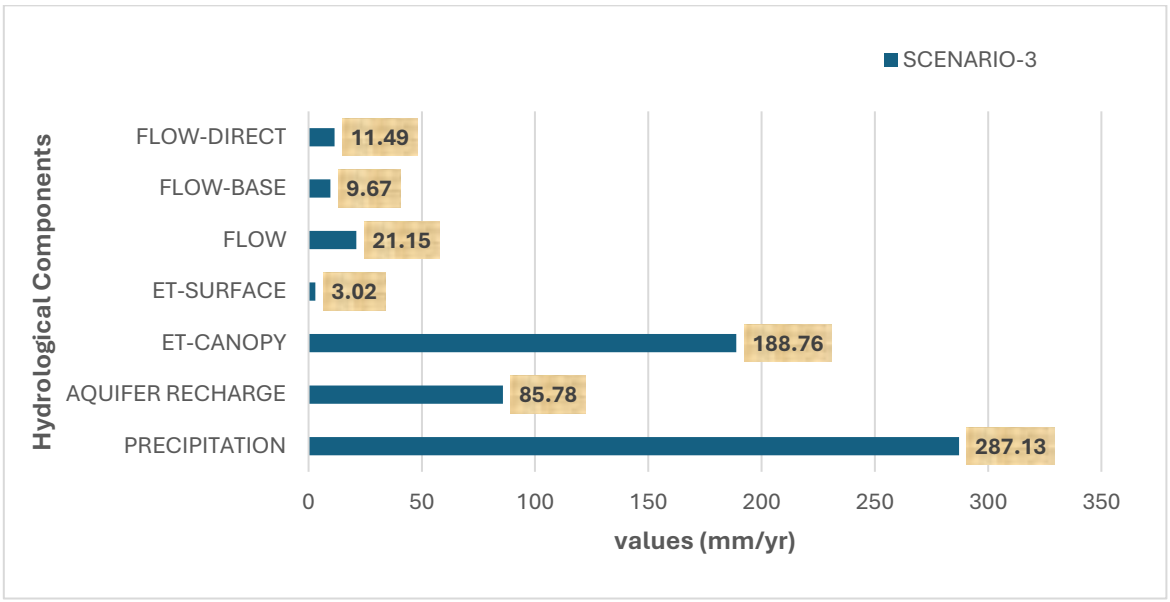

Figure 73. 100yrs Mean Annual Water Balance for Gheba Basin for Prolonged Dry Scenario

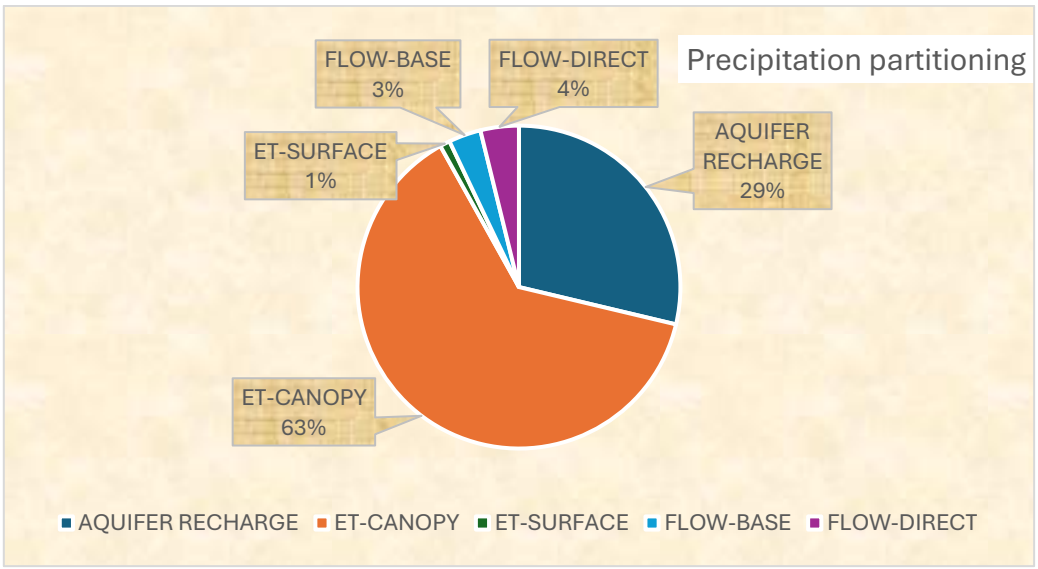

Figure 74. 100yrs Mean Annual Precipitation partitioning (%) for Gheba Basin for Prolonged Dry Scenario

5.5.5. SUMMARY OF THE HYDROLOGIC PARTITIONING FOR STOCHASTIC EXPERIMENTS

Table 11. Summary of 100yrs Mean Annual Hydrologic Partitioning for stochastically generated experiments

Hydrological Components Mean annual for 100yrs	CURRENT CLIMATE (mm)	SCENARIO-1 (mm)	SCENARIO-2 (mm)	SCENARIO-3 (mm)
Precipitation	503.91	553.62	775.78	287.13
Aquifer Recharge	180.93	213.77	330.63	85.78
Et-Canopy	299.28	313.15	336.45	188.76
Et-Surface	3.23	2.46	20.55	3.02
Flow-Base	20.07	23.75	36.52	9.67
Flow-Direct	20.21	22.14	79.24	11.49
Flow-Total	40.28	45.89	115.76	21.15

Comparing Scenario 2 with Scenario 1, the intensified rainfall pattern leads to a 40% increase in precipitation beyond the moderate increase scenario. This results in a 55% increase in aquifer recharge (from 213.77 mm mm/yr to 330.63 mm mm/yr), indicating that a significant portion of the excess rainfall is stored as groundwater. However, direct runoff sees the most dramatic shift, with Scenario 2 producing nearly four times the direct flow of Scenario 1 (79.24 mm/yr vs. 22.14 mm mm/yr). This indicates that Scenario 2 presents a much more volatile hydrological balance, shifting towards flash flood conditions. The increase in total flow from 45.89 mm mm/yr in Scenario 1 to 115.76 mm mm/yr in Scenario 2 (152% increase) suggests that excess rainfall in Scenario 2 does not translate proportionally to groundwater recharge, highlighting a higher risk of rapid surface runoff and potential erosion.

When comparing the moderate increase scenario (Scenario 1) with the prolonged dry scenario (Scenario 3), the contrast in water availability becomes evident. Scenario 3 has 48% less total flow, 60% less aquifer recharge, and significantly lower ET canopy losses, reflecting the impacts of extended dry conditions. While Scenario 1 enhances storage and maintains a stable hydrological balance, Scenario 3 shifts the system into a state of extreme water scarcity, where both surface and groundwater supplies are reduced.

Comparing Scenario 2 with Scenario 3 highlights the two extreme ends of hydrological response. Scenario 2 experiences a 187% increase in total flow compared to Scenario 3, emphasizing intensified runoff and flood risks, whereas Scenario 3 faces water scarcity and reduced groundwater recharge. ET canopy in Scenario 3 is 44% lower than in Scenario 2, reinforcing the stress on vegetation and reduced atmospheric moisture exchange. Direct flow in Scenario 3 is 85% lower than in Scenario 2, demonstrating the shift from flood-prone conditions to extreme drought.

The comparative analysis shows that Scenario 1 presents a balanced increase in water availability, improving groundwater storage while maintaining a stable hydrological system. Scenario 2 introduces extreme rainfall patterns, increasing flood risks and surface runoff, potentially leading to soil erosion and water management challenges. Scenario 3, in contrast, highlights severe reductions in water availability, emphasizing the vulnerability of the Gheba Basin to prolonged dry conditions.

These findings underscore the need for adaptive water resource management strategies to mitigate the risks associated with both extreme wet and dry climate futures.

While the hypothetical scenarios were designed to represent different hydrological extremes, the resulting simulations reveal some deviations from initial expectations. For instance, Scenario 3 was structured to introduce a 30% reduction in mean precipitation, yet the total precipitation decrease observed in the stochastic simulations was 43%. This discrepancy likely arises from the inherent variability in the 100-year synthetic dataset, which is based on a 4-year observed precipitation record. Stochastic generation introduces fluctuations that may not always align perfectly with the predefined scenario assumptions, particularly over shorter sample periods. These variations highlight the complexity of hydrological responses and emphasize the importance of interpreting results within the broader statistical context of long-term climate simulations.

The imposed scenario modifications aimed to simulate distinct hydrological responses, yet the model outputs showed some deviations from expectations. In Scenario 1, the 10% precipitation increase led to a 9.9% rise, closely aligning with expectations.

Scenario 2 (Intensified Rainfall): The imposed 30% increase in 24-hour mean precipitation imposed and 50% increase in 24-hour variance likely contributed to the larger-than-expected 54% increase in total precipitation instead of the intended 30%. This suggests that the model's stochastic structure amplified extreme rainfall events more than anticipated. The increase in variance essentially made the precipitation distribution more uneven, favouring high-intensity rainfall events, which explains the stronger surface runoff response rather than proportional groundwater recharge.

Scenario 3 (Prolonged Dry Periods): The imposed 30% precipitation reduction and 10–25% increase in dry fraction likely intensified the effects of the 30% reduction in mean precipitation, causing the actual total precipitation to drop by 43% instead. This suggests that more frequent and prolonged dry spells were generated

6. CONCLUSION

The Gheba Basin exhibits highly variable rainfall patterns with strong seasonal fluctuations, making accurate precipitation estimation crucial for hydrological modeling and water resource management. The evaluation of global precipitation datasets revealed that CHIRPS and TRMM performed best, with CHIRPS showing lower bias and a strong correlation (0.74 at Adigudom station), while TRMM overestimated light rainfall and underestimated intense events. ERA5 and TerraClimate datasets exhibited significant biases, limiting their suitability for hydrological simulations in this region. The HEC-HMS model was successfully calibrated using observed precipitation, achieving a Nash-Sutcliffe Efficiency (NSE) of 0.719, demonstrating strong model performance in simulating streamflow dynamics.

A 100-year hourly precipitation dataset was generated using a Bartlett-Lewis stochastic model, calibrated with interpolated precipitation from HEC-HMS simulations for the 1999–2002 period. The statistical properties of the generated dataset were compared against observed precipitation, showing strong agreement in mean, variance, and wet-dry cycle patterns. While the generator underestimated extreme events, it effectively captured seasonal variability, confirming its applicability in semi-arid environments.

The HEC-HMS model was validated using observed streamflow data from the Gheba station (1999–2002), with results demonstrating strong model performance in simulating the basin's hydrology. The simulated peak discharge (83.5 m^3/s on 27 July 2000) closely aligned with observed peak discharge (104.5 m^3/s on 2 August 2001). The total simulated volume (200.55 mm) was slightly higher than the observed 195.09 mm, showing a good match in overall water balance. The Nash-Sutcliffe Efficiency (NSE) of 0.719 and a percent bias of -12.36% indicate a strong ability to capture general flow dynamics despite minor underestimations of extreme peak flows.

Simulations using CHIRPS and TRMM precipitation datasets were also conducted to evaluate the applicability of global datasets. CHIRPS-based simulations yielded a peak discharge of 94.5 m^3/s, with an NSE of 0.557, indicating moderate model performance but slight overestimations in total flow (219.44 mm, compared to 195.09 mm observed). TRMM-based simulations performed better, with a simulated peak discharge of 116.6 m^3/s and an NSE of 0.578, demonstrating reasonable accuracy in water balance representation. Streamflow analysis across different datasets confirmed that CHIRPS consistently produced lower streamflow values, while TRMM tended to overestimate peak flows. Despite discrepancies, all three datasets captured seasonal variations effectively, reinforcing their utility in hydrological assessments for the Gheba Basin.

For the stochastic experiments, the baseline water balance results indicated that evapotranspiration (ET canopy 57%) and aquifer recharge (34%) dominated precipitation partitioning, while direct flow (4%) and base flow (4%) contributed less. This highlights the water-limited nature of the basin, where most rainfall is lost through evapotranspiration rather than streamflow.

Scenario 1 (Moderate Increase, RCP8.5) resulted in a 10% increase in precipitation, leading to an 18% rise in aquifer recharge and a 5% increase in ET canopy. While total flow increased by 14%, the relative proportions of direct flow and base flow remained stable, indicating that additional precipitation contributed mainly to storage rather than increasing flood risks.

Scenario 2 (Intensified Rainfall Scenario, +30% mean, +50% variance) resulted in a 54% increase in precipitation, dramatically increasing aquifer recharge (83%) and total flow (187%), with direct flow

surging by 292%. This indicates higher flood risks and a shift towards rapid surface runoff, which could lead to flash floods and erosion hazards.

Scenario 3 (Prolonged Dry Scenario, -30% mean precipitation, increased dry fraction) led to a 43% decline in precipitation, causing a 53% reduction in aquifer recharge and a 37% drop in ET canopy. Total flow decreased by 48%, and direct flow fell by 43%, highlighting severe reductions in water availability, streamflow depletion, and increased drought stress.

Comparing Scenarios 2 and 3 reveals the extremes of hydrological response. While Scenario 2 leads to excessive runoff and flood risks, Scenario 3 results in severe water shortages, emphasizing the need for adaptive water resource management strategies.

These discrepancies between the imposed scenario changes and the model outputs are explained by considering that the 100-year baseline dataset generated is just one of the infinite numbers of possible realizations. While the model is calibrated to preserve, on average, key statistical properties of the observed data, a single stochastic generation may exhibit significant deviations from this average The use of multiple stochastic simulations would likely yield results that align more closely with expectations. Nonetheless, this study provides valuable insights into hydrological shifts under different climate scenarios, demonstrating Gheba Basin's vulnerability to both extreme wet and dry conditions. These findings reinforce the importance of adaptive water resource management, ensuring resilience against increasing climatic variability in semi-arid regions.

7. RECOMMENDATIONS

Given these findings, integrating advanced technologies into precipitation estimation, hydrological modeling, and climate adaptation planning is crucial.

Flood risk mitigation strategies should be enhanced through watershed conservation, reservoir optimization, and improved flood forecasting systems, particularly under intensified rainfall conditions. Conversely, drought resilience measures such as rainwater harvesting, groundwater recharge projects, and precision irrigation techniques must be prioritized to ensure sustainable water availability under prolonged dry conditions. Hydrological model projections should be integrated into regional water management policies to develop climate-resilient infrastructure and sustainable water allocation frameworks. Such hydrological projections should expand on the analyses presented here, by exploring multiple scenarios from a whole set of climate models, in order to produce an ensemble estimation of possible changes in the hydrologic balance associated with climatic changes, along with a measure of uncertainty.

This study underscores the critical role of accurate precipitation dataset selection, stochastic weather generators, and climate scenario-based hydrological modeling in sustainable water resource management. The findings emphasize the need for proactive planning, improved dataset integration, and innovative technological approaches to mitigate both extreme rainfall and prolonged drought conditions in semi-arid regions.

8. BIBLIOGRAPHY

1. Berhe AG, Misgna SH, Abraha GG, Abraha AZ. Impacts of climate change on crop growing season characteristics in Northern Ethiopia. J Water Clim Change [Internet] 2023 [cited 2025 Feb 20];14(6):1977–90. Available from: https://iwaponline.com/jwcc/article/14/6/1977/95673/Impacts-of-climate-change-on-crop-growing-season

2. Gebremicael TG, Mohamed YA, Van Der Zaag P. Attributing the hydrological impact of different land use types and their long-term dynamics through combining parsimonious hydrological modelling, alteration analysis and PLSR analysis. Sci Total Environ [Internet] 2019 [cited 2024 Dec 25];660:1155–67. Available from: https://linkinghub.elsevier.com/retrieve/pii/S0048969719300920

3. Nyssen J, Clymans W, Descheemaeker K, Poesen J, Vandecasteele I, Vanmaercke M, et al. Impact of soil and water conservation measures on catchment hydrological response—a case in north Ethiopia. Hydrol Process [Internet] 2010 [cited 2024 Dec 25];24(13):1880–95. Available from: https://onlinelibrary.wiley.com/doi/10.1002/hyp.7628

4. Hiben MG, Gebeyehu Awoke A, Adugna Ashenafi A. Estimation of Current Water Use over the Complex Topography of the Nile Basin Headwaters: The Case of Ghba Subbasin, Ethiopia. Adv Civ Eng [Internet] 2022 [cited 2024 Dec 25];2022(1):7852100. Available from: https://onlinelibrary.wiley.com/doi/10.1155/2022/7852100

5. Hölting B, Coldewey WG. Hydrological Cycle: Water Balance [Internet]. In: Hydrogeology. Berlin, Heidelberg: Springer Berlin Heidelberg; 2019 [cited 2024 Dec 25]. page 63–89.Available from: http://link.springer.com/10.1007/978-3-662-56375-5_8

6. Deshmukh MM, Elbeltagi A, Kouadri S. Climate Change Impact on Groundwater Resources in Semi-arid Regions [Internet]. In: Panneerselvam B, Pande CB, Muniraj K, Balasubramanian A, Ravichandran N, editors. Climate Change Impact on Groundwater Resources. Cham: Springer International Publishing; 2022 [cited 2024 Dec 25]. page 9–23.Available from: https://link.springer.com/10.1007/978-3-031-04707-7_2

7. Wilks DS. Interannual variability and extreme-value characteristics of several stochastic daily precipitation models. Agric For Meteorol [Internet] 1999 [cited 2025 Feb 18];93(3):153–69. Available from: https://linkinghub.elsevier.com/retrieve/pii/S0168192398001257

8. Rodriguez-iturbe,I., Cox,D. R., Isham, V. Some models for rainfall based on stochastic point processes. Proc R Soc Lond Math Phys Sci [Internet] 1987 [cited 2025 Feb 18];410(1839):269–88. Available from: https://royalsocietypublishing.org/doi/10.1098/rspa.1987.0039

9. Semenov MA, Barrow EM. Use of a Stochastic Weather Generator in the Development of Climate Change Scenarios. Clim Change [Internet] 1997 [cited 2025 Feb 18];35(4):397–414. Available from: http://link.springer.com/10.1023/A:1005342632279

10. Marani M. PROCESSI E MODELLI DELL'IDROLOGIA Un'introduzione.

11. Beven K. Rainfall-Runoff Modelling: The Primer [Internet]. 1st ed. Wiley; 2012 [cited 2024 Dec 25]. Available from: https://onlinelibrary.wiley.com/doi/book/10.1002/9781119951001

12. Feldman AD. HEC-HMS Technical Reference Manual. US Army Corps Eng Hydrol Eng Cent HEC 2000;

13. USACE. HEC-HMS Technical Reference Manual. 2023;

14. Todd H. Development and Application of a Continuous Soil Moisture Accounting Algorithm for the Hydrologic Engineering Center Hydrologic Modeling System (HEC-HMS). Thesis MS 1998;

15. HEC-HMS: Hydrologic Modeling System Technical Reference Manual. 2000;

16. Clark CO. Storage and the Unit Hydrograph. Trans Am Soc Civ Eng [Internet] 1945 [cited 2025 Feb 18];110(1):1419–46. Available from: https://ascelibrary.org/doi/10.1061/TACEAT.0005800

17. Kull DW, Feldman AD. Evolution of Clark's Unit Graph Method to Spatially Distributed Runoff. J Hydrol Eng [Internet] 1998 [cited 2025 Feb 23];3(1):9–19. Available from: https://ascelibrary.org/doi/10.1061/%28ASCE%291084-0699%281998%293%3A1%289%29

18. Berhanu B, Seleshi Y, Melesse AM. Surface Water and Groundwater Resources of Ethiopia: Potentials and Challenges of Water Resources Development [Internet]. In: Melesse AM, Abtew W, Setegn SG, editors. Nile River Basin. Cham: Springer International Publishing; 2014 [cited 2024 Dec 26]. page 97–117.Available from: https://link.springer.com/10.1007/978-3-319-02720-3_6

19. Gebrehiwot T, Van Der Veen A, Maathuis B. Spatial and temporal assessment of drought in the Northern highlands of Ethiopia. Int J Appl Earth Obs Geoinformation [Internet] 2011 [cited 2024 Dec 26];13(3):309–21. Available from: https://linkinghub.elsevier.com/retrieve/pii/S030324341000139X

20. Climate Classification of Ethiopia. Ethiop J Sci 2006;2(1):23–4.

21. Berhe AG, Misgna SH, Abraha GGS, Abraha AZ. Variability and trend analysis of temperatures, rainfall, and characteristics of crop-growing season in the eastern zone of Tigray region, northern Ethiopia. Theor Appl Climatol [Internet] 2023 [cited 2024 Dec 26];152(1–2):25–43. Available from: https://link.springer.com/10.1007/s00704-023-04364-w

22. Gebremicael TG, Mohamed YA, Van Der Zaag P, Hagos EY. Quantifying longitudinal land use change from land degradation to rehabilitation in the headwaters of Tekeze-Atbara Basin, Ethiopia. Sci Total Environ [Internet] 2018 [cited 2024 Dec 25];622–623:1581–9. Available from: https://linkinghub.elsevier.com/retrieve/pii/S0048969717327298

23. Gebreyohannes T, De Smedt F, Walraevens K, Gebresilassie S, Hussien A, Hagos M, et al. Application of a spatially distributed water balance model for assessing surface water and groundwater resources in the Geba basin, Tigray, Ethiopia. J Hydrol [Internet] 2013 [cited 2024 Dec 25];499:110–23. Available from: https://linkinghub.elsevier.com/retrieve/pii/S0022169413004691

24. Muñoz-Sabater J, Dutra E, Agustí-Panareda A, Albergel C, Arduini G, Balsamo G, et al. ERA5-Land: a state-of-the-art global reanalysis dataset for land applications. Earth Syst Sci Data [Internet] 2021 [cited 2025 Jan 5];13(9):4349–83. Available from: https://essd.copernicus.org/articles/13/4349/2021/

25. Muñoz-Sabater J, Dutra E, Agustí-Panareda A, Albergel C, Arduini G, Balsamo G, et al. ERA5-Land: A state-of-the-art global reanalysis dataset for land applications [Internet]. 2021 [cited 2024 Dec 27];Available from: https://essd.copernicus.org/preprints/essd-2021-82/essd-2021-82.pdf

26. Funk C, Peterson P, Landsfeld M, Pedreros D, Verdin J, Shukla S, et al. The climate hazards infrared precipitation with stations—a new environmental record for monitoring extremes. Sci Data [Internet] 2015 [cited 2024 Dec 27];2(1):150066. Available from: https://www.nature.com/articles/sdata201566

27. Abatzoglou JT, Dobrowski SZ, Parks SA, Hegewisch KC. TerraClimate, a high-resolution global dataset of monthly climate and climatic water balance from 1958–2015. Sci Data [Internet] 2018 [cited 2024 Dec 27];5(1):170191. Available from: https://www.nature.com/articles/sdata2017191

28. Willmott C, Matsuura K. Advantages of the mean absolute error (MAE) over the root mean square error (RMSE) in assessing average model performance. Clim Res [Internet] 2005 [cited 2025 Feb 9];30:79–82. Available from: http://www.int-res.com/abstracts/cr/v30/n1/p79-82/

29. Legates DR, McCabe GJ. Evaluating the use of "goodness-of-fit" Measures in hydrologic and hydroclimatic model validation. Water Resour Res [Internet] 1999 [cited 2025 Feb 9];35(1):233–41. Available from: https://agupubs.onlinelibrary.wiley.com/doi/10.1029/1998WR900018

30. Chai T, Draxler RR. Root mean square error (RMSE) or mean absolute error (MAE)? – Arguments against avoiding RMSE in the literature. Geosci Model Dev [Internet] 2014 [cited 2025 Feb 9];7(3):1247–50. Available from: https://gmd.copernicus.org/articles/7/1247/2014/

31. Willmott CJ. ON THE VALIDATION OF MODELS. Phys Geogr [Internet] 1981 [cited 2025 Feb 18];2(2):184–94. Available from: https://www.tandfonline.com/doi/full/10.1080/02723646.1981.10642213

APPENDIX A: STOCHASTIC MODEL CALIBRATION OUTPUT

A1. STATISTICAL SUMMARY OF THE OBSERVATION DATA

This appendix presents the raw output from the stochastic model calibration process used in this study. The dataset, identified as GHEBA_MODEL2.DAT, which was the observation daily precipitation data over the study basin and was processed through an iterative calibration procedure to estimate key statistical parameters for each month.

These values were used to fine-tune the stochastic precipitation generator, ensuring that the simulated precipitation patterns align with observed historical data.

Month	Mean 24h (mm)	Variance 24h (mmÂ²)	Correlation 24h	Dry Fraction 24h	Variance 48h (mmÂ²)	Dry Fraction 48h
1	0.177083	1.133911	0.667223	0.923611	3.073897	0.888889
2	0.059167	0.196256	0.477372	0.958333	0.378952	0.916667
3	0.444444	2.736036	0.096092	0.826389	7.011618	0.777778
4	0.479861	3.890708	0.449358	0.791667	10.438946	0.694444
5	0.58125	4.204967	0.411495	0.736111	11.155304	0.652778
6	1.236806	10.374922	0.197603	0.638889	24.880417	0.527778
7	5.84375	75.341919	0.052485	0.125	165.422409	0.055556
8	6.70625	73.89325	0.184701	0.138889	164.925034	0.027778
9	1.097917	19.322273	0.150664	0.680556	41.211266	0.5
10	0.088194	0.107304	0.001	0.888889	0.213162	0.805556
11	0.102083	0.502411	0.547448	0.944444	1.363014	0.902778
12	0.123611	0.806325	0.108531	0.916667	1.669575	0.875

A2. STATISTICAL SUMMARY OF THE 100-YEAR STOCHASTICALLY GENERATED BASELINE DATA

This appendix presents the statistical summary of the 100-year stochastically generated baseline precipitation dataset for the GHEBA Basin.

Month	Mean 24h (mm)	Variance 24h (mmÂ²)	Correlation 24h	Dry Fraction 24h	Variance 48h (mmÂ²)	Dry Fraction 48h
1	0.126908	0.480484	NaN	0.938333	1.455281	0.906111
2	0.051664	0.153164	NaN	0.959334	0.360433	0.928667
3	0.464216	3.041309	0.073314	0.874166	6.906896	0.781111
4	0.489661	3.553438	0.120013	0.848055	10.001172	0.742778
5	0.529529	3.503556	0.131539	0.849722	9.663276	0.751667
6	1.278572	11.675473	0.17838	0.655	28.491228	0.527778
7	5.280403	60.231594	0.039786	0.200833	126.179688	0.061667
8	6.083771	73.601189	0.137017	0.19	169.795975	0.061667
9	1.578448	31.462099	0.183848	0.677778	76.762787	0.495556
10	0.267797	4.071529	0.00001	0.878611	8.44127	0.777222
11	0.108221	0.408444	NaN	0.943333	1.182664	0.899444
12	0.105175	0.571564	0.117397	0.938055	1.319286	0.886111

APPENDIX B: STOCHASTIC MODEL PRECIPITATION OUTPUT

B1. ANNUAL PRECIPITATION ACCUMULATION ACROSS ALL SCENARIOS

This section presents the total annual precipitation accumulation for each year over the 100-year period across all scenarios. These values represent the sum of daily precipitation throughout each year, providing insight into long-term precipitation trends and potential shifts in overall water availability.

YEAR	100YRS - BASELINE Precipitation(mm)	100YRS-SCENARIO1 Precipitation(mm)	100YRS-SCENARIO-2 Precipitation(mm)	100YRS-SCENARIO-3 Precipitation(mm)
1	442	528	501	477
2	551	501	607	342
3	475	646	635	337
4	489	510	627	235
5	568	562	873	206
6	591	700	770	276
7	490	571	635	228
8	351	566	597	338
9	526	628	716	301
10	464	522	790	252
11	474	518	653	440
12	450	448	1263	243
13	551	481	704	322
14	530	384	801	270
15	448	458	578	261
16	644	578	662	194
17	486	497	560	327
18	626	624	796	284
19	428	420	581	264
20	355	754	978	246
21	550	586	720	339
22	524	487	751	213
23	703	475	957	290
24	403	506	514	242
25	414	524	628	275
26	545	502	729	177
27	411	436	813	197
28	684	513	831	335
29	502	503	493	311
30	527	662	745	279
31	414	558	699	200
32	543	504	949	250
33	485	533	611	584
34	458	598	707	412
35	511	713	734	391

36	391	677	556	345
37	426	526	675	287
38	392	565	803	200
39	399	592	942	223
40	472	600	982	270
41	515	589	721	308
42	433	625	802	354
43	478	580	1394	284
44	617	625	998	335
45	543	683	841	319
46	527	607	1013	193
47	401	704	985	194
48	596	421	603	362
49	400	661	584	320
50	453	501	657	267
51	523	684	920	225
52	448	680	711	293
53	512	420	1286	207
54	447	615	964	235
55	409	495	650	249
56	542	507	1164	247
57	554	475	853	278
58	643	649	910	221
59	560	552	586	280
60	653	565	811	318
61	436	473	915	164
62	438	570	1515	293
63	673	565	642	396
64	522	478	583	301
65	416	561	1019	348
66	387	498	691	251
67	454	583	1318	355
68	513	486	678	272
69	398	667	1025	273
70	454	585	684	146
71	624	514	894	278
72	686	452	831	219
73	472	546	639	212
74	516	457	1251	329
75	642	539	578	229
76	531	576	982	266
77	719	579	600	300
78	509	608	541	480
79	579	544	522	213
80	477	510	623	214
81	485	348	630	352
82	384	698	618	397

83	550	534	551	327
84	466	518	713	218
85	501	511	627	256
86	495	585	724	198
87	585	402	951	321
88	837	568	711	233
89	560	543	543	386
90	589	554	525	330
91	644	579	610	262
92	394	519	1181	282
93	494	558	814	365
94	421	640	467	234
95	361	646	983	364
96	362	524	765	355
97	365	549	615	258
98	312	546	872	253
99	598	549	461	250
100	597	606	1045	381

B2. DAILY MAXIMUM PRECIPITATION ACROSS ALL SCENARIOS

This section displays the highest single-day precipitation recorded each year over the 100-year period across all scenarios. These values help identify extreme daily rainfall events, which are crucial for understanding changes in storm intensity and flood risk

YEAR	100YRS - BASELINE Precipitation(mm)	100YRS-SCENARIO1 Precipitation(mm)	100YRS-SCENARIO-2 Precipitation(mm)	100YRS-SCENARIO-3 Precipitation(mm)
1	18.6	57.2	45.9	25.4
2	22.8	6.4	58.8	7.9
3	16.0	6.0	21.9	21.0
4	23.7	8.9	33.7	7.5
5	25.7	5.0	135.8	7.8
6	19.1	6.5	55.6	14.8
7	21.6	6.5	34.4	12.7
8	15.0	6.2	29.3	11.7
9	31.0	7.5	66.3	18.6
10	15.5	6.8	107.3	24.0
11	11.8	9.0	20.4	15.5
12	13.6	4.5	485.1	8.7
13	18.8	4.7	72.9	34.5
14	16.2	5.4	111.0	14.9
15	16.5	4.1	20.3	9.7
16	16.5	5.9	28.1	7.4
17	17.1	6.5	53.1	22.1
18	19.0	7.6	27.2	10.2
19	16.6	6.2	21.8	10.2
20	7.9	6.3	273.8	14.0

21	19.4	5.5	166.3	18.0
22	16.4	5.2	124.3	8.9
23	41.2	6.3	320.6	12.8
24	21.0	4.3	18.7	13.0
25	15.9	7.8	16.9	28.2
26	20.4	6.6	94.6	11.9
27	11.7	7.5	159.8	13.6
28	27.3	3.7	150.0	14.3
29	22.0	5.8	12.4	24.1
30	18.7	9.0	39.0	19.8
31	22.8	9.8	91.7	10.2
32	49.6	6.2	152.5	8.9
33	13.0	9.1	83.3	35.3
34	21.6	7.0	99.0	11.3
35	11.4	6.1	77.2	16.3
36	12.2	5.5	34.9	12.3
37	19.5	6.4	142.2	30.6
38	9.6	5.9	74.2	12.2
39	11.6	11.9	412.6	8.6
40	16.9	6.7	312.6	14.5
41	19.2	8.2	115.0	15.6
42	10.6	6.4	88.4	22.6
43	10.1	9.7	199.8	11.8
44	17.5	5.9	248.6	12.9
45	16.9	5.9	102.9	15.8
46	37.4	7.9	191.1	9.3
47	14.4	23.0	201.3	10.0
48	87.0	3.5	55.5	20.5
49	16.1	19.3	51.2	11.6
50	15.7	5.7	16.9	10.9
51	11.4	5.6	98.8	17.3
52	10.7	5.7	120.0	9.7
53	14.3	4.6	365.1	17.5
54	35.5	9.4	184.5	19.1
55	14.9	8.0	74.4	9.0
56	17.1	8.4	245.2	16.2
57	25.7	11.8	113.5	12.3
58	18.9	6.3	207.7	10.4
59	18.4	8.3	87.8	16.2
60	17.7	8.0	205.2	19.9
61	15.2	5.4	82.5	9.9
62	14.9	10.1	439.2	10.1
63	23.3	5.9	72.9	24.5
64	23.5	31.4	84.9	11.7
65	24.7	6.2	364.9	20.9
66	16.8	5.6	161.6	9.5
67	15.4	5.8	252.1	13.5

68	17.0	3.9	45.7	13.4
69	12.2	12.1	166.4	9.1
70	13.3	6.0	18.3	7.7
71	19.0	5.2	275.5	11.3
72	23.8	6.3	97.3	7.8
73	18.0	10.4	31.3	5.8
74	23.6	3.9	328.2	27.3
75	22.8	7.0	60.8	10.3
76	12.9	4.6	161.3	19.2
77	19.4	6.1	14.1	25.4
78	12.7	9.8	11.6	12.9
79	19.4	5.7	17.7	6.9
80	14.3	4.6	75.7	6.7
81	17.0	5.3	52.6	45.1
82	9.4	5.8	49.4	26.2
83	67.9	6.4	24.7	13.1
84	11.3	6.8	94.4	8.3
85	13.5	7.4	17.0	7.8
86	19.5	8.3	77.2	22.2
87	31.3	6.5	174.7	5.6
88	22.8	9.4	103.6	13.3
89	16.2	5.6	28.2	16.7
90	20.8	3.6	25.4	17.3
91	26.7	7.1	29.3	12.6
92	12.0	6.1	235.4	17.2
93	14.0	6.4	95.7	24.0
94	14.1	11.8	36.8	8.8
95	12.1	5.0	264.9	13.3
96	12.7	6.1	155.5	20.4
97	12.8	6.2	14.3	10.6
98	10.7	5.9	319.5	11.5
99	29.1	6.8	18.8	15.3
100	17.8	6.5	290.2	24.7

ANNEX1: Additional Resources & Documentation

📎 Downloadable Resources

🔗 Extracted Precipitation Data (CSV & Geo TIFF)

🔗 Google Earth Engine (GEE) Scripts Repository

📑 Dataset Documentation & Metadata

Dataset Name	Resolution	Time Period	Processing Steps
ERA5-Land	Hourly (~10km)	1999-2002/2019	Extracted hourly precipitation, aggregated, and exported as CSV/GeoTIFF
CHIRPS	Daily (~5km)	1999-2002/2019	Processed daily & annual precipitation for basin-wide analysis
TRMM 3B42	3-Hourly (~27km)	1999-2002/2019	Converted 3-hourly to daily precipitation, exported for hydrological modeling
TerraClimate	Monthly (~4.6km)	1999-2019	Extracted precipitation and PET for long-term climate trends

🚀 Citation & Contact

📖 Hundesa Siraj Mohammed (2025), "Basin-scale hydrological impacts from climatic changes: a model assessment in the Horn of Africa," University of Padua, Department of Water and Geological Risk Engineering.

✉️ ***Contact: hundesiraj65@gmail.com***